INFORMATION TO USERS

This manuscript has been reproduced from the microfilm master. UMI films the text directly from the original or copy submitted. Thus, some thesis and dissertation copies are in typewriter face, while others may be from any type of computer printer.

The quality of this reproduction is dependent upon the quality of the copy submitted. Broken or indistinct print, colored or poor quality illustrations and photographs, print bleedthrough, substandard margins, and improper alignment can adversely affect reproduction.

In the unlikely event that the author did not send UMI a complete manuscript and there are missing pages, these will be noted. Also, if unauthorized copyright material had to be removed, a note will indicate the deletion.

Oversize materials (e.g., maps, drawings, charts) are reproduced by sectioning the original, beginning at the upper left-hand corner and continuing from left to right in equal sections with small overlaps.

Photographs included in the original manuscript have been reproduced xerographically in this copy. Higher quality 6" x 9" black and white photographic prints are available for any photographs or illustrations appearing in this copy for an additional charge. Contact UMI directly to order.

Bell & Howell Information and Learning
300 North Zeeb Road, Ann Arbor, MI 48106-1346 USA
800-521-0600

Université d'Ottawa • University of Ottawa

REGIONAL GEOPHYSICAL MODELLING AND PALEO-RECONSTRUCTION IN AND AROUND THE SOUTHERN SLAVE STRUCTURAL PROVINCE.

by

© Karen Anne Bernice Shepley

A thesis submitted to the School of Graduate Studies and Research

in partial fulfillment of the requirements

for the degree of M.Sc. in Earth Sciences

Ottawa-Carleton Geoscience Centre

And

University of Ottawa

Ottawa, Canada

Abstract

The rocks of northwestern Canada represent over 4.0 Ga of geological history. This study focuses on two periods from that history: geophysical modeling in the south-central Archean Slave Structural Province and a reconstruction of the Early Proterozoic Great Slave Lake Shear Zone (GSLSZ) using the regional magnetic fabric.

One of the goals of the modelling in the Slave Province was to constrain the depth extent and shapes of the exposed plutons and greenstone belts. This was extremely successful. The greenstone belts are steeply dipping toward the east and the plutons are laccolithic in shape, often folded, and are about 1-2 km thick. These results correlate with a cross-section of the western part of the south-central Slave Province (Wouter Bleeker, personal communication). However, it was not possible to confirm or rule out the presence of the greenstones beneath the metasediments of the Yellowknife Basin, as either model was feasible. The depth to basement, however, is constrained at 8-9 km, in either case.

The reconstruction of the GSLSZ was performed using a technique developed by Roest and Pilkington (1994). First, the effects of the Bathurst and MacDonald Fault Zones were removed. These fault zones are brittle features that bound the Slave Province to the northeast and southeast and resulted from the collision of the Hottah Terrane to the west. Motion due to this collision was taken up by compression at the leading edge of the indentor and by the escape of a large block of material to the north. The motion of the indentation and, thus was to the northeast.

Reconstruction of the GSLSZ was performed using the regional magnetic fabric after the removal of the effects of the Bathurst and MacDonald Fault Zones. One possible combination of plate geometries is assumed. The results of the reconstruction show that the Slave Province experienced a clockwise rotation approximately 16° with respect to the Churchill Province and moved toward the northeast. It was not possible to correlate the units to the north and south of the shear zone, except for the Taltson and Thelon Magmatic Zones, which have been shown to belong to the same unit through geological, geochemical, and geochronological studies in the area. The reconstruction only depicts one stage in the collisional event. Any brittle component of the shear zone that may have occurred is assumed to have eroded away, with the exception of cataclastic mylonites found within the GSLSZ (Hanmer, 1988), and is not factored into the reconstruction models.

Although widely separated in time, the two tectonic phases addressed in this study depicts two phases in the process of craton formation. Future work in the Slave Province can be directed at producing a 3-D model of the Yellowknife basin. Future work for the reconstruction of the shear zone may include applying the reconstruction technique to other plate geometry combinations and by considering the other stages of motion along the shear zone.

Résumé

Les roches du nord ouest du Canada ont une histoire géologique de plus de 4 milliards d'années. Cette étude se concentre sur deux périodes spécifiques de cette histoire. D'abord, nous discutons de la modélisation des données gravimétriques dans le domaine sud de la Province Structurale Archéenne du Slave, en essayant de comprendre la structure 3D des plutons qui y existent. Après, nous faisons une reconstitution du mouvement le long de la zone d'une déformation transformante: Great Slave Shear Zone.

La gémétrie des plutons et des ceintures de roches vertes dans la domaine de Yellowknife est bien contrainte par les données gravimétriques. Cette étude a démontré que les roches vertes ont une attitude verticale, avec une inclination vers l'est. Les formations plutoniques sont, en général, d'une forme laccolithique, souvent plissées, et ont une extension en profondeur de 1 à 2 km. De plus, la profondeur du socle est bien contrainte, soit entre 8 et 9 km. Ces résultats sont en accord avec le modèle de Bleeker et al. (Bleeker, comm. pers.), qui ont construit une section verticale de la Province du Slave. Les modèles gravimétriques ne peuvent pas discriminer entre une configuration ayant des roches vertes à la base du basin structural de Yellowknife, telle que préféré par Bleeker et al, ou une absence de ces roches vertes en dessous des métasédiments.

La reconstitution des mouvements tectoniques le long la zone transformante du Grand Lac des Esclaves a été effectuée à l'aide de la technique développée par Roest et Pilkington (1994). D'abord, les effets de la déformation cassante le long des failles Bathurst et

MacDonald ont été reconstruites. Ce mouvement cassant a été suivi par une compression et par un mouvement rigide. Le modèle préféré est que ce mouvement a été initié par un mouvement du terrain Hottah en direction nord est.

Finalement, le mouvement ductile le long la zone de GS a été reconstruit, en utilisant les données aéromagnétiques. Nous avons essayé de faire des corrélations entre les domaines géologiques au nord et au sud de la zone transformante. À l'exception des zones Taltson et Thelon, il est difficile de faire une corrélation robuste. Néanmoins, cette reconstitution peut être utilisée pour étudier le mouvement relatif entre le craton Slave et le craton Churchill. Plus de données géochronologiques et paléomagnétiques sont nécessaire pour vérifier notre modèle cinématique.

Les deux parties de cette étude, même si elles s'intéressent à des temps géologiques très différents, illustrent des périodes de construction d'un continent. Dans le futur, un modèle gravimétrique en 3D pour le basin de Yellowknife devra être construit. Aussi, différents scénarios cinématiques doivront être considérée pour la zone transformante du GSL.

Table of Contents

List of Tables

List of Figures

Introduction

The rocks of northwestern Canada represent over 4.0 Ga of varied and complex geological history. They include the Archean granite-greenstone terrain of the Slave Structural Province (SSP), the Proterozoic Wopmay Orogen with its associated Hottah Terrane, and the Proterozoic Western Churchill Province, which is known to be underlain by Archean basement.

Presented here are the results of a two-part geophysical study, located in northwestern Canada (Fig. 0.1). Figures 0.2-0.4 show the regional geology, aeromagnetic, and gravity maps of the study area respectively. The regional geology and the data processing techniques used for the regional data sets and the gravity profiles are presented. This provides a firm foundation for the discussion of the modelling and analyses of the gravity profiles and the results of the paleo-reconstruction of the Great Slave Lake Shear Zone.

While the two studies are focussed on events that are distinct and widely separated in time, together they provide a good example of the sorts of events that contribute to the processes of plate tectonics and the building of cratons. The events within the Archean Slave Structural Province are not well understood and there is a wide variety of interpretations of the data that has been acquired there (explained in section 1.29); however, these events were crucial in forming the Slave Craton. In contrast to this, the Great Slave Lake Shear Zone has been primarily linked to the collision of the Slave Province with the Western Churchill Province.

Starting in the Archean, the results of the gravity modelling in the south-central Slave

Province are presented. The focus is on the analysis and modelling of three gravity profiles, which cross the south-central SSP, and modelling of a profile which extends from the southwestern SSP as far west as the Fort Simpson Terrane (Slave-Northern Cordillera Lithospheric Evolution (SNORCLE) Transect 1), with detailed modelling and analysis of the eastern end of this profile. The purpose of this modelling is to constrain the depth extent and shape of the various units in the Yellowknife Basin, particularly the plutons and the greenstone belts.

Then, shifting to the Early Proterozoic, the results of the reconstruction of the Great Slave Lake Shear Zone, separating the SSP from the Churchill Structural Province to the south, are presented, first taking into account the effects of the later Bathurst and MacDonald Fault Zones. After considering different original plate geometries, a reconstruction technique developed by Roest and Pilkington (1994) is then applied to the simplest of them. The GSLSZ was active 2.0-1.9 Ga ago, during the collision of the SSP with the western Churchill Province. The focus of this study is to constrain the geometry of the collision and deformation. It may aid in understanding why the shear zone does not penetrate further into the Churchill Province and it may help explain the current distribution of units to the north and south of the shear zone.

All regional aeromagnetic and gravity data were collected by the Geological Survey of Canada (GSC) and Geomatics Canada (GC). The targeted gravity data was collected along Lithoprobe SNORCLE Transect 1 in the summer of 1996, and along the three Cameron profiles in the south-central SSP in the summer of 1997. The data collection was led by Roy

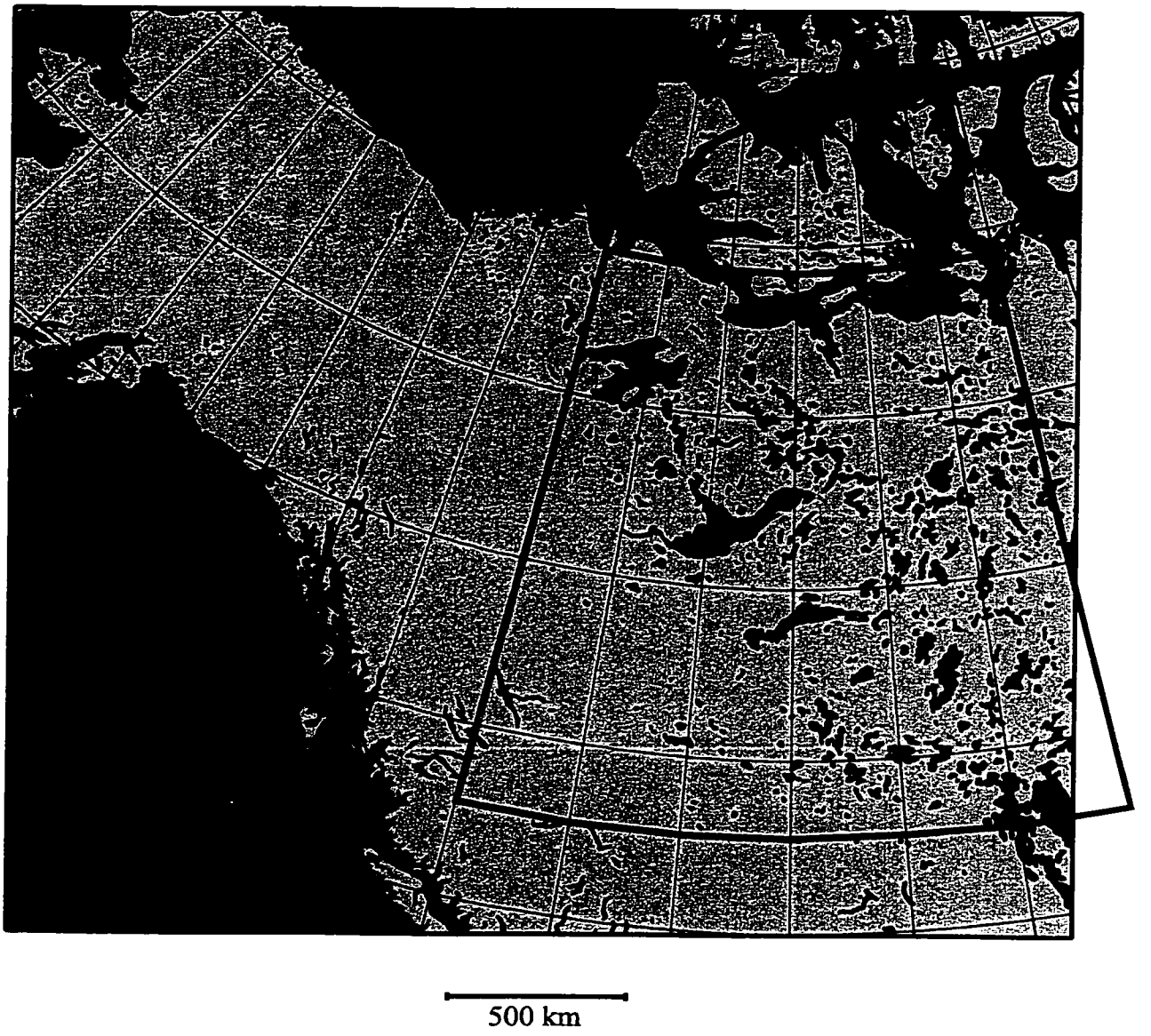

Figure 0.1. Location map. The red box encompasses both study areas: the gravity modelling in the Slave Province and the reconstruction of the GSLSZ.

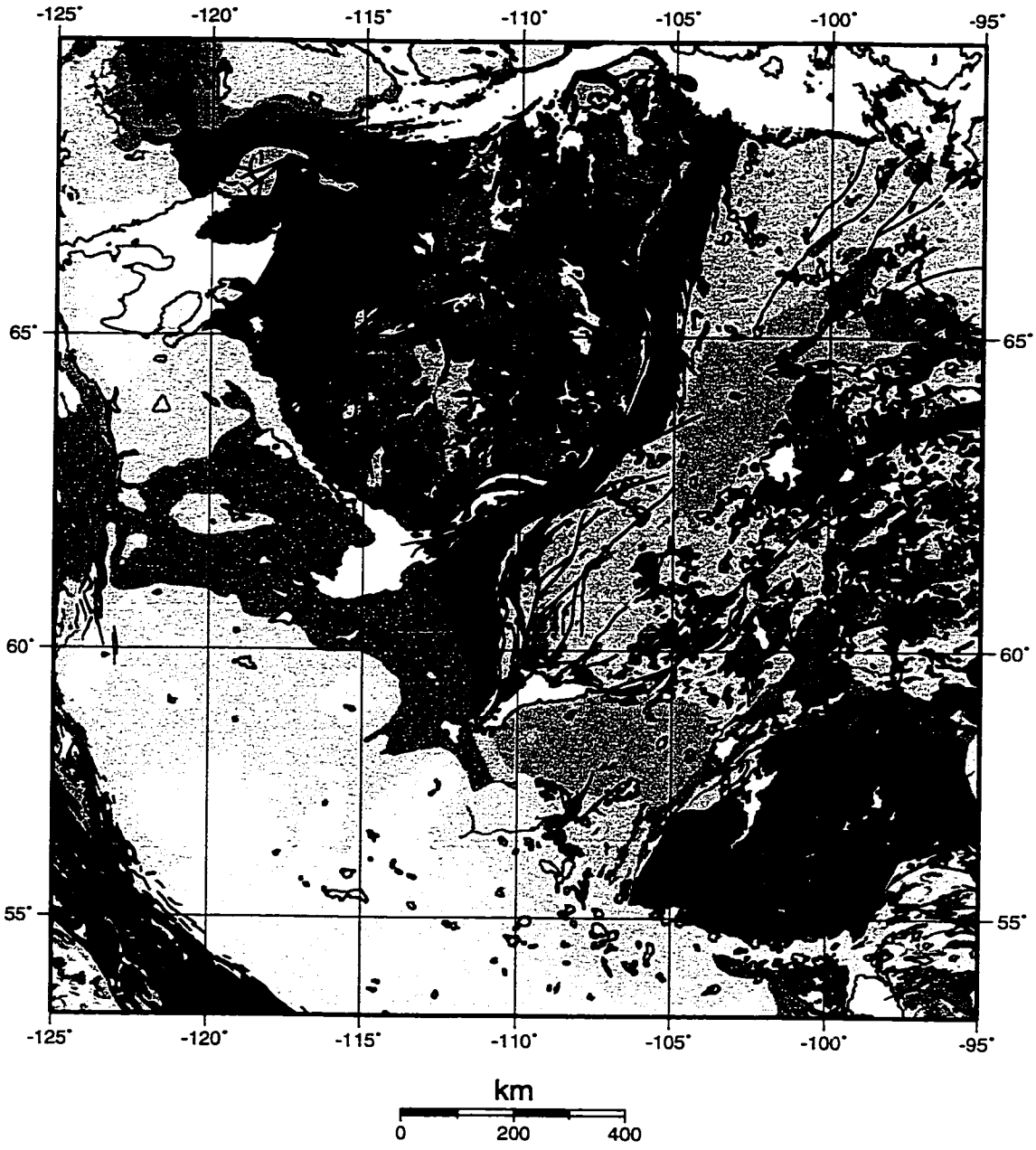

Figure 0.2. Regional geology of the study area.
Taken from the Geological Map of Canada.

Legend/Légende

CENOZOIC ROCKS
ROCHES DU CÉNOZOÏQUE
- shale sandstone conglomerate / conglomérats de schiste argileux avec grès
- volcanic rocks / roches volcaniques
- tonalite / tonalite

MESOZOIC-CENOZOIC ROCKS
ROCHES DU MÉSOZOÏQUE-CÉNOZOÏQUE
- shale sandstone conglomerate / conglomérats de schiste argileux avec grès

MESOZOIC ROCKS
ROCHES DU MÉSOZOÏQUE
- shale sandstone conglomerate / conglomérats de schiste argileux avec grès
- Cretaceous sedimentary rocks / roches sédimentaires du Crétacé
- Cretaceous-Triassic sedimentary rocks / roches sédimentaires du Crétacé-Trias
- Jurassic sedimentary rocks / roches sédimentaires du Jurassique
- Triassic-Jurassic sedimentary rocks / roches sédimentaires du Trias-Jurassique
- Triassic sedimentary rocks / roches sédimentaires du Trias

PALEOZOIC ROCKS
ROCHES DU PALÉOZOÏQUE
- granite syenite / granite syénite
- gabbro diorite anorthosite / gabbro diorite anorthosite
- ultramafic intrusions / intrusions ultramafiques
- mafic volcanic rocks / roches volcaniques mafiques
- undivided carbonate and siliciclastic rocks / roches carbonatées et siliciclastiques non divisées
- Silurian carbonate and siliciclastic rocks / roches carbonatées et siliciclastiques du Silurien
- Cambrian-Silurian carbonate and siliciclastic rocks / roches carbonatées et siliciclastiques du Cambrien-Silurien
- Cambrian-Ordovician carbonate and siliciclastic rocks / roches carbonatées et siliciclastiques du Cambrien-Ordovicien
- Cambrian sedimentary rocks / roches sédimentaires du Cambrien

NEOPROTEROZOIC ROCKS
ROCHES DU NÉOPROTÉROZOÏQUE
- gabbro diorite anorthosite / gabbro diorite anorthosite
- undivided sedimentary rocks / roches sédimentaires non divisées

MESOPROTEROZOIC-NEOPROTEROZOIC ROCKS
ROCHES DU MÉSOPROTÉROZOÏQUE-NÉOPROTÉROZOÏQUE
- undivided sedimentary rocks / roches sédimentaires non divisées

MESOPROTEROZOIC ROCKS
ROCHES DU MÉSOPROTÉROZOÏQUE
- gabbro diorite anorthosite / gabbro diorite anorthosite
- undivided gneiss / gneiss non divisés
- undivided sedimentary rocks / roches sédimentaires non divisées
- volcanic rocks / roches volcaniques

PALEOPROTEROZOIC-MESOPROTEROZOIC ROCKS
ROCHES DU PALÉOPROTÉROZOÏQUE-MÉSOPROTÉROZOÏQUE
- undivided sedimentary rocks / roches sédimentaires non divisées

PALEOPROTEROZOIC ROCKS
ROCHES DU PALÉOPROTÉROZOÏQUE
- gabbro diorite anorthosite / gabbro diorite anorthosite
- undivided gneiss / gneiss non divisés
- granite monzonite syenite/granulite-facies granitoids / granite monzonite syénite/granitoïdes à faciès granulite
- granulite-facies paragneiss / paragneiss à faciès granulite
- orthogneiss / orthogneiss
- granulite-facies volcanic rocks / roches volcaniques à faciès granulite

ARCHEAN-PALEOPROTEROZOIC ROCKS
ROCHES D'ARCHÉEN-PALÉOPROTÉROZOÏQUE
- undivided gneiss / gneiss non divisés
- granite monzonite syenite/granulite-facies granitoids / granite monzonite syénite/granitoïdes à faciès granulite
- undivided granulite-facies gneiss / gneiss à faciès granulite non divisés
- granulite-facies sedimentary and volcanic rocks / roches sédimentaires et volcaniques à faciès granulite
- metasedimentary rocks / roches métasédimentaires
- metasedimentary and metavolcanic rocks / roches métasédimentaires et métavolcaniques

ARCHEAN ROCKS
ROCHES D'ARCHÉEN
- gabbro diorite anorthosite / gabbro diorite anorthosite
- undivided gneiss / gneiss non divisés
- granite monzonite syenite / granite monzonite syénite
- granulite-facies mafic rocks / roches mafiques à faciès granulite
- granulite-facies sedimentary rocks/metasedimentary rocks / roches sédimentaires à faciès granulite/roches métasédimentaires
- metasedimentary and metavolcanic rocks/metavolcanic rocks / roches métasédimentaires et métavolcaniques/roches métavolcaniques

Continuation of Figure 0.2.

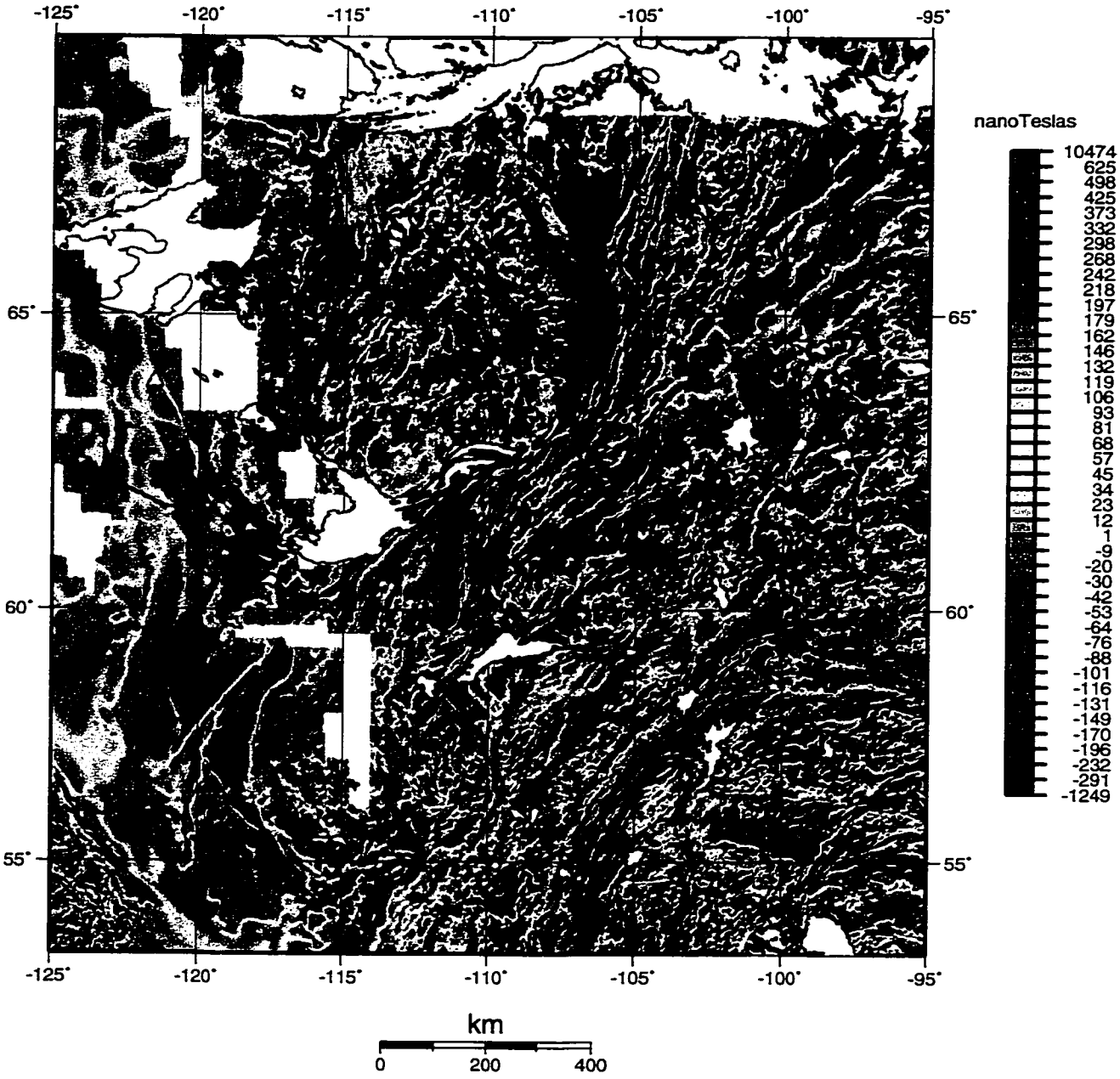

Figure 0.3. Regional aeromagnetic map of study area.

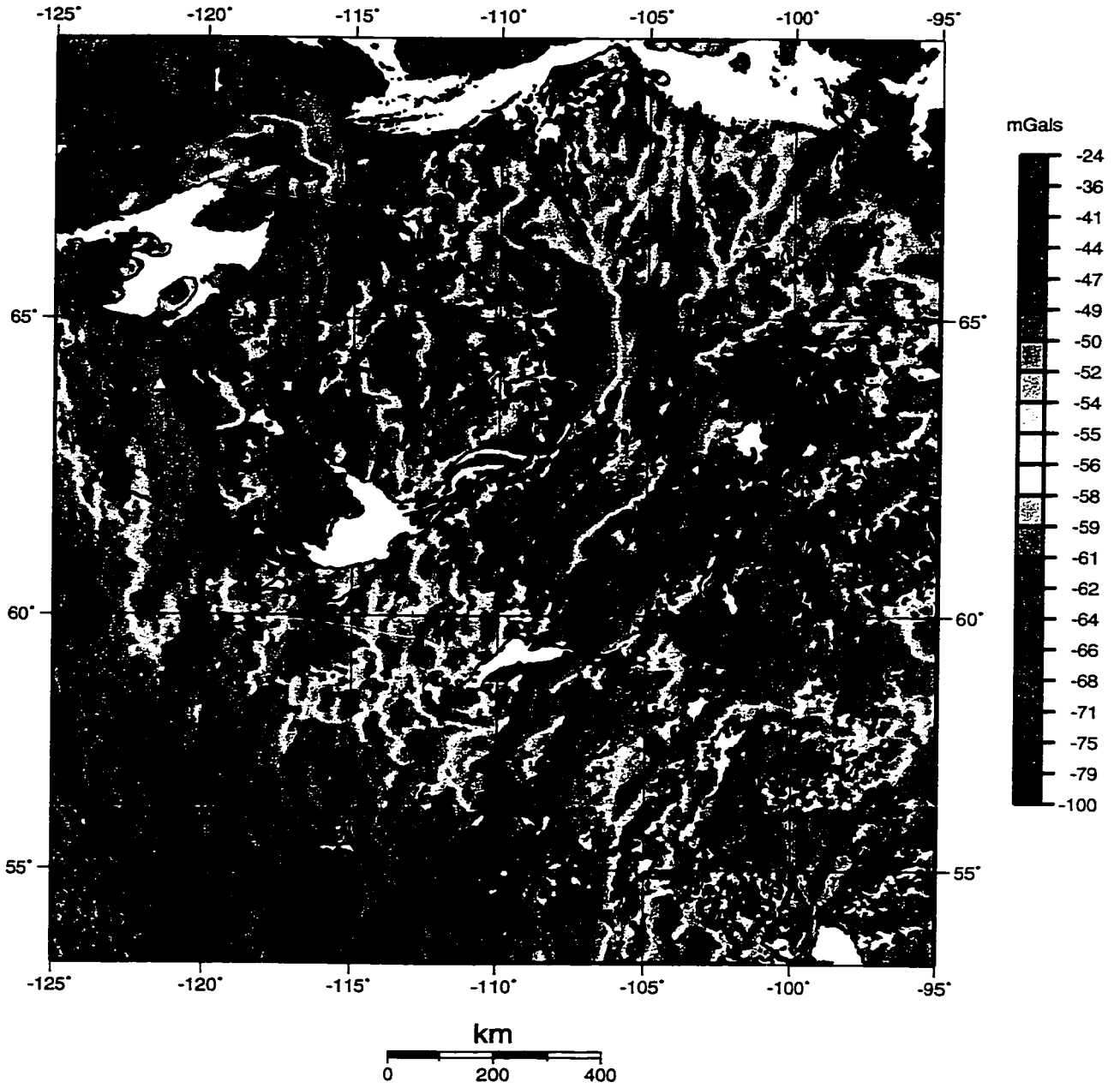

Figure 0.4. Regional Bouguer gravity map of the study area.

Cooper of GC. Processing of the targeted gravity data was carried out by Bryne Hearty of GC. Regional gravity data were processed by the Gravity Group of the GSC and the regional aeromagnetic data were processed by Warner Miles of the Regional Geophysics Section of the GSC. All interpretation and analyses of data presented in this thesis were carried out by the author using the facilities at the Regional Geophysics Section of the GSC. Any other data presented in thesis is used to constrain and support the analyses and these data are contributed by various parties. These contributions will be acknowledged as the data is presented.

Chapter 1: Geology

1.1 Introduction

The area of study includes the south-central Slave Structural Province, the northwestern part of the Churchill Structural Province, the Wopmay Orogen, and the Great Slave Lake Shear Zone (Fig. 1.1). The geology, structure, and tectonic history of these areas will be discussed

1.2 Slave Structural Province

1.21 Introduction

The Slave Structural Province (SSP) lies in the northwestern part of the Canadian Shield. It is bound by the Coronation Gulf to the north, the Wopmay Orogen to the west, the Thelon Magmatic Arc to the east, and the Great Slave Lake Shear Zone to the south (Fig. 1.1). The SSP can be divided into two regions; the eastern, which is largely underlain by juvenile crust, and the western half, which is underlain by Archean basement (Bleeker and Davis, 1999) (Fig. 1.2). This is supported by Pb isotopic data (Thorpe et al., 1992) and Nd isotopic data (Davis and Henger, 1992), which define a boundary between 112°W and 110°30'W. Throughout the western SSP there are a number of occurrences of basement rocks, numerous north to north-east trending greenstone belts, traceable marker sequences, and various basins of metasediments.

The gravity modeling in this study focuses on the south-central part of the SSP, known as the Yellowknife Domain (the Yellowknife-Hearne Lake area of Henderson (1985);

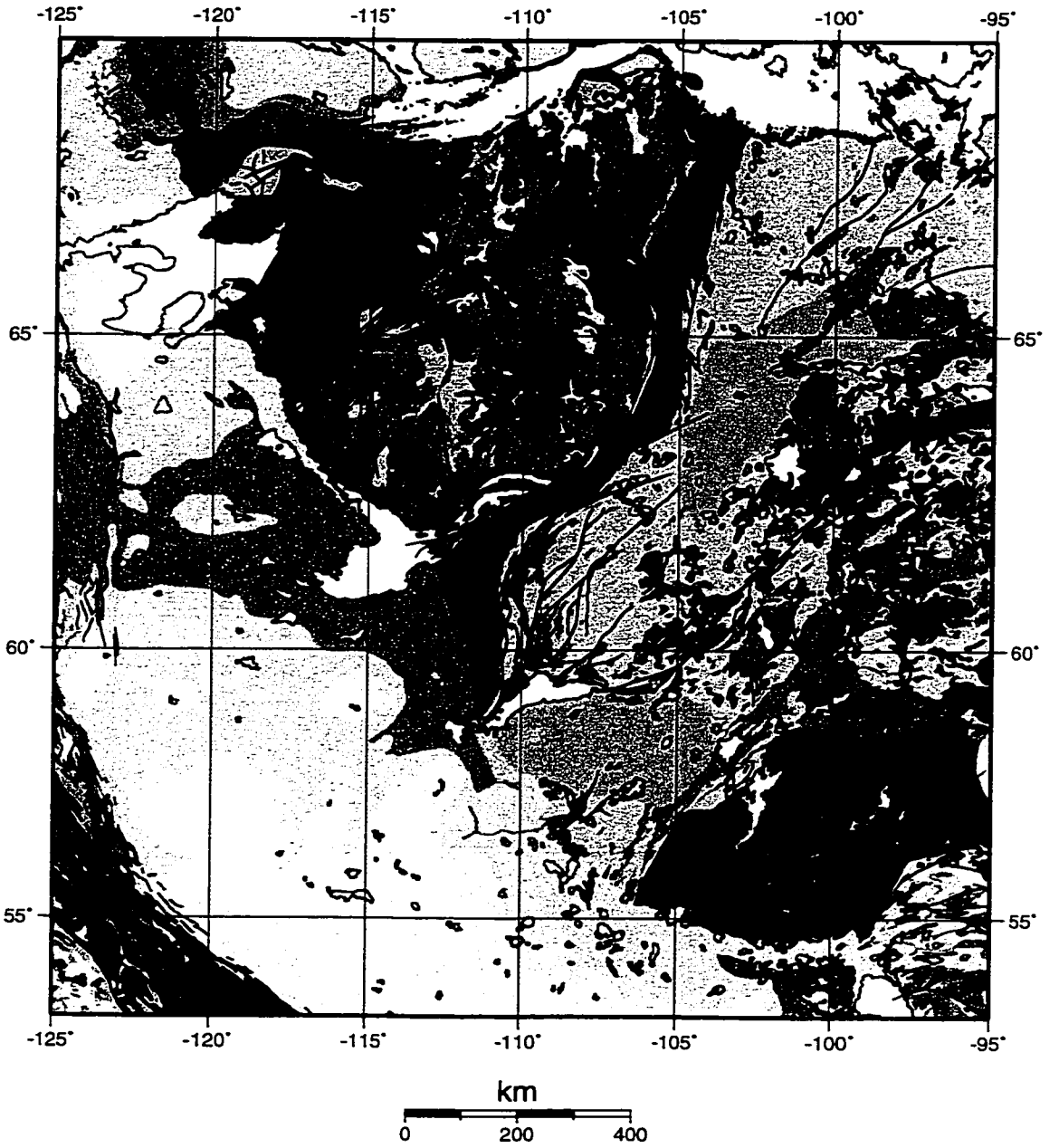

Figure 1.1. Regional Geology of the study area

Legend/Légende

CENOZOIC ROCKS
ROCHES DU CÉNOZOÏQUE
- shale sandstone conglomerate
  conglomérats de schiste argileux avec grès
- volcanic rocks
  roches volcaniques
- tonalite
  tonalite

MESOZOIC-CENOZOIC ROCKS
ROCHES DU MÉSOZOÏQUE-CÉNOZOÏQUE
- shale sandstone conglomerate
  conglomérats de schiste argileux avec grès

MESOZOIC ROCKS
ROCHES DU MÉSOZOÏQUE
- shale sandstone conglomerate
  conglomérats de schiste argileux avec grès
- Cretaceous sedimentary rocks
  roches sédimentaires du Crétacé
- Cretaceous-Triassic sedimentary rocks
  roches sédimentaires du Crétacé-Trias
- Jurassic sedimentary rocks
  roches sédimentaires du Jurassique
- Triassic-Jurassic sedimentary rocks
  roches sédimentaires du Trias-Jurassique
- Triassic sedimentary rocks
  roches sédimentaires du Trias

PALEOZOIC ROCKS
ROCHES DU PALÉOZOÏQUE
- granite syenite
  granite syénite
- gabbro diorite anorthosite
  gabbro diorite anorthosite
- ultramafic intrusions
  intrusions ultramafiques
- mafic volcanic rocks
  roches volcaniques mafiques
- undivided carbonate and siliciclastic rocks
  roches carbonatées et siliciclastiques non divisées
- Silurian carbonate and siliciclastic rocks
  roches carbonatées et siliciclastiques du Silurien
- Cambrian-Silurian carbonate and siliciclastic rocks
  roches carbonatées et siliciclastiques du Cambrien-Silurien
- Cambrian-Ordovician carbonate and siliciclastic rocks
  roches carbonatées et siliciclastiques du Cambrien-Ordovicien
- Cambrian sedimentary rocks
  roches sédimentaires du Cambrien

NEOPROTEROZOIC ROCKS
ROCHES DU NÉOPROTÉROZOÏQUE
- gabbro diorite anorthosite
  gabbro diorite anorthosite
- undivided sedimentary rocks
  roches sédimentaires non divisées

MESOPROTEROZOIC-NEOPROTEROZOIC ROCKS
ROCHES DU MÉSOPROTÉROZOÏQUE-NÉOPROTÉROZOÏQUE
- undivided sedimentary rocks
  roches sédimentaires non divisées

MESOPROTEROZOIC ROCKS
ROCHES DU MÉSOPROTÉROZOÏQUE
- gabbro diorite anorthosite
  gabbro diorite anorthosite
- undivided gneiss
  gneiss non divisés
- undivided sedimentary rocks
  roches sédimentaires non divisées
- volcanic rocks
  roches volcaniques

PALEOPROTEROZOIC-MESOPROTEROZOIC ROCKS
ROCHES DU PALÉOPROTÉROZOÏQUE-MÉSOPROTÉROZOÏQUE
- undivided sedimentary rocks
  roches sédimentaires non divisées

PALEOPROTEROZOIC ROCKS
ROCHES DU PALÉOPROTÉROZOÏQUE
- gabbro diorite anorthosite
  gabbro diorite anorthosite
- undivided gneiss
  gneiss non divisés
- granite monzonite syenite/granulite-facies granitoids
  granite monzonite syénite/granitoïdes à faciès granulite
- granulite-facies paragneiss
  paragneiss à faciès granulite
- orthogneiss
  orthogneiss
- granulite-facies volcanic rocks
  roches volcaniques à faciès granulite

ARCHEAN-PALEOPROTEROZOIC ROCKS
ROCHES D'ARCHÉEN-PALÉOPROTÉROZOÏQUE
- undivided gneiss
  gneiss non divisés
- granite monzonite syenite/granulite-facies granitoids
  granite monzonite syénite/granitoïdes à faciès granulite
- undivided granulite-facies gneiss
  gneiss à faciès granulite non divisés
- granulite-facies sedimentary and volcanic rocks
  roches sédimentaires et volcaniques à faciès granulite
- metasedimentary rocks
  roches métasédimentaires
- metasedimentary and metavolcanic rocks
  roches métasédimentaires et métavolcaniques

ARCHEAN ROCKS
ROCHES D'ARCHÉEN
- gabbro diorite anorthosite
  gabbro diorite anorthosite
- undivided gneiss
  gneiss non divisés
- granite monzonite syenite
  granite monzonite syénite
- granulite-facies mafic rocks
  roches mafiques à faciès granulite
- granulite-facies sedimentary rocks/metasedimentary rocks
  roches sédimentaires à faciès granulite/roches métasédimentaires
- metasedimentary and metavolcanic rocks/metavolcanic rocks
  roches métasédimentaires et métavolcaniques/roches métavolcaniques

Continuation of Figure 1.1.

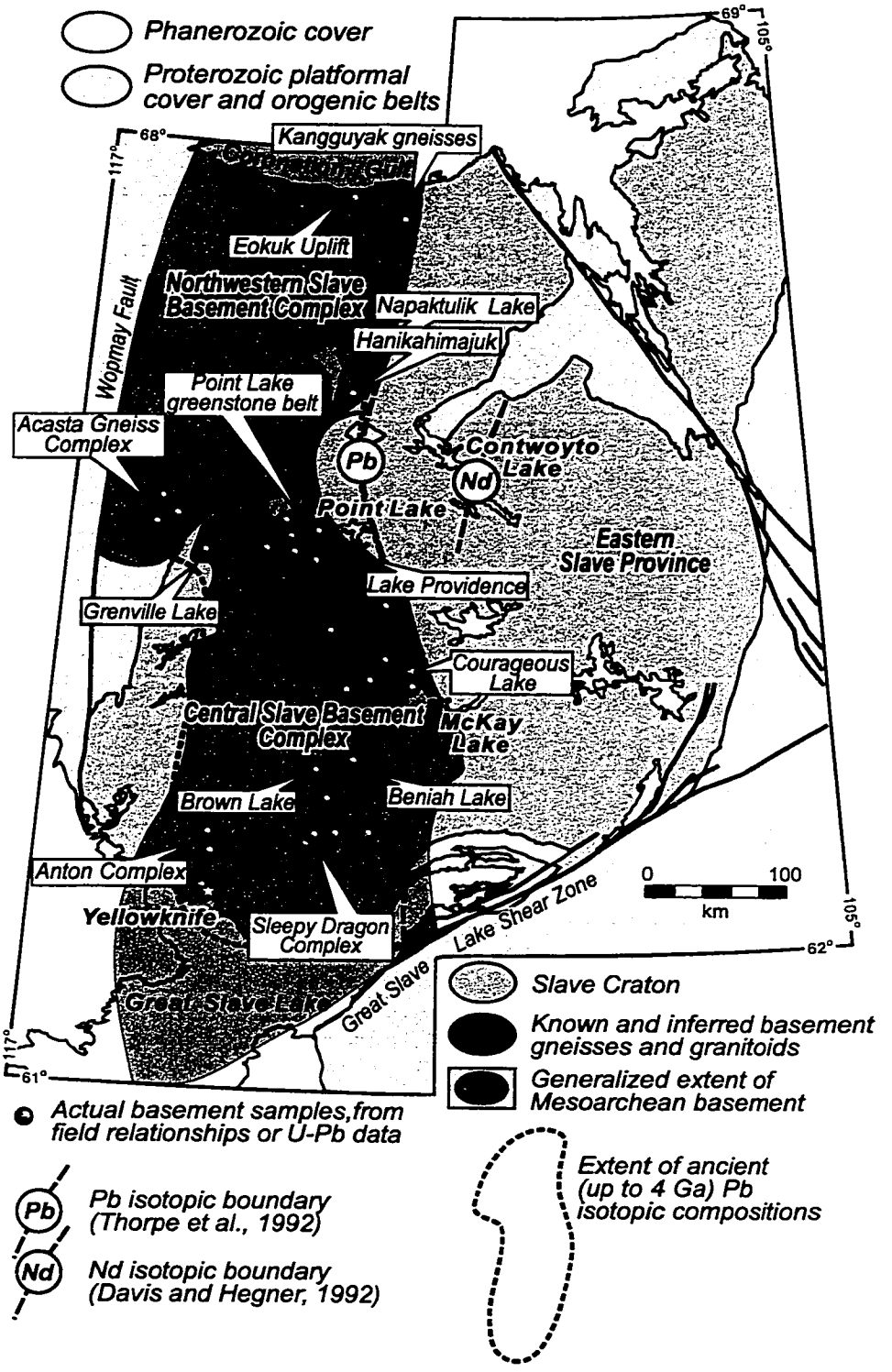

Figure 1.2. Map of the Slave Structural Province showing the division between old and juvenile basement terrains (from Bleeker & Davis, 1999).

Fig. 1.3), crossing the Yellowknife Basin, a metasedimentary basin which is bound to the west by the Yellowknife Greenstone Belt and to the east by the Cameron River Greenstone Belt (Fig. 1.3). There are also two basement gneiss complexes present in the Yellowknife Domain: the Anton Complex to the west of the Yellowknife Greenstone Belt, and the Sleepy Dragon Complex, which lies Between the Cameron River and Beaulieu River Greenstone Belts. The entire area has been affected by syn- and post-volcanic plutonism.

Description of the SSP will be taken from the work of Henderson (1985) and Lambert (1988), unless otherwise stated. The discussion of the geology will be brief and will only include those units that are crossed by the gravity profiles. This will be followed by a treatment of the structural geology and the tectonic hypotheses that have been proposed.

1.22 Central Slave Basement Complex

The Archean basement underlying much of the western SSP has been designated the Central Slave Basement Complex (CSBC) by Bleeker and Ketchum (1998). The age range of the basement rocks is > 4.0 - 2.8 Ga.

The SDC is a basement cored anticlinorium (discussed further in the section on structural geology). The gneisses are heterogeneous, and in some places are migmatitic, granodioritic to dioritic to tonalitic gneisses with a well defined foliation. In the south the foliation trends to the northwest and in the north the foliation swings around to a northeast trend. These gneisses have been dated at 3.0-2.8 Ga (van Breemen et al., 1992; Isachsen and Bowring, 1994; Bleeker et al., 1997). They have not been formally subdivided.

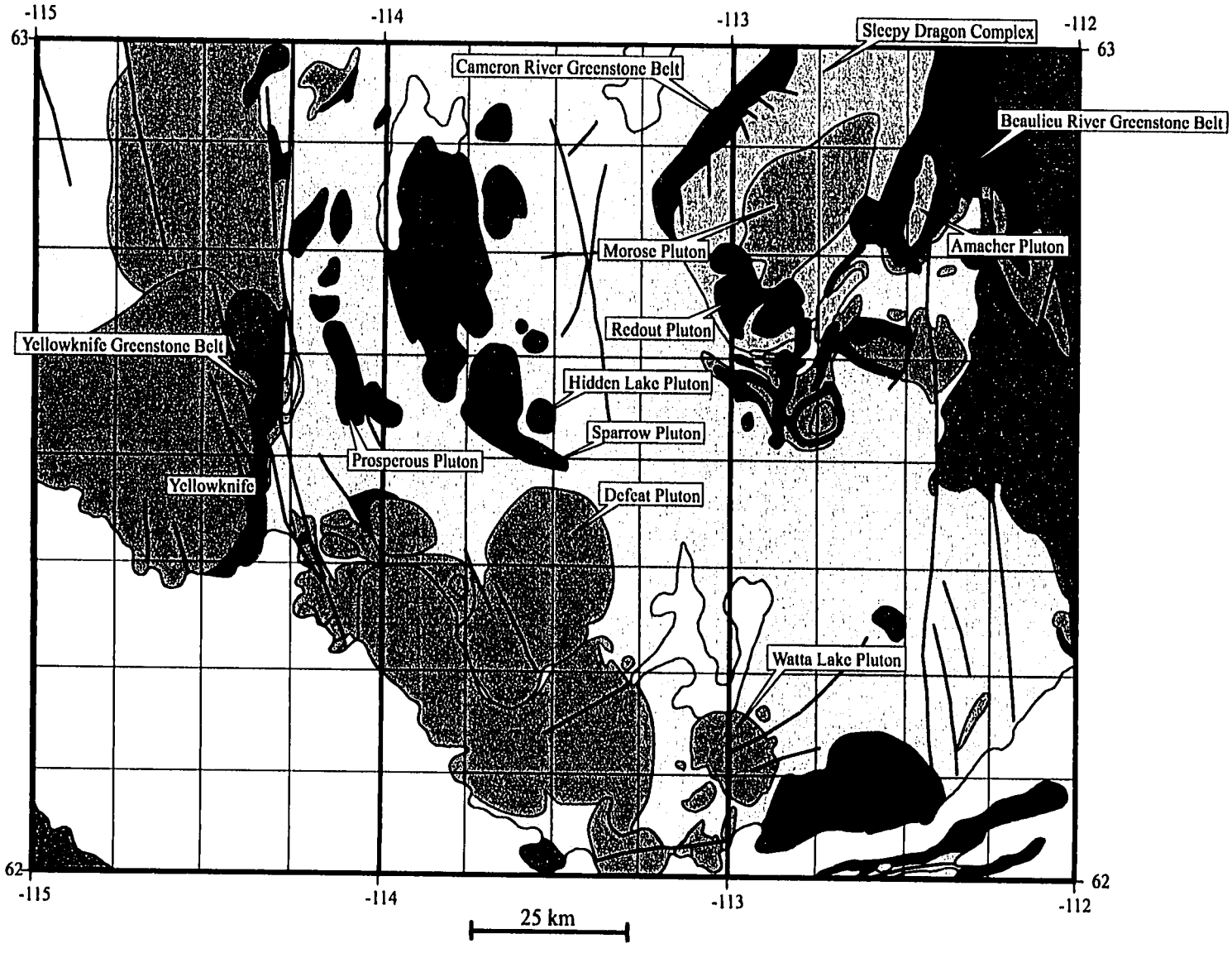

Figure 1.3. The geology of the Yellowknife Domain (from Hoffman and Hall, 1993). The main units are labelled.

Legend

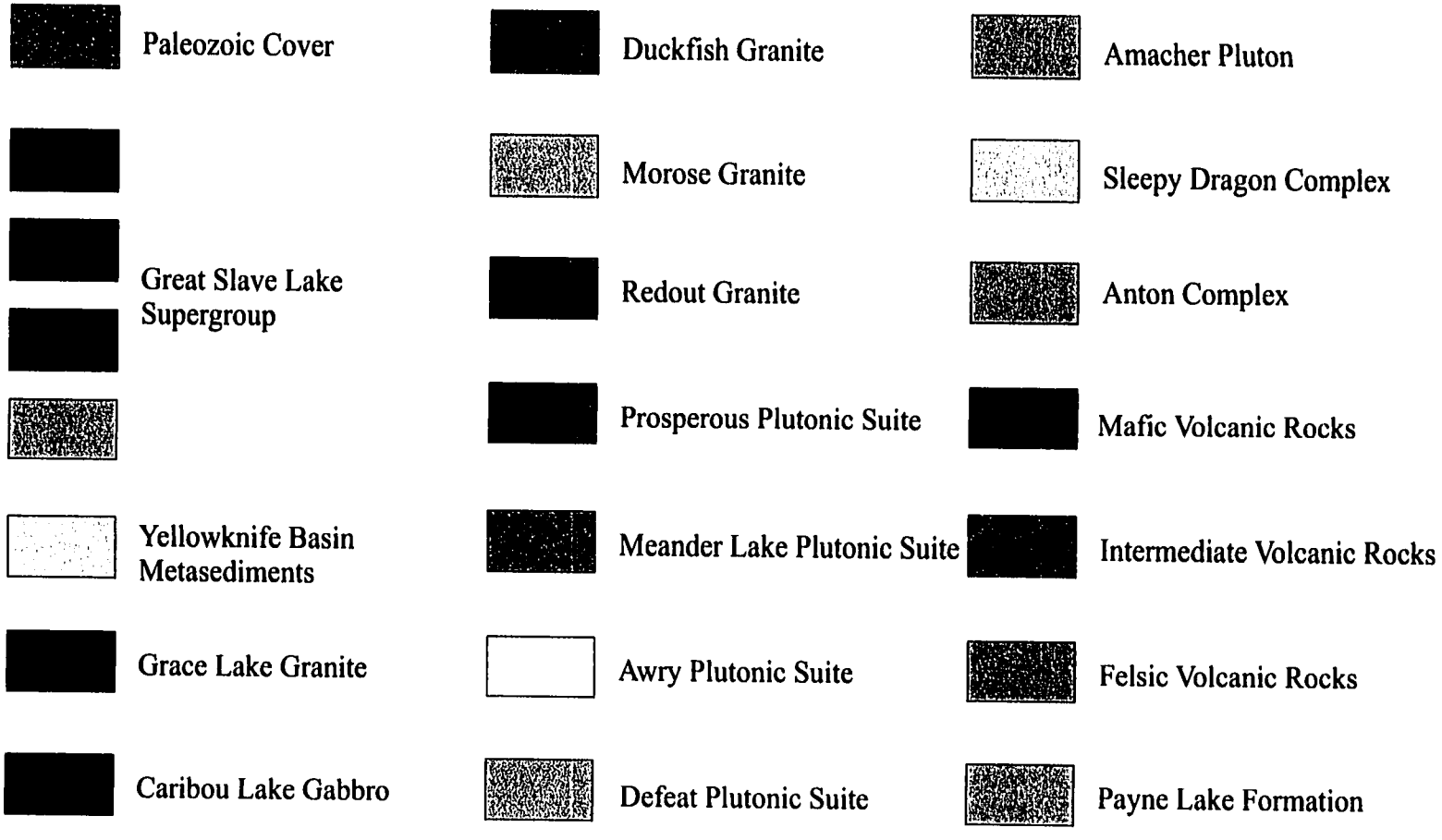

Continuation of Figure 1.3.

1.23 Central Slave Cover Group (CSCG)

The CSCG (Bleeker and Ketchum, 1998) can be identified throughout the western SSP, associated with the greenstone belt-basement contact (the unit is too thin to be identified in Fig. 1.3). It consists of a basal unit of mafic or ultramafic volcanic rocks overlain by conglomerates, immature quartz-rich grits, chromite-bearing fuschitic quartzites, and silicate or oxide banded iron formation. This sequence is evidence of a shelf setting.

1.24 Greenstone Belts

The Yellowknife Greenstone Belt (Helmstaedt and Padgham, 1986; Isachsen and Bowring, 1997) lies to the west of the Yellowknife basin (Fig.1.3). It is a north-trending, east-facing, steeply dipping homoclinal succession, which is approximately 5 km wide and 52 km long. The belt formed ca. 2.72-2.66 Ga. The Kam Group, from the base of the greenstone belt up, includes: the Chan Formation, composed of massive and pillowed basalts with gabbroic bodies and sheeted mafic dykes; the Crestaurium Formation, which includes massive and pillowed mafic flows and numerous laterally continuous cherts and felsic tuffs; the Townsite Formation, comprises two lenticles of felsic flows which are interbedded with rhyodacite breccias, tuffs, welded tuffs, and pillowed dacites; the Yellowknife Bay Formation is composed of massive and pillowed flows and flow breccia, with lenticular flows abundant at the base of the formation. The Banting Group includes: the Ingraham Formation, composed of the Shot Lake Member, which consists of sheared quartz-monzonite that grades into quartz-feldspar and is overlain by mafic lavas, breccia, felsic fragmental flows, and

bedded tuffs, and the Grayling Member, which consists of medium to course-grained quartz-feldspar porphyry; the Prosperous Formation, composed of massive to bedded felsic tuffs with interbedded mafic flows and tuffs, turbidites and conglomerates; the Duck Formation, which contains mafic to intermediate volcanic rocks, with individual flows of mattress-shaped pillows separated by thin zones of pillow breccia, and is located on the eastern side of Yellowknife Bay. The Duncan Lake Group includes the Burwash Formation, composed largely of turbidites (discussed in more detail below) and the Walsh Formation, which is a lateral equivalent of the Burwash Formation.

The Cameron River Greenstone Belt (Fig. 1.3) bounds the Yellowknife basin to the east. It comprises 85% basalt (Cameron River Basalt) at the base of the belt, which is composed of a series of flows containing pillowed and massive lavas and pillow breccias of amphibolite; 10% andesite (Webb Lake Andesite) which is composed of pillowed lavas and pillow breccias of andesite and basaltic andesite; 3% rhyolite to dacite domes, which are found in three separate domes; and 2% represented by the Dome Lake Basalt, a bell shaped body of amphibolite which is defined by alternating units of pillowed lavas and volcaniclastic units in the lower half and massive to crudely layered lavas topped by pillowed flows in the upper half. The package forms a north-trending, upright to steeply-dipping, west-facing homocline, 95 km in length and is metamorphosed to amphibolite facies (defined by the cordierite isograd). Its contact with the underlying Sleepy Dragon Complex is highly sheared and it is in conformable contact with the Burwash Formation.

On the eastern side of the SDC lies the Beaulieu River Greenstone Belt (Fig. 1.3), a

north-trending, upright to steeply-dipping, east-facing homoclinal succession. It includes the Sunset Lake Basalt, the Alice Formation, the Payne Lake Formation, rhyolite, and ultramafic rocks. It is largely of amphibolite grade, except for a 4 km wide north-northwest trending zone that follows the valley of Sunset Lake. The Sunset Lake Basalt comprises 70% of the greenstone belt and is the oldest member of the formation. Primary structures within the basalts are dominantly pillows and pillow breccia with minor amounts of layered volcanics and massive lavas which have been tectonically flattened and sheared. The contact between the basalts and the SDC on the western side of the belt is intensely sheared. The Alice Formation lies in a northerly trending belt that is centred on Sunset Lake. It overlies the Sunset Lake Basalt conformably and interfingers with it and rhyolites at the south end of Sunset Lake. The formation includes two members, one andesitic and one dacitic. The Payne Lake Formation forms the southeastern arm of the volcanic belt and is a complex succession of volcaniclastic sediments. These sediments consist of dominantly layered schists and gneisses and is divided into three main lithologies: 1) amphibole-rich schists, which are derived from mafic volcanics, 2) biotite-muscovite-quartz-feldspar schists, which are derived from felsic volcanics, and 3) quartz feldspar schists, which are interpreted as metarhyolite or detritus derived from rhyolites. There are also intravolcanic sediments which are similar to the Burwash sediments.

1.25 Burwash Formation

The Burwash Formation underlies much of the Yellowknife Basin (Fig. 1.3). It is

largely composed of graywacke-mudstone layered pairs, interbedded with each other. These rocks are turbiditic and often preserve internal sedimentary structures. They are composed largely of quartz, along with rock fragments and feldspar, which indicate a mixed felsic volcanic and granitic provenance (McGlynn and Henderson, 1972). Conglomerates occur occasionally at the contact between the metasediments and the greenstone belts, and are interpreted as possible conglomerate on the flanks of volcanic piles; otherwise this contact seems conformable.

This sedimentary package has been metamorphosed and highly deformed. Due to the intense deformation, the thickness of the formation is not known, but has been estimated at 300-600 m to 4500 m (McGlynn and Henderson, 1972). The formation is metamorphosed to greenschist facies and amphibolite facies. The amphibolite facies isograd tends to follow the contacts and trends of the major plutonic suites in the area (Prosperous, Defeat, and Blachford Lake Suites) and directly related to the effects of the intrusion themselves, but has been attributed to the heat from the event which generated the plutons (Henderson, 1985). The rocks of amphibolite grade are schistose and include various mineral assemblages of quartz-plagioclase-biotite-muscovite-cordierite-andalusite-sillimanite-staurolite-garnet. The rocks of greenschist grade are largely the interbedded graywacke-mudstone layers, with some siltstone. There is cleavage developed throughout the Burwash Formation; this will be discussed in Section 1.28, Structural Geology.

1.26 Plutonism

The Amacher Pluton (Fig. 1.3) is a northerly-trending pluton located in the Beaulieu River Greenstone Belt. It cores an antiform which is part of a synform-antiform pair within the greenstone belt. It is a biotite granite and leucogranite, approximately 15 km long and 3 km wide. It is medium- to coarse-grained, massive, and consists of 15-45% quartz. The pluton is in sharp intrusive contact with the surrounding mafic volcanics and in its northern part it includes large blocks of these rocks. It has a fine grained margin that is approximately 100 m wide and shows none of the penetrative deformation that is evident in the volcanics. Its texture is variable, from massive to porphyritic, and was emplaced into a shallow environment. There is no reliable age data on the Amacher Granite, but due to observed field relationships (high discordance with surrounding rocks and high metamorphic grade despite shallow emplacement) it has been recognized as synvolcanic and one of the oldest plutons in the area.

There are two plutonic suites that intrude the Burwash Formation: the Prosperous Granites and the Defeat Plutonic Suite (Fig. 1.3). The bulk of the Prosperous Granite lies northeast of Yellowknife and forms multiple plutons of biotite-muscovite granodiorite and granite. The fabric of these plutons is parallel with the D_2 deformation in the surrounding Burwash Formation. They are white to buff to light pink, homogeneous, and medium- to coarse-grained. The plutons critical to the gravity modelling in this study are the Sparrow Pluton and the Hidden Lake Pluton. The Prosperous Granite has been dated at 2596±2 Ma (Bleeker and Davis, 1999).

The plutonic complexes of the Defeat Plutonic Suite lie to the east and west of Yellowknife. This study focuses on the complex to the east of Yellowknife, which lies between the Ingraham Trail and the north shore of Great Slave Lake. It has been dated at 2628 +7/-20 Ma (Bleeker and Davis, 1999). It is composed largely of tonalite, trondjhemite, and granodiorite, containing plagioclase and biotite, and the plutons are generally massive, homogeneous, medium-grained, and equigranular. The contacts with the supracrustal rocks are generally concordant. Gravity profiles in the present study cross the Defeat Lake Pluton, the Watta Lake Pluton, and the small pluton which underlies the large island in upper Watta Lake as well as part of its north shore.

There are two large plutons which intrude the SDC: the Redout Granite and the Morose Pluton (Fig 1.3). Both of these are crossed by gravity profiles modelled in this study. The Redout Granite forms five irregular bodies in the extreme south of the SDC. It is massive to irregularly foliated and is a fine- to medium-grained, equigranular, heterogeneous, biotite-muscovite granite. It is generally pink to pinkish-gray. Pegmatites are commonly associated with it and contacts with surrounding units, while intrusive, are diffuse. While the geochronological data are not entirely clear, the age of the Redout Granite can probably be bracketed between approximately 2515-2440 Ma.

The Morose Pluton (Fig. 1.3) is a large, coarse-grained, heterogeneous, megacrystic quartz monzonite. It is generally white and contains potassium feldspar megacrysts. It has been dated at 2586±2 Ma (Davis and Bleeker, in press) and is one of the youngest plutons in the area. This granite forms the core of the SDC.

1.27 Structural Geology

The SSP is structurally complex. Fyson (1982) contends that the southern SSP has undergone four generations of deformation, which he further divides into subgenerations, a highly complex picture. Bleeker and Beaumont-Smith (1995), disagree with this, and argue that the western SSP has undergone three generations of deformation, the first two accompanied by major crustal scale folding and the D_3 showing a strong S_3 cleavage, but with no associated folding found to date. F_1-F_2 fold interference structures can be found throughout the western SSP, and the Sleepy Dragon Complex is an example of such a structure, forming a classic "mushroom fold" or Type 2 fold interference pattern. These three generations of deformation are identifiable throughout the Burwash Formation metasediments, but are not as readily defined in the volcanic sequences that border them.

In addition to the folding and cleavage formation there are numerous shear zones throughout the western SSP, namely those at the basement-cover contact. There are also late structures, including locally-developed small kinks and brittle fault sets.

The following description of the structural history of the western SSP is taken from Bleeker and Beaumont-Smith (1995) unless otherwise stated.

D_1 deformation is characterized by a series of high amplitude, upright, open to tight chevron folds. These F_1 folds have doubly plunging axes and are the dominant fold pattern in the area. F_1 fold hinges are often associated with quartz saddle reefs and en échelon vein arrays.

Within the Burwash Formation there is a well developed slaty cleavage that parallels

the F_1 fold axes. It is identifiable on a local scale, in areas of low grade metamorphism. In addition, many primary sedimentary features are flattened parallel to S1.

Unlike the Burwash Formation metasediments, the volcanic belts do not show the same intensity of folding internally. Generally, the internal deformation is manifested in the form of foliations and lineations (Lambert, 1988). The flattening of pillows also attests to the deformation. While the Yellowknife and Cameron River Greenstone Belts are homoclinal successions, the Beaulieu River Greenstone Belt contains an anticline-syncline pair. The anticline is cored by the Amacher Pluton. There are marker units within the greenstone belts that do record the deformation events, such as the CSCG described above.

The F_1 folds were formed under low-grade metamorphic conditions, and the formation of these folds predates all post-volcanic granitoid intrusions. They postdate the deposition of the Burwash Formation turbidites and the gabbroic sill complexes which intrude the Burwash Formation. The age of the folding has been estimated at approximately 2640-2630 Ma.

F_2 folds are steeply plunging. Their axial trace parallels the intersection lineation between the S_2 axial planar cleavage and the F_1 folds. The S_2 cleavage is subvertical and trends northwest-southeast. The F_2 folds and S_2 cleavage overprint felsic porphyry dykes which are the earliest signs of the Defeat Suite plutonism. However, the plutons themselves show a weak S_2 foliation, if any. This suggests that the D_2 event occurred during the initial stages of Defeat Suite plutons, but did not outlast it. The age of the D_2 event is 2620-2600 Ma. Also associated with D_2 are discrete shear zones which pervade the area.

Evidence for D_3 deformation exists in the form of a generally subvertical, northeast-southwest-trending S_3 foliation. This foliation is defined by a crenulation cleavage and it locally overprints the regional S_2 foliation. Bleeker and Beaumont-Smith (1995) speculate that the S_3 foliation may be related to an F_3 generation of folds that refolds F_2 and S_2 about a suvertical axis. No mesoscopic F_3 folds have been identified, but there may be macroscopic F_3 responsible for the S_3 foliation.

The basement-cover contact was interpreted by Kusky (1988, 1990) as a high strain thrust zone along which oceanic crust was thrust onto continental crust from southeast to northwest, indicating that the supracrustal rocks are allochthonous with respect to the basement. However, later work (Bleeker and Ketchum, 1998) suggests that the supracrustal rocks moved toward the southwest, over the CSBC and its cover, dated at between 2734 Ma and 2687 Ma (Bleeker and Davis, 1999). Since, as discussed above, mafic dykes, although not directly traceable across the basement-cover contact, have been identified as feeders to the volcanics, the supracrustal sequence is parautochthonous (it has moved with respect to, but is still overlying its original basement rock). The contact zone is anywhere from one to several kilometres in width. It contains basement rocks which vary from strongly foliated to protomylonites or gneisses to well developed mylonites. Transposed mafic dykes can be seen. Stretching lineations pitch 20°-65°. This contact is a regional-scale décollement, with movement northeast to southwest and a minimum displacement of >10 km is estimated (Bleeker and Ketchum, 1998).

1.29 Tectonic Models

While most workers have generally come to agree on the structure and geology of the western SSP, and the SSP as a whole, the interpretation of these observations has been diverse. A period of intense deformational events in the Archean has distorted the tectonic picture. One of the fundamental problems is defining the original relationship between the basement and its cover sequence.

Initial models proposed for the development of the western SSP suggested an ensialic rift model (McGlynn and Henderson; 1970 and Henderson, 1985). In such a model, rifting of the thinner sialic Archean crust occurred, volcanism occurring along the normal faults of the rifted basin(s). These rifts grew large enough to allow deep water deposition of sediments. This model implies that the area is underlain by a single basement block.

In contrast to this, some workers suggested that the greenstone belts were remnants of oceanic crust which have been obducted onto continental crust (Kusky, 1990, Helmstaedt et al., 1986, and MacLachlan and Helmstaedt, 1995). Kusky bases his conclusions on observations of the Cameron River and Beaulieu River Greenstone Belts, while Helmstaedt et al. and MacLachlan and Helmstaedt based theirs on a study of the Yellowknife Greenstone Belt. In general, the process started with early rifting of a continental margin, followed by the formation of oceanic crust, possibly in a back arc setting. This marginal ocean basin then closed to result in the thrusting of oceanic crust onto the continental crust. Kusky stresses that the greenstone belts may not belong to the same unit and that the area may be a tectonic collage of slivers of ocean floor.

More recently Bleeker and Ketchum (1998) proposed, like Kusky, that the western SSP is underlain by one older basement terrain. However, in contrast to Kusky's allochthonous supracrustal sequence, they suggest the sequence is parautochthonous, and that movement along the basement cover contact was the result of large-scale, regional folding. This conclusion is based on observations of a cover unit, the Central Slave Cover Group described above, associated with the basement-cover contact in various areas throughout the western SSP. The presence of a single, older basement terrain is also supported by Pb isotopic data (Thorpe et al., 1992) and Nd isotopic data (Davis and Henger, 1991). Thus, the rift model is still valid, but the rifting never reached the ocean floor-forming stage. Bleeker and Ketchum (1998) suggest that greenstones everywhere underlie the metasediments of the Burwash Formation, on the evidence of observed marker horizons associated with the basement-cover contact throughout the western SSP. This implies that all the greenstone belts belong to a single unit.

1.3 The Western Churchill Structural Province

1.31 Introduction

The Archean and Early Proterozoic Churchill Structural Province (CSP) lies in the western portion of the Canadian Shield, bounded by Hudson Bay and the Superior Structural Province to the east and south and the Slave Structural Province and the Cordillera to the north and west (eastern portion of Fig. 0.2). The western half of the CSP lies beneath Paleozoic cover. For the purposes of the second part of this study, the reconstruction of the

Great Slave Lake Shear Zone, interest lies in six of the geological units in the northwestern CSP. Listed chronologically, oldest to youngest, they are the Nova Terrane, the Buffalo Head Terrane, the Chinchaga Low, the Ksituan High (Magamatic Arc), the Taltson Magmatic Arc, and the Thelon Magmatic Arc. These terranes border the GSLSZ, as do the SSP and the Wopmay Orogen that are discussed above, (Fig. 1.4) and some are only recognized by their magnetic signature on the regional aeromagnetic map (Fig. 1.5) and by drill core data. Trends given refer to the general trends of the units away from the GSLSZ; close to the shear zone the units are transposed into a northeasterly trend. Each unit will be discussed in the order given above and their locations can be found in Fig. 1.4. The reader is referred to Ross et al. (1990) and Villeneuve et al. (1993), for much of the geology and geochronology of the region. The following discussion will be based on their work unless otherwise referenced.

1.32 The Nova Terrane

The Nova Terrane lies furthest to the west, against the eastern extent of the Cordilleran deformation. It is defined by a north-trending aeromagnetic high which is bound to the northwest by the GSLSZ and to the east it is separated from the Ksituan High by a narrow aeromagnetic low, which has been interpreted as a fault. This low merges with the Kiskatinaw Low. It lies beneath the Paleozoic cover and, thus, all information has been obtained through geophysical data and drill core samples. The extent of the Nova Terrane to the southwest is unknown.

From this unit, three drill cores have been examined. Two samples are rhyolites, one

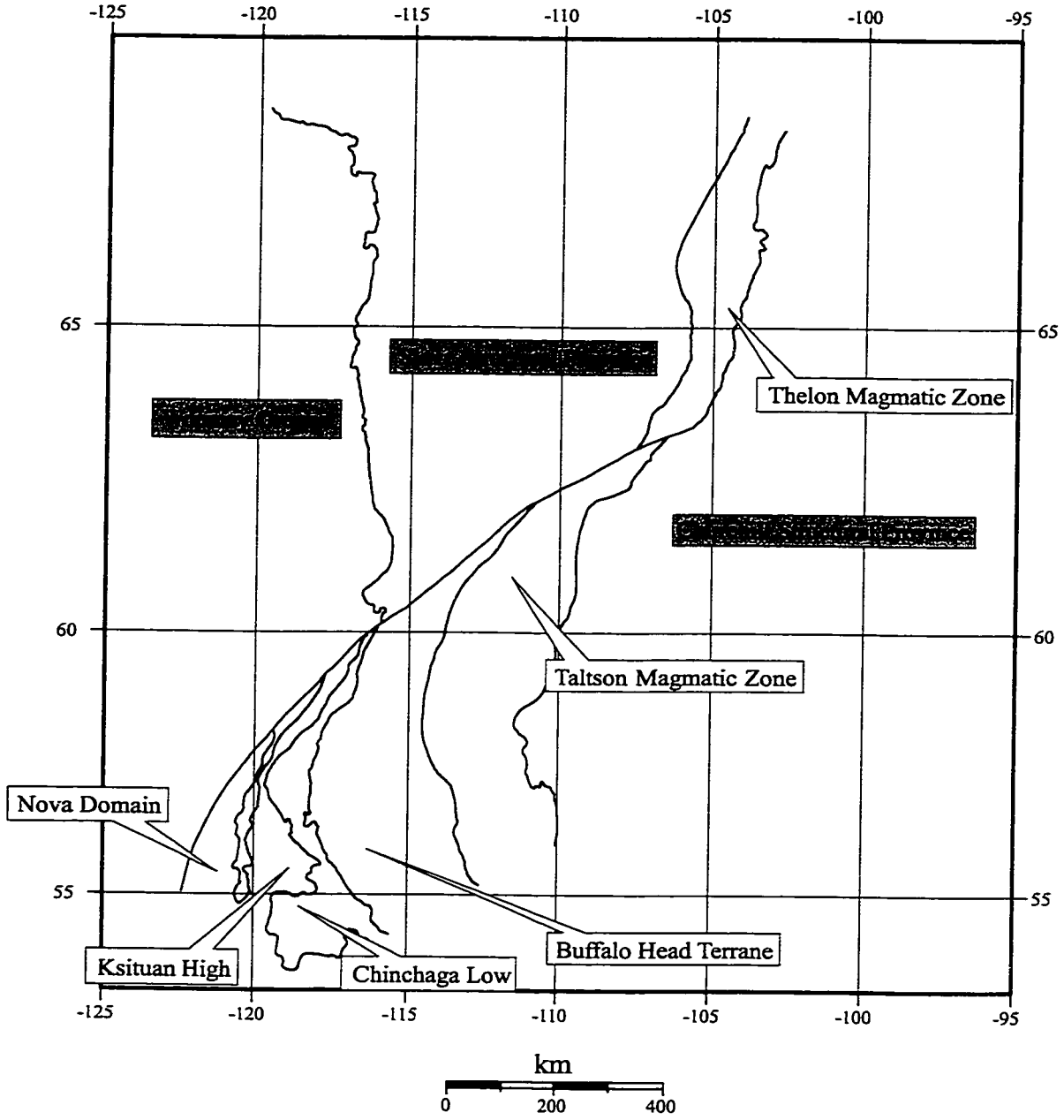

Figure 1.4. A map showing the boundaries of those terranes that border the Great Slave Lake Shear Zone (modified from Villeneuve et al, 1993).

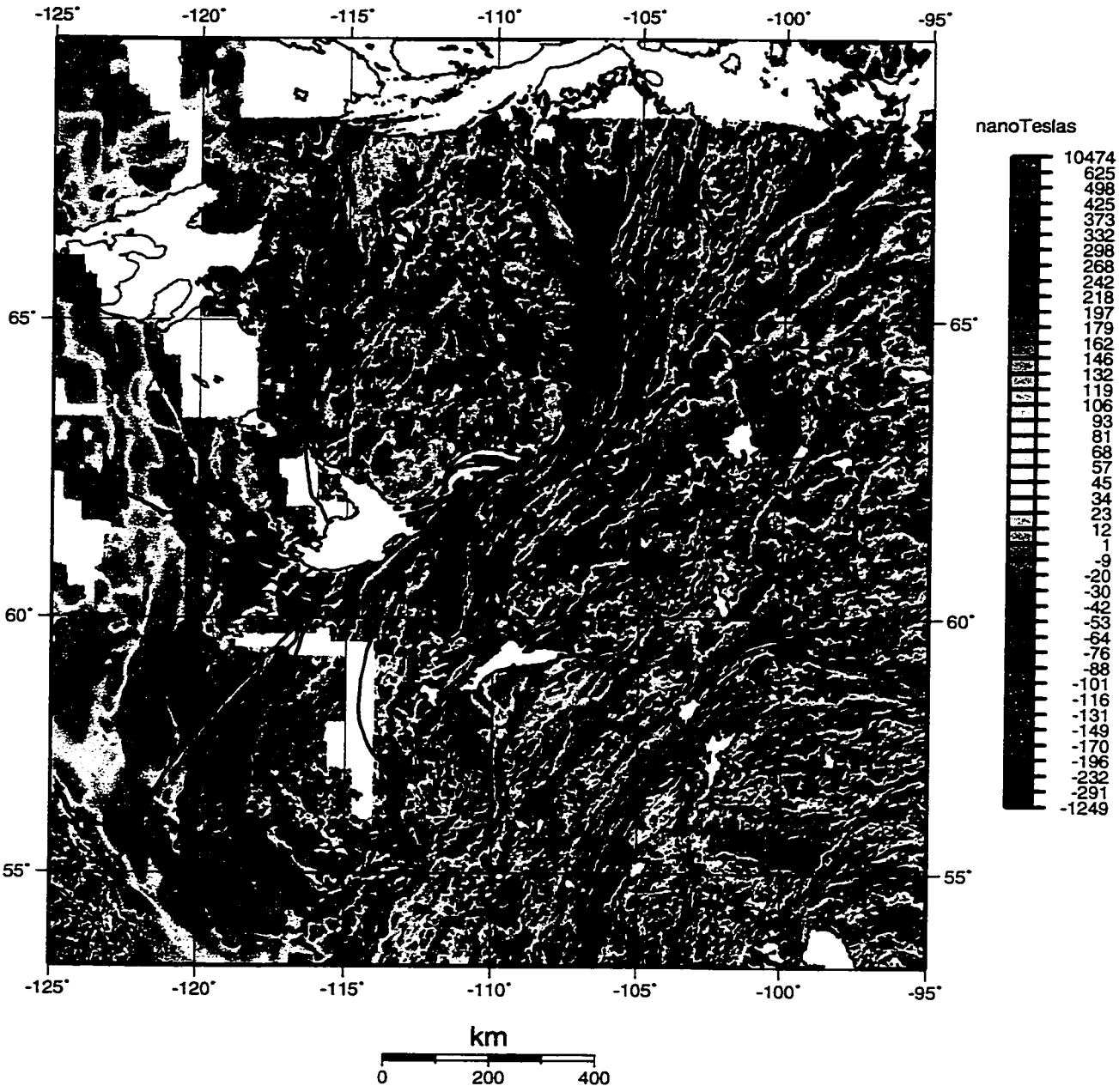

Figure 1.5. The terrane boundaries shown superimposed on the regional aeromagnetic map. The distinct nature of the terranes' magnetic signature is obvious.

of which may be a metasediment. The metasedimentary core gave inconclusive age data. The other rhyolite sample, a foliated, quartz-rich rock, was dated at ~1.99 Ga. The third sample is a 2.8 Ga mylonitic, melanocratic gneiss, which is composed of red feldspar and quartz grains set in a biotite-chlorite-rich ground mass. Thus, at least part of the Nova Terrane is clearly Archean.

1.33 The Buffalo Head Terrane

This north-trending unit shows up as a broad, moderately positive region on the aeromagnetic map, which defines an arcuate domain, with concavity to the east. It is bounded to the northwest by the GSLSZ, to the west by the Chinchaga Low, to the east by the Taltson Magmatic Arc, and to the south against the Wabamun High by a splay of the Snowbird Tectonic Zone.

Based on the aeromagnetic signature, the Buffalo Head Terrane can possibly be divided into three subdomains: the Buffalo Head High, a region of positive aeromagnetic ridges with separating negative ridges, the Utikuma Belt, an area characterized by weaker positive anomalies, and a region of low aeromagnetic signature to the southwest where geochronology suggests older (2.3 Ga) metaplutonic rocks. Felsic to intermediate metaplutonic rock types dominate the Buffalo Head Terrane, but felsic metavolcanic rocks and high-grade gneisses are also present. Ages range from 2.32-2.0 Ga.

1.34 The Chinchaga Low

This is recognized as a prominent, curvilinear low on the regional aeromagnetic map, with concavity to the east. It is bounded to the east by the Buffalo Head Terrane, to the north and northwest by the Ksituan High, and to the south against the Wabamun High by a fault splay of the Snowbird Tectonic Zone. A small portion of the Chinchaga Low borders the GSLSZ to the north. Drill cores from the basement of the Chinchaga Low indicates it is composed of metaplutonic and metasedimentary gneisses that range in age from 2.17-2.08 Ga.

1.35 The Ksituan High

The Ksituan High shows as a prominent, curvilinear high on the regional aeromagnetic map, with concavity to the east. It is bound to the east by the Chinchaga Low and to the west by the Kiskatinaw Low (not described here). A small portion to the north borders the GSLSZ. It is a magmatic arc that is characterized by hornblende-bearing metaplutonic rocks, ranging in age from 1.99-1.90 Ga.

1.36 The Taltson Magmatic Zone

The northeastern end of the Taltson Magmatic Arc is exposed. Here it trends to the northeast, along the GSLSZ, and in the southwest it swings abruptly to a north-south trend, most of which lies below Paleozoic cover. Part of its exposed section has been mapped (Bostock, 1987). All dating has been done by Bostock et al. (1987) and the age has been

bracketed between 2.0 Ga and 1.9 Ga. The oldest rocks, based on intrusive relationships, are metasediments and metavolcanics. The metasediments are largely semipelitic and pelitic gneisses and much of the area is metamorphosed to amphibolite-lower granulite grade, with sillimanite-cordierite-K feldspar assemblages present. There are also local bands of calc-silicate and quartz-rich beds. These have not been dated, but are assumed to be Archean. Both sinistral and dextral kinematic indicators have been found.

The Taltson Magmatic Arc can be traced southward, beneath the Paleozoic cover, on the bases of drill core samples and aeromagnetic anomalies. The ages and rock types correlate with those exposed to the north. The eastern boundary of the arc on the aeromagnetic map is sharp, with discordance of magnetic fabric between it and the Rae Terrane to the east, indicating a structural boundary. To the west, it is bordered by the Buffalo Head Terrane.

1.37 The Thelon Magmatic Arc

The Thelon Magmatic Arc, which lies to the north of the Great Slave Lake Shear Zone, is the northern equivalent of the Taltson Magmatic Zone. The age of magmatic events in the Thelon Magmatic zone, as in the Taltson, has been bracketed between 2.0 and 1.9 Ga. It is bound to the west by the Slave Structural Province and to the east by the basement gneisses of the Western Churchill Province. Its contact with the SSP is complex and somewhat diffuse (Thompson et al., 1986 and Culshaw, 1990). Culshaw (1990) describes it as comprising three zones: the Archean foreland of the Slave Craton, the craton-edge, which

lies further east and is the part of the Slave Craton that was remobilized in the Proterozoic, and the Proterozoic granulites and granites of the Thelon Magmatic Zone.

A wide assortment of granitoid gneisses make up the Thelon Magmatic Arc. Pink and gray granitoid gneisses and migmatites and orthopyroxene-bearing gneisses have been described, both in the north (Thompson et al., 1986) and in the south (the Darrell River gneiss of James, 1986). This is a similar lithology to the Taltson Magmatic rocks described above. In addition, there are rusty quartzofeldspathic gneisses, coarse augen gneisses, mafic gneisses, foliated leucogranites and diatexites that grade into migmatites. This zone of rocks trends north-northeast and has a strong foliation, with the same trend, that dips moderately to steeply to the east. To the north, granulite grade metamorphism predominates, but to the south it becomes increasingly more amphibolitic in grade, though the core of the zone remains at granulite grade.

1.38 Tectonic Models

The Nova Terrane lies furthest to the west, completely under the Paleozoic cover. Because of this and its unknown extent, the nature of the Nova Terrane is ambiguous. It is probably an accreted terrane and is thought by some workers to be a possible southwestward extension of the Slave Craton (Ross et al., 1990 and Villeneuve et al., 1993).

The Buffalo Head Terrane is considered to be a terrane that was accreted to the Rae Province of the Western CSP (Villeneuve et al., 1993). The association of the Buffalo Head Terrane and the Chinchaga Low is unclear, but they overlap in time. The sharp aeromagnetic

gradient between the terranes suggests they may be in faulted contact. The Ksituan High is considered to be a magmatic arc, which lies to the west of the Buffalo Head Terrane and the Chinchaga Low.

The Taltson Magmatic Zone is the southern extension of the Thelon Magmatic Zone (Bostock, 1987, Bostock et al., 1987, Hoffman, 1987, and Hanmer et al., 1992). This correlation is based on the geological, geochronological, and geophysical data and Hanmer et al. (1992) have traced it across the contemporaneous Great Slave Lake Shear Zone. The entire magmatic arc is the result of the eastward subduction of the SSP beneath the Western CSP, between 2.0 Ga and 1.9 Ga. This event will be discussed in more detail in the section on the Great Slave Lake Shear Zone.

1.4 The Great Slave Lake Shear Zone

1.41 Introduction

The Great Slave Lake Shear Zone (GSLSZ) is a vertical, northeast-trending, transcurrent, crustal scale shear zone with dextral displacement which was active ca. 2.0-1.9 Ga (Hanmer and Lucas, 1985 and Hanmer, 1988). The age has been determined by dating the protolith and from field relationships (Hanmer et al., 1992). It is the result of the convergence and collision between the Slave Structural Province (SSP) and the Western Churchill Province (WCP). Approximately 1300 km in length and 25 km at its widest, the GSLSZ stretches from the foothills of the Rocky Mountains to the eastern edge of the Thelon magmatic zone. Along much of its length, it lies under Paleozoic Cover and has been

inferred from its strong presence on the regional aeromagnetic map as a sharp truncation of units to the north and south of it and the clockwise deflection of the major north-south trend of the regional magnetic fabric (see Fig. 1.5). It has accommodated up to 700 km of displacement, determined by restoring displacement of units using the aeromagnetic map (Hoffman, 1987).

1.42 Geology

The GSLSZ, in the area of MacDonald and Laloche Lakes southeast of the east arm of Great Slave Lake, can be divided into 5 mylonitic belts (Fig. 1.6), each of a different age and metamorphic grade (Hanmer, 1988). The first three belts can be recognized by the mineral assemblages they preserve: granulite facies and upper amphibolite facies. The other two belts, the Laloche River and Hornsby Channel ultramylonite belts, are in the greenschist facies. The protolith to the mylonites is the Laloche Batholith.

The Laloche Batholith is a megacrystic, leucocratic biotite-hornblende granite to tonalite. The northwestern boundary of the batholith is marked by the chlorite-bearing mylonite zone of the GSLSZ and its southeastern boundary extends from the vicinity of Thubin Lakes to near Laloche Lakes. Very few individual plutons can be recognized within the batholith. The Laloche Batholith intrudes the sillimanite-cordierite-garnet granites and migmatitic paragneiss of the WCP.

Mylonite belt #1 is in the granulite facies of metamorphism. There are metapelites carrying the mineral assemblage of garnet-sillimanite-cordierite-biotite-plagioclase-K

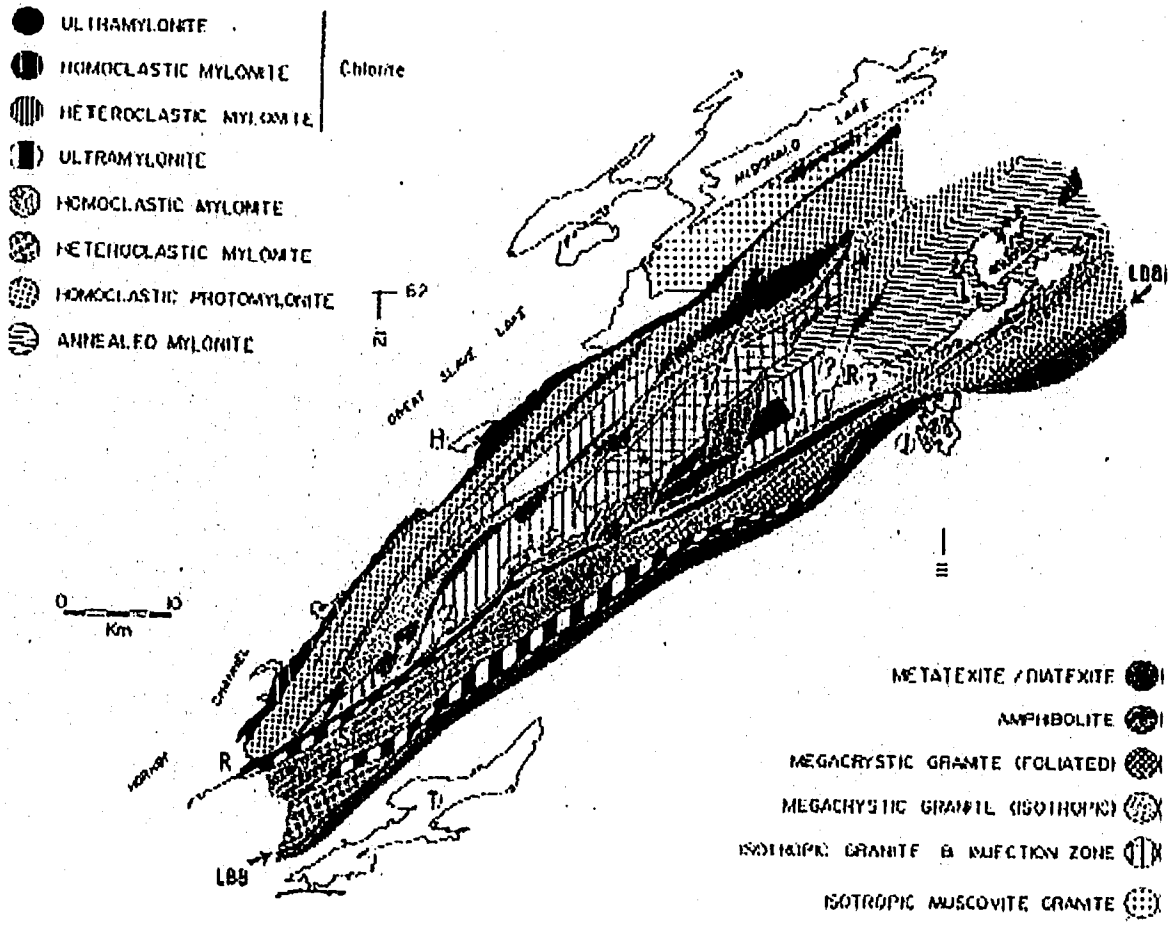

Figure 1.7. The geology of the Great Slave Lake Shear Zone (Hanmer, 1988).

feldspar-quartz in addition to melt. There are also metagranitoids and associated mylonites with the mineral assemblage garnet-orthopyroxene-biotite-plagioclase-K feldspar-quartz, and amphibolites, which are locally two pyroxene-bearing or garnetiferous. These are the most complex of the GSLSZ mylonites, both at the outcrop and map scales. These mylonites can be traced into coarse-grained protoliths.

Amphibolite facies mylonitization characterizes mylonite belts #2 and #3. The metapelites in belt #2 comprise a garnet-sillimanite-cordierite-biotite-plagioclase-K feldspar-quartz mineral assemblage. The amphibolites are locally garnetiferous. This belt is composed of homogeneous ribbon mylonites, but is compositionally banded on the decimetre scale in some places. It is up to 10 km wide and is eclipsed by finely homoclastic protomylonites with small, well rounded, well sorted feldspar porphyroclasts. Locally, these protomylonites pass into mylonites and ultramylonites.

Belt #3 metapelites contain the mineral assemblage garnet-sillimanite-white mica-biotite-plagioclase-K feldspar-quartz. This belt, with 5 km maximum width, is also composed of ribbon mylonites and is largely composed of heteroclastic and homoclastic mylonites. The northwest and southeast boundaries of the belt are each composed of a continuous ultramylonite belt, up to 2 km wide and 70 km long.

The ultramylonite belts of the greenschist facies are characterized by the mineral assemblage chlorite-white mica-albite-epidote±quartz. The belts are completely identical and are 1.0-1.5 km in width. They include monotonous, dark-green to white, fissile ultramylonite to heteroclastic mylonite with an ultrafine matrix.

All the mylonite belts are cut by a 500 m wide zone of breccias. The breccia is in turn cut by discrete, east-west-trending vertical fault planes, which have a dextral sense of motion. Cutting across both the breccia zone and the faults are pseudotachylite veins, which are also present in belt #3. Everything is then cut by quartz veins.

1.43 Structural Geology

There is a mylonitic foliation and lithologic layering that strike northeast-southwest and are vertical to steeply dipping. Throughout the GSLSZ, there is an extension lineation that is subhorizontal except for a central stretch on the northwest border of belt #3, where it tends to be steep to vertical. This indicates that the central part of the shear zone has a highly transpressive component. The extension lineation is defined by the alignment of mineral grains and quartzo-feldspathic aggregates, the presence of boudinage, and the alignment of isoclinal folds. Dextral shear is consistently indicated by shear criteria, such as rotated inclusions and porphyroclasts, shear band foliation, asymmetrical pull-aparts, C and S fabrics, rotated fold axial planes, and asymmetrical pressure shadows.

There is no preservation of metamorphic gradients within the GSLSZ, but Hanmer (1988) has demonstrated that the higher grade assemblages are older than the lower grade assemblages, as the entire mylonite belt started out at granulite facies. With a decrease in temperature the central part of the mylonite zone stiffened as the strain rate decayed and the strain was concentrated in narrower belts at lower grades. This progression of strain localization moved outward from the centre, until the greenschist facies mylonites were

formed, each belt being abandoned when conditions no longer supported ductile deformation within them.

1.44 Tectonic Model

The GSLSZ has been recognized as a transform fault (Hoffman, 1987) and later as an intra-arc transform fault (Hanmer et al., 1992). It accommodated northeast-trending, oblique subduction of the SSP beneath the Western CSP, with relative movement at a small angle to the shear zone itself. Included in this event is the convergence of the two provinces, the collision between them, and later indentation (producing the conjugate Bathurst and MacDonald Fault Zones; Henderson et al., 1990). With decreasing metamorphic grade during convergence, motion along the steeply-dipping subduction zone changed to dextral strike-slip (Culshaw, 1990 and Hanmer et al., 1992). This was followed by the collision and initiation of westward-directed thrusting along the Thelon Front (boundary between the Thelon Magmatic Zone and the SSP).

Hanmer et al. (1992) suggested an escape model, where a large block of material is squeezed out along escape faults to help accommodate the shortening related to the convergence of the two provinces. A similar model was proposed for the later indentation of the SSP into the Western CSP, coincident with the formation of the Bathurst and MacDonald Fault Zones (Gibb, 1978).

The movement along the GSLSZ produced a clockwise deflection of the aeromagnetic grain in the CSP. Note that terranes such as the Buffalo Head Terrane and the Chinchaga Low are older than the GSLSZ, but are not present north of the shear zone.

Chapter 2: Data Processing

2.1 Gravity Data

2.11 Introduction

Gravity is not uniform over the Earth's surface. It is affected by the latitude, elevation, surrounding topography, tides, and lateral density variations. In gravity exploration, the lateral density variations are important, and anomalies due to these variations are small when compared to latitude and elevation. It is for this reason the effects of latitude and elevation, as well as topographic and tidal effects, must be removed. There are a number of corrections which can be applied to gravity data in order to come up with the density anomalies due to lateral density variations. These corrections reduce gravity data to values that would have been measured on a common datum equipotential surface: the geoid or a surface parallel to it.

Regional data were collected by Geomatics Canada and the Geological Survey of Canada using LaCoste and Romberg gravimeters and Scintrex gravimeters. Various surveys were conducted over land, glaciers, lake and sea ice, and on lake and ocean bottoms, and station spacing ranged from 6-20 km. The targeted gravity data was collected at ~1 km station spacings, using the LaCoste and Romberg gravimeters.

The following discussion will define the geoid and will describe each of the data correction procedures routinely used on raw gravity data (both regional and targeted): latitude correction, free-air correction, Bouguer correction, terrain correction, Earth-tide correction, instrument drift correction, and isostatic correction. The equations discussed here

are taken from Telford et al. (1990). Equations used by the GSC and GC may not use the same terminology, but the resulting corrections are the same. The reader is referred to Telford et al. (1990) for an in depth discussion of gravity theory and data collection and processing.

2.12 The Geoid

The Earth is spheroidal in shape due to the centrifugal force, and for this reason gravitational acceleration is not uniform over the Earth's surface. The geoid is the reference spheroid that defines the mean sea level of the Earth.

2.13 Latitude Measurement

Due to the rotation of the Earth, there is an equatorial bulge and centrifugal acceleration. The equatorial bulge causes the geoid to be further away from the Earth's centre of mass at the equator than at the poles, causing gravitational acceleration to increase with increasing latitude. Centrifugal acceleration produces the same affect, reducing the affects of gravitational acceleration near the equator relative to the poles, as it is greatest at the equator and least at the poles. Thus, with increasing latitude, gravity also increases. The correction for latitude is given by the equation:

$$g_t = 978{,}031.846\ (1 + 0.005{,}278{,}895\ \sin^2\varphi + 0.000{,}023{,}426\ \sin^4\varphi)\ \text{mGal}$$

where φ is the latitude. There is no need for correction at the equator, and the correction

increases toward the poles. It is added to g as the equator is approached. The latitude must be known precisely for this correction to be accurate.

2.14 Free-air Correction

Gravitational acceleration decreases with the square of the distance from the Earth's centre of mass. The free-air correction is applied to the data to correct for the effects of elevation, bringing the data to a common datum plane (this does not take into account the effects of material between the station and the datum plane). The correction is defined by the equation:

$$\frac{\delta g_{FA}}{\delta R} = \frac{2\gamma M_e}{R_e^3} = \frac{2g}{R_e} = -0.3086 mGal/m$$

at 45°, where g is the measure of gravity, g_{FA} is the Free Air gravity, R is the radius from the Earth's centre of mass to the point of the measurement, R_e is the radius of the Earth, M_e is the mass of the Earth, and γ is the universal gravitational constant and is equal to 6.672×10^{-11}. The correction is added to the gravity reading when the station is above the datum plane and subtracted from the gravity reading when the station is below the datum plane.

2.15 Bouguer Correction

This correction takes into account the material that exists between the station and the datum plane that was ignored in the free-air correction. The correction is calculated by the

following equation:

$$\frac{\Delta g_B}{\Delta R} = 2\pi\gamma\rho = 0.04192\rho mGal / m$$

where ρ is the density of the material between the station and the datum plane, with two assumptions: 1) the rock is uniform in thickness and density and 2) it is of infinite horizontal extent. If the density is assumed to be the average crustal density, the value becomes 0.112 mGal/m.

The Bouguer correction is applied in the opposite sense than the free-air correction. The two are often combined to give an elevation correction given by:

$$\frac{\Delta g_E}{\Delta R} = \frac{\Delta g_{FA}}{\Delta R} - \frac{\Delta g_B}{\Delta R} = (0.3086 - 0.0419\rho)mGal / m$$

The elevation correction is applied in the same way as the free-air correction.

2.16 Terrain Correction

Irregularities in the terrain around the gravity station affects the gravity readings. Hills around the station tend to pull upward on the gravimeter and valleys fail to pull down on the gravimeter, both of which affect the gravity readings in the same sense. Although there are various methods for calculating the terrain correction for a given station, a detailed knowledge of the topography of the area around the station must be acquired. A common

method is to divide the area into sections and compare the elevations in each section. Routinely, the template uses concentric circles with radial lines, drawn around the station so that area of each sector increases away from the station outward. The gravity effect of one sector is calculated with the following equation:

$$\delta g_t(r,\theta) = \gamma\rho\theta\{(r_o - r_i) + (r_i^2 + \Delta z^2)^{1/2} - (r_o^2 + \Delta z^2)^{1/2}\}$$

where θ is the sector angle in radians, $\Delta z = |z_s - z_a|$, z_s is the station elevation and z_a is the average elevation in the sector, and r_o and r_i are the outer and inner radii of the sector respectively.

2.17 Earth-tide Correction

Gravimeters are sensitive enough to detect the change in gravity due to the movement of the sun and moon. These changes depend on latitude and time, and knowledge of the positions of the sun and moon are essential for the calculation, but generally, since the variation is so slow and smooth, it is included in the instrument drift correction.

2.18 Instrument Drift Correction

When setting up a gravity instrument for measurement, it must be calibrated. This calibration is done by occupying at least two stations at which the gravity values are known. If the difference in the gravity readings between the two stations is large enough to cover a reasonable fraction of the range of the gravimeter, the response between them is considered

to be linear.

At each station the gravimeter must be carefully levelled to give a stable null reading. This null reading drifts through time due to creep in the springs of the instrument (and partly due to the Earth-tide effects, see 2.17). This correction is carried out by returning to some previous stations, roughly every 3-4 hours, and re-calibrated as necessary.

2.19 Isostatic Correction

Gravity values can vary due to large-scale fluctuations in crustal thickness (eg. between oceans and continents). This is only crucial for very large gravity surveys.

2.110 Bouguer Anomalies

The Bouguer anomaly is the value obtained after all of the above corrections have been made. It is given by the equation:

$$g_B = g_{obs} - g_t + (\Delta g_L + \Delta g_{FA} - \Delta g_B - \Delta g_T)$$

where g_{obs} is the station reading, g_t is the theoretical gravity value, and the other values correspond to the corrections described above. This equation is for a station south of the reference latitude in the northern hemisphere and that is above the datum plane. If the station was below the datum plane the signs for Δg_{FA} and Δg_B would be opposite to those used above. If the value of Δg_B (and sometimes Δg_T) were to be removed from the equation, the result would be the free-air anomaly.

2.2 Aeromagnetic Data

2.21 Introduction

The Earth has a magnetic field, due largely to the convective currents of conductive material within the Earth's outer core. There is also an external magnetic field, which results from the electric currents in the upper ionosphere. Rocks on the Earth's surface have characteristic susceptibilities, dependent upon their magnetic mineral content (most importantly magnetite and pyrrhotite). This susceptibility dictates how easily the rocks can acquire an induced magnetic field. This induced field is of interest in magnetic surveys.

The regional magnetic data were acquired by the Geological Survey of Canada during a number of airborne surveys, flown at 805 m line-spacings at approximately 300 m above the Earth's surface, and is available from the GSC's Geophysical Data Centre. In the area covered by this study, the data were recorded prior to 1970 and, therefore, in analogue fashion. Data were measured with a fluxgate magnetometer. Magnetic data is not affected by the same variables as gravity data. There are a number of factors that have to be considered, such as instrument drift, the magnetic field generated by the aircraft, temporal variations in the magnetic field due to events such as sunspot activity or magnetic storms, the main magnetic field of the Earth, and variations in altitude between flight lines and different surveys. Corrections applied to the data will be described below. The reader is referred to Telford et al. (1990) for a description of magnetic theory, survey techniques, and processing and interpretation methods. For an in-depth description of the acquisition and processing of the GSC aeromagnetic data, the reader is referred to Dods et al. (1985) and Redford et al.

(1990).

2.22 Digitization

The aeromagnetic data were originally collected in analog form and were plotted on a map on which contour lines were hand-drawn. These were later digitized at the intersection of the contour lines with the flight lines. This process essentially acted as a low-pass filter, where anomalies less than the contour interval are not represented in the digitized data (Warner Miles, personal communication). The data were then converted to geographical coordinates.

2.23 Instrument Drift and the Effects of the Aircraft's Magnetic Field

Instrument drift for data collected with the Fluxgate magnetometer was significant with respect to more modern instruments. Drift rates could be as high as 10 nT/hour, and this had to be corrected for in the data.

The magnetic field of the aircraft includes the permanent magnetisation, the magnetisation induced by the motion of the aircraft through the Earth's magnetic field, and the magnetisation due to the electrical currents moving through the aircraft. These factors were generally corrected for before the survey took place. Inside the aircraft was an array of electrical coils and the electrical current was varied through each of these until the permanent magnetism of the aircraft was neutralized. The aircraft was rotated on the ground, over a fixed spot, while varying the currents, until a constant reading was obtained. The modern

method includes flying the aircraft around in a square, while performing various manoeuvres. This is done over an area of low magnetic relief. The aircraft are compensated in real time by modelling packages and the flying and manoeuvring establishes the model parameters, which are then used to neutralize any induced magnetic effects. Whatever effects are not removed from this technique are taken care of in the levelling of the data.

2.24 Removal of the Earth's Regional Magnetic Field

Removal of the Earth's regional magnetic field is important in order to isolate those anomalies which are due entirely to magnetic variations in the Earth's crust. This is done by subtracting the Earth's main magnetic field, usually taken to be the International Geomagnetic Reference Field (IGRF), a model of the secular variation in the Earth's magnetic field.

2.25 Line-to-line Levelling

In an aeromagnetic survey, control or tie lines (ties) are flown in addition to the regular survey lines in order to give duplicate readings at particular points. These lines are grouped according to flight. After a reference or principal tie is chosen, the method for levelling the data can be broken down into four components: levelling the ties, drifting the flight lines to the ties, drifting the lines individually to the ties, and drifting the ties individually to the lines. For an in-depth discussion, see Luyendyk (1997).

Line-to-line levelling removes the effects of temporal variations in the geomagnetic

field, as well as navigational error and any error that still exists due to the permanent magnetic field of the aircraft.

2.26 Survey-to-survey Levelling

Levelling of the data between surveys removes the effects of the temporal variations between surveys, as well as the variation of altitude and magnetic datum between different survey blocks. After gridding the data of each individual survey at a grid size of 812.8 m, the various survey blocks were adjusted to a common datum, determined by flying control lines, so that high frequency differences were minimized. This method may introduce a long wavelength error.

Since this time, the data for each survey have been re-gridded to an integral size of 200 m, which then had to be re-levelled. Levelling of the 200 m grid was accomplished by draping the unlevelled grid over the previous 812.8 m grid to produce a levelled grid. Then, the long wavelength levelling error, the regional effects, and the high frequency geological effects were removed. The result is the level error, which was then subtracted from the unlevelled profile data. These data were then gridded at 200m integral size, to produce a levelled grid. As each survey was digitized from analog data, there was no over-lapping of the survey areas. The levelled grid was subject to a low-pass filter and the final grid was created by gridding the levelled profile data, using the Brigg's minimum curvature algorithm.

Chapter 3: Gravity Modelling

3.1 Introduction

Gravity profiles modelled in this study cross the Yellowknife Greenstone Belt, the Prosperous and Defeat Plutonic Suites, and the Sleepy Dragon Complex, including the Cameron River and Beaulieu River Greenstone Belts and the Morose, Redout, and Amacher plutons (Fig. 3.1). Major gravity anomalies are present over the greenstone belts and over a variety of granitoid plutons of the Prosperous and Defeat Suites and the Morose Granite. Figures 3.2 and 3.3 show the profiles superimposed on the regional aeromagnetic and gravity maps respectively. In general, the gravity profiles show excellent correlation with the known geology (Bleeker et al., 1998) and help in constraining the deep structure of the area.

The geological evolution of the southern Slave Province has been under debate for many years. One of the main issues under contention is the correlation between the various greenstone belts, and the relationship between greenstones and basement rock complexes. A significant question is, do the greenstone belts extend beneath the turbidite packages? Detailed gravity modelling of the transects in the southern Slave Province help to shed new light on these issues, by providing estimates for the overall subsurface dip and depth extent of contacts between the various rock units. The modelling also provides constraints on the shape of some of the plutons, which, combined with field and magnetic fabric studies may shed new light on their emplacement history (Spark et al., 1999).

All modelling was done using the modelling program, GM-SYS, produced by Northwest Geophysical Associates, Inc.. The following discussion gives the results of the

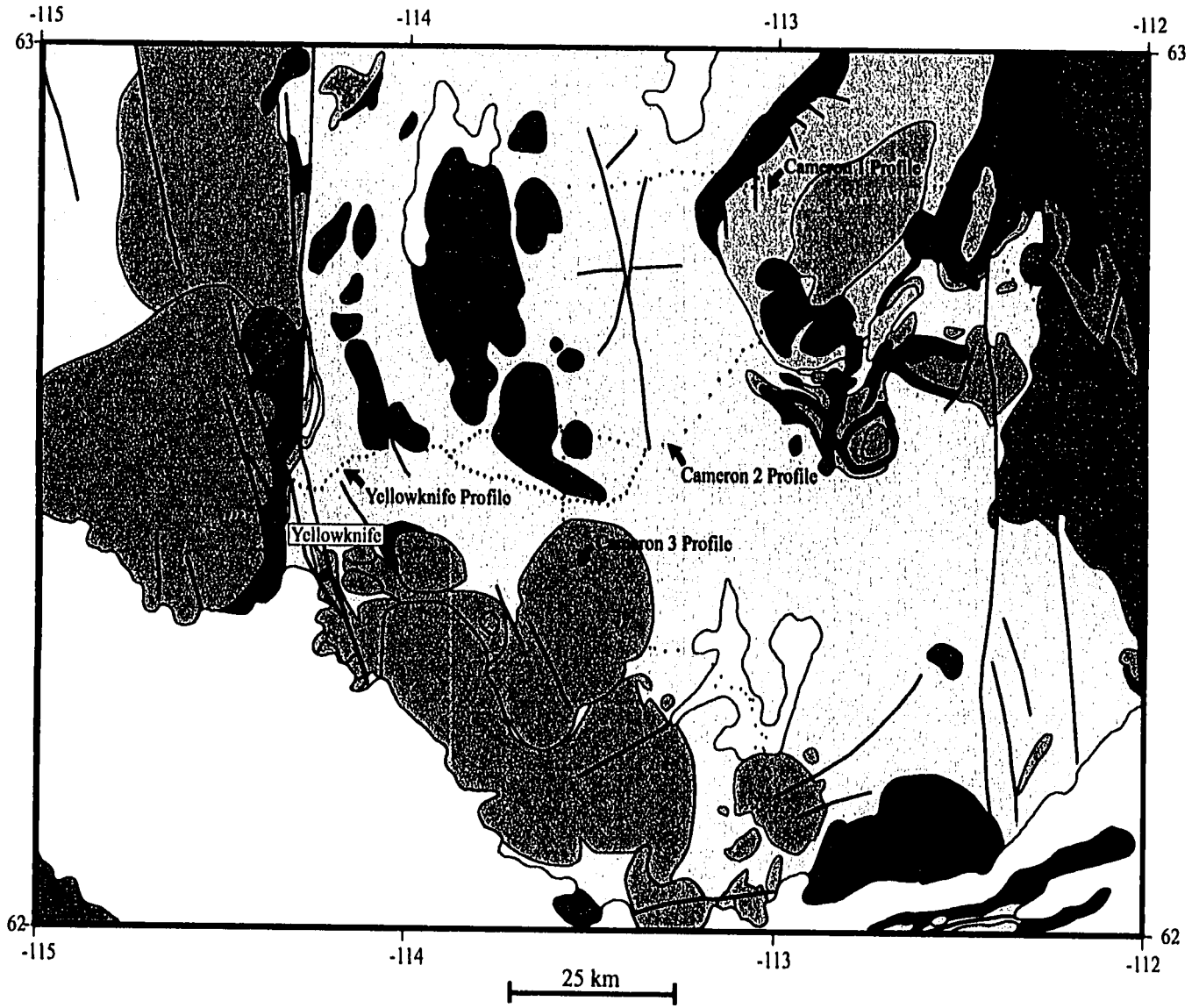

Figure 3.1. The four profiles superimposed on the regional geology of the Yellowknife Domain (from Hoffman and Hall, 1993). Please note that the scale is the same on all Yellowknife Domain maps in Chapter 3.

Legend

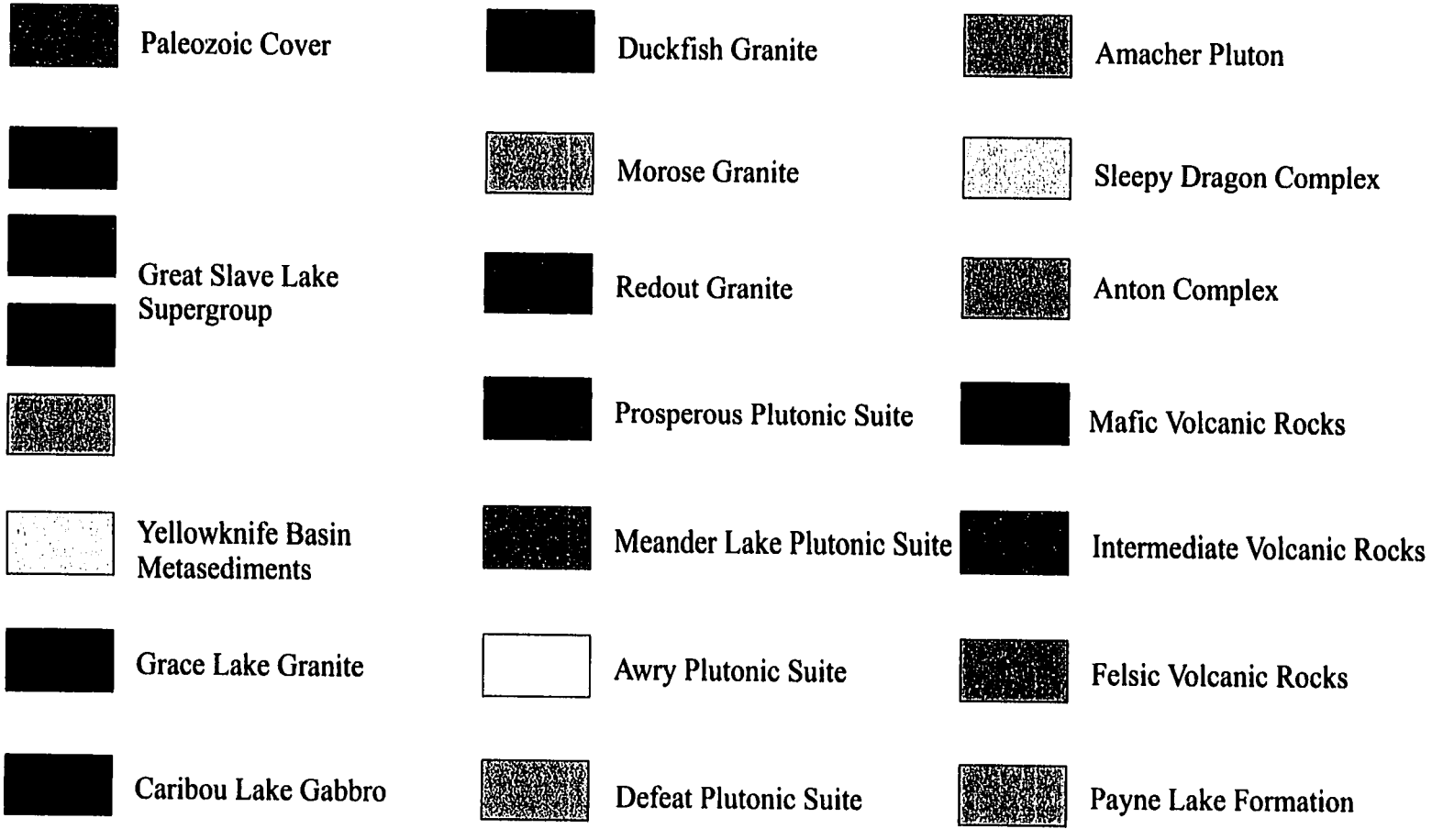

Continuation of Figure 3.1..

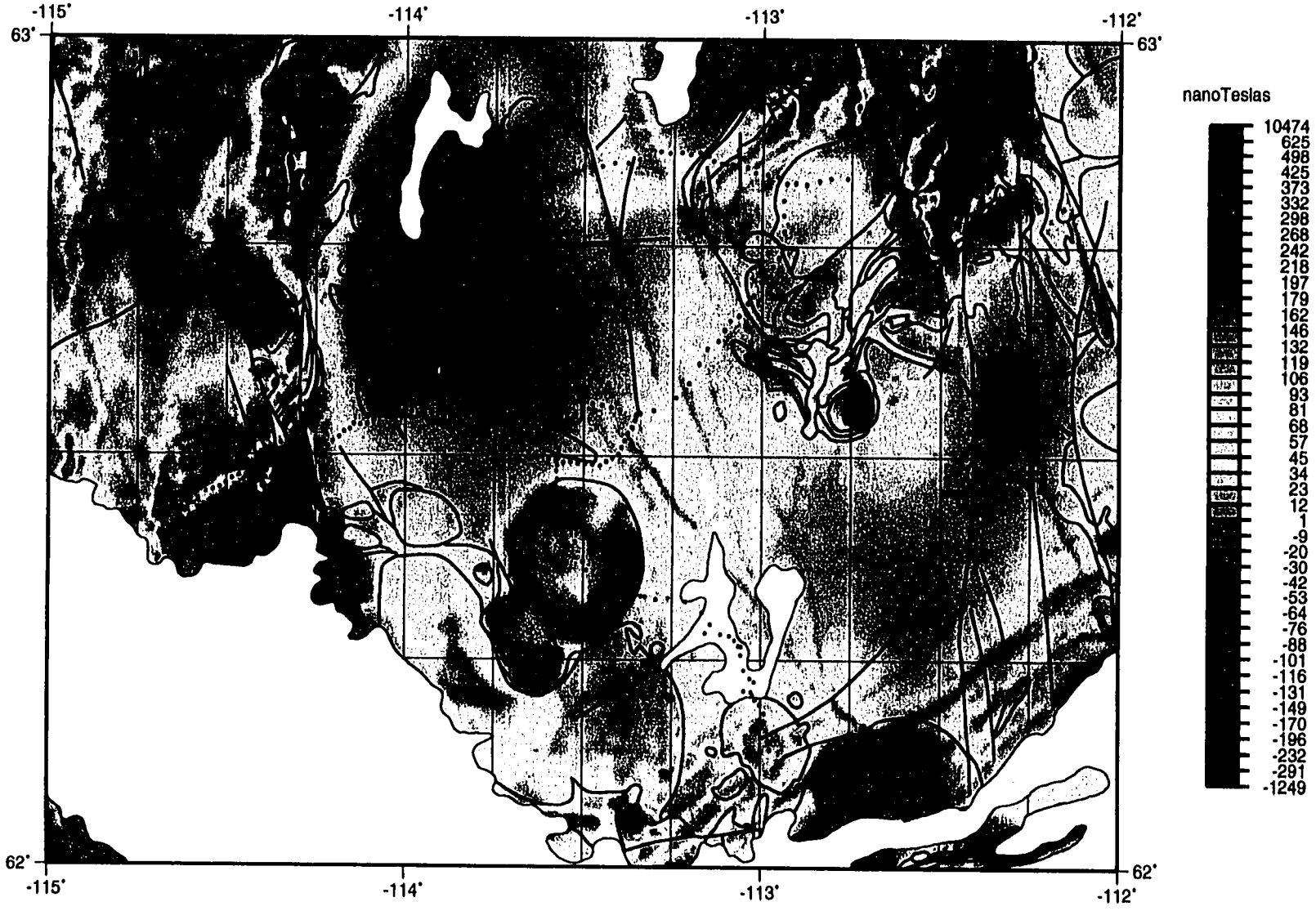

Figure 3.2. The gravity profiles superimposed on the regional aeromagnetics of the Yellowknife Domain.

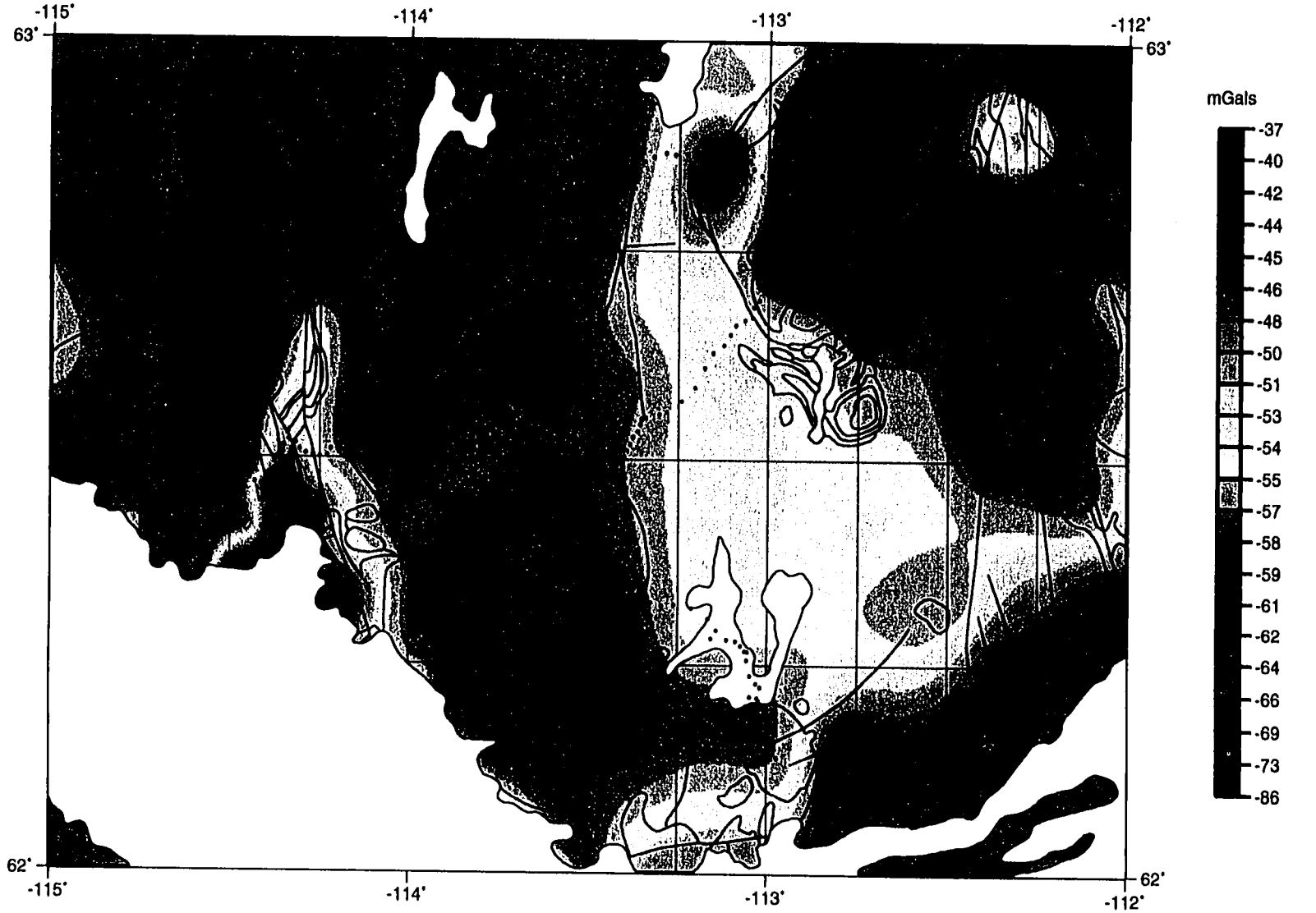

Figure 3.3. The gravity profiles superimposed on the regional Bouguer gravity of the Yellowknife Domain.

modelling of the Yellowknife and Cameron profiles, including examples of models with and without the greenstone belts extending beneath the metasediments. Models shown are the preferred models for each profile, and the reader is referred to the legend in Figure 3.1 for correlation of the units in the models (note that in the models light gray represents the low grade metasediments and dark gray represents the high grade metasediments). Where greenstones extend beneath the metasediments, they are assumed to be1 km thick, consisting of 750 m of basalts and 250 m of intermediate-felsic volcanics (chosen on the basis of the field observations of Bleeker, personal communication). Maximum and minimum depths to the top of the basement are presented, along with estimates of the shape and depth-extent of the plutons crossed by the profiles. The ranges of models shown are based on the models in which the greenstone belt does extend beneath the metasediments.

Constraints used in the modelling include the densities of the bodies (measured by the author), dips and dip directions of the contacts at the surface, and, in the case of the Yellowknife profile, a seismic reflection profile. Densities used in the modelling are listed in Table 3.1, along with the magnetic susceptibilities of the rocks. Densities were obtained by measuring the weight of rock samples of each unit (for numbers and sample types, please refer to the raw data in appendix A). Measurements were taken in air and in water, and the densities were calculated using the equation:

$$density = \frac{dry}{dry - wet}$$

Unit	Density (g/cm^3)	Magnetic Susceptibility ($x\ 10^{-3}$)
Sleepy Dragon Complex/Basment	2.75	0.63
Burwash Formation – greenschist grade	2.73	0.33
Burwash Formation – amphibolite grade	2.78	0.38
Jackson Lake Formation	2.72	0.45
Basalts	2.99	0.77
Felsic – Intermediate	2.82	0.03
Prosperous Suite	2.63	0.04
Defeat Suite	2.65	0.27
Morose Pluton	2.64	0.07
Redout Pluton	2.63	0.1
Amacher Pluton	2.69	0.16

Table 1. Densities used in gravity modelling for all profiles.
(refer to Appendix A for the raw data).

The densities of air and water are negligible, and were ignored. The error of the scale used to measure the weights was ±0.2 grams and the error for the calculated densities is 0.005 g/cm^3. The densities of the rock samples were then averaged to give an average density for each unit. A complete table of the rock samples measured can be found in Appendix 1.

3.2 The Yellowknife Profile

The Yellowknife profile is the eastern end of the Lithoprobe SNORCLE transect 1. It runs from approximately 20 km west of Yellowknife to the eastern end of the Ingraham Trail. The profile was re-projected on a straight line segment (Fig. 3.4)

The Bouguer gravity profile values are plotted against the distance along the profile (Fig. 3.5). Note the significant gravity high at the western end of the profile, which corresponds to the Yellowknife Greenstone Belt, and the gravity lows, which correspond to the Prosperous and Sparrow Plutons of the Prosperous Suite.

The seismic reflection profile for the Yellowknife Profile (taken from Snyder et al., 1999) is shown (Fig. 3.6). A cartoon drawing depicts an interpretation in which the high velocity layer at approximately 3 to 4 seconds is the greenstone belt lying on top of the basement, placing it at 10 km depth.

Gravity modelling of the Yellowknife profile suggests the presence of greenstones beneath the metasediments of the Yellowknife Basin (Fig. 3.7). The bottom of the basin has been modelled flat because there are no constraints on the structures, thicknesses and densities of bodies at depth. The only exception may be the seismic reflection profile (Fig.

Figure 3.4. The Yellowknife gravity profile superimposed on the regional geology of the Yellowknife Domain (from Hoffman and Hall, 1993). The purple line shows the profile's re-projection.

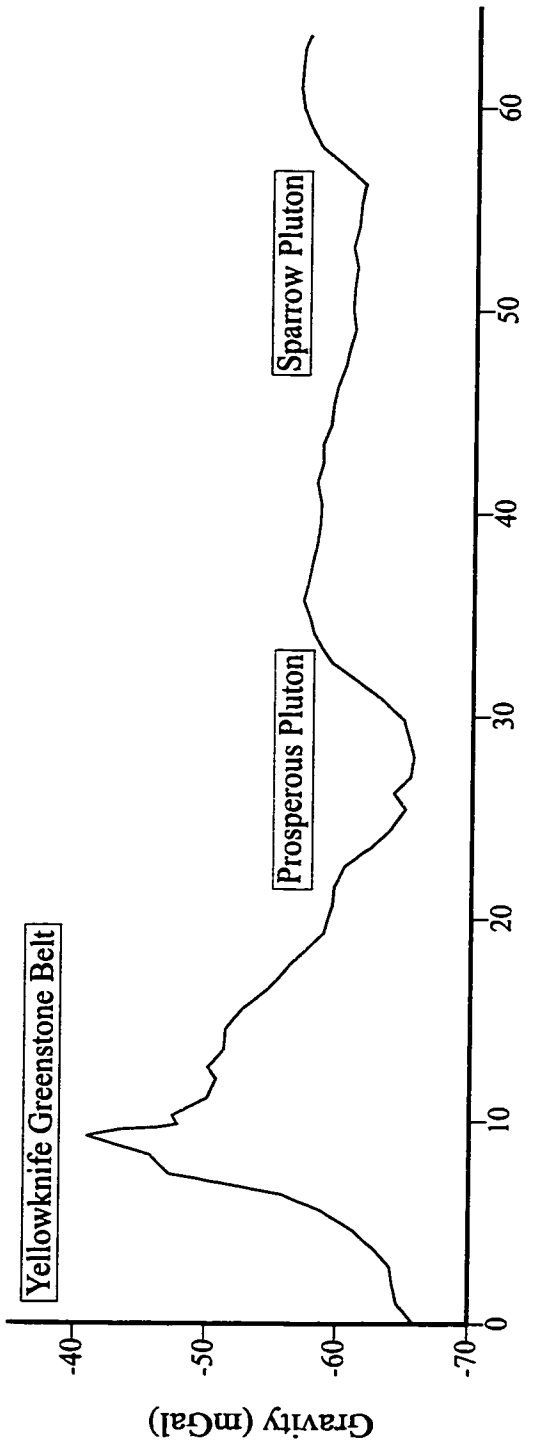

Figure 3.5. Yellowknife Bouguer gravity profile.

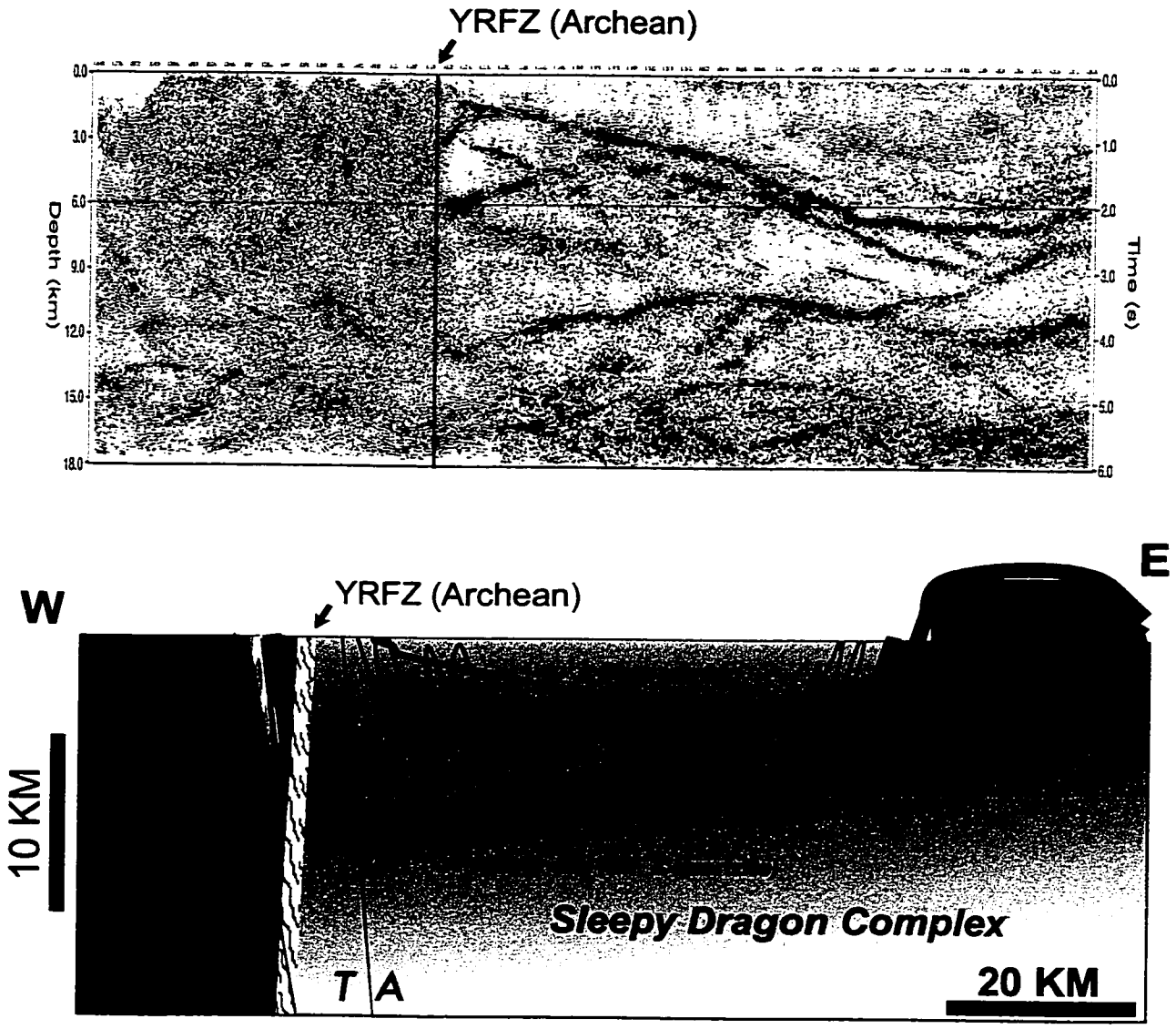

Figure 3.6. The Yellowknife end of the SNORCLE seismic reflection profile shown with a cartoon drawing of an interpretation of the data. The thick greenish-blue line represents the greenstone belt, which has been interpreted to lie above the basement, at about 8-10 km depth from east to west respectively. Taken from Snyder et al. (1999).

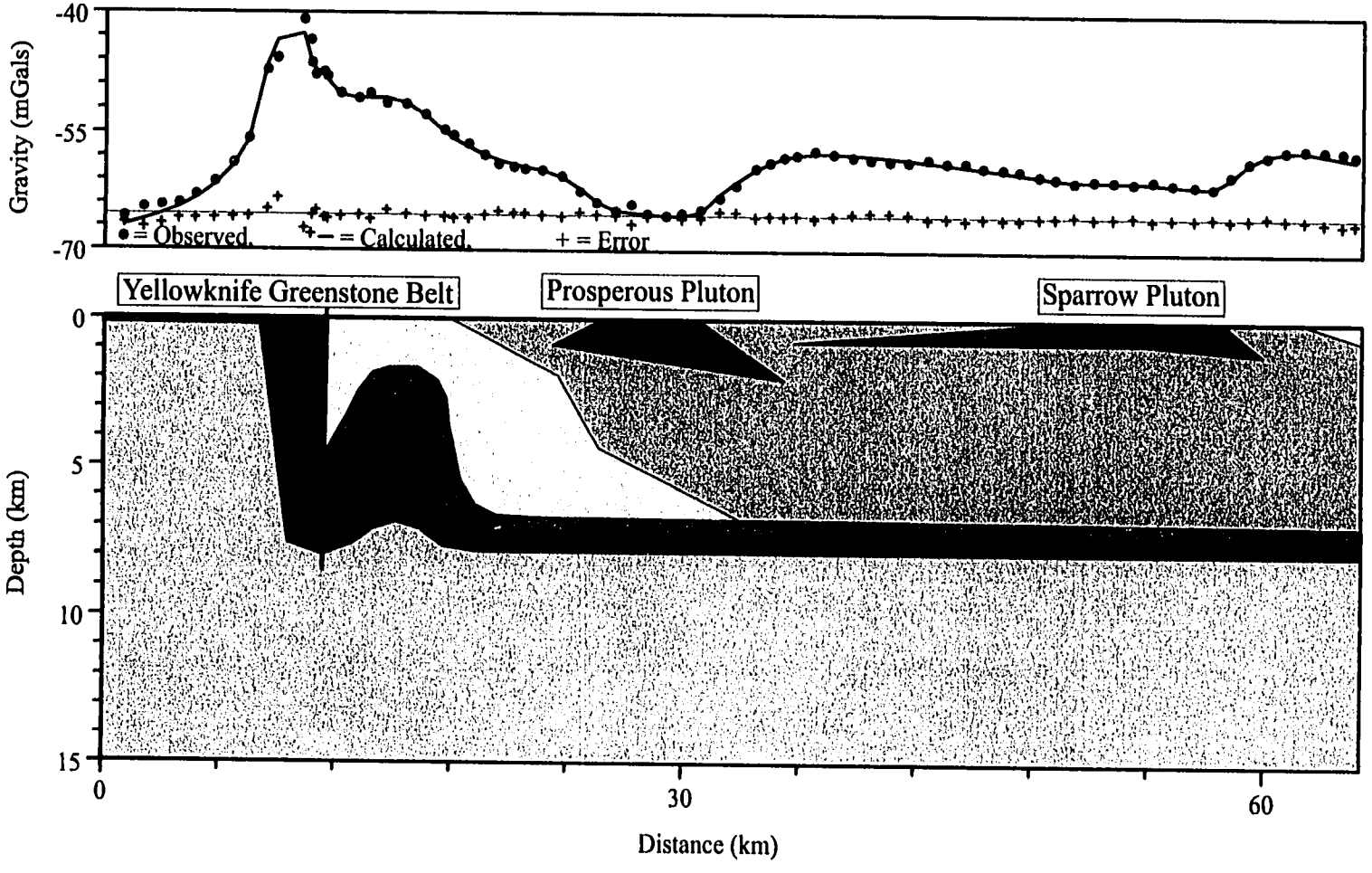

Figure 3.7. Preferred model for the Yellowknife gravity profile showing the greenstone belt extending beneath the metasediments of the Yellowknife Basin. Depth to basement is 8 km. The vertical red line represents the Yellowknife River Fault Zone.

3.6). What is significant, is the structure of the greenstone belt in the vicinity of the vertical Yellowknife River Fault Zone (YRFZ, the red line on Fig. 3.7, 3.8, and 3.9). The greenstone belt that outcrops to the west of the YRFZ is responsible for the prominent gravity high, and a thick package of greenstones beneath the surface east of the fault zone, is necessary for the broad high in the gravity profile. The greenstone belt west of the YRFZ, was found to be steeply dipping on its western side, and is cut by the fault zone to the east. It is approximately 2.5 km thick. East of the fault zone the thick package of greenstones is interpreted as an anticline at a depth of 1.5 km, which is cut by the fault zone to the west. This assumption is based on the presence of an anticline cored by greenstones which occurs to the south of the profile (Henderson, 1970; McGrath et al., 1983). In Figure 3.7, the bottom of the greenstones on either side of the YRFZ extend to 8 km depth (which is 2 km shallower than suggested by the seismic reflection profile in Fig. 3.6). The profile can also be modelled such that the greenstones to the west of the fault zone extend to a greater depth, 8 km, than the greenstones to the east of the fault zone, which extend to 7 km depth (Fig. 3.8). Due to the flat nature of the bottom of the basin, layers representing the greenstones can be removed with little effect on the profile, particularly the eastern end of it (Fig. 3.9). However, the eastern portion of the broad gravity high does not fit in the model in Fig. 3.9 as well as it does in the model in Fig. 3.8, suggesting that the greenstone belt must extend much further to the east. The poor fit to the observed gravity profile in this area is the result of an improper density contrast used in the model. It is not known if the proper density contrast is possible in such a model if more variations in the model were tested. In the model in which no

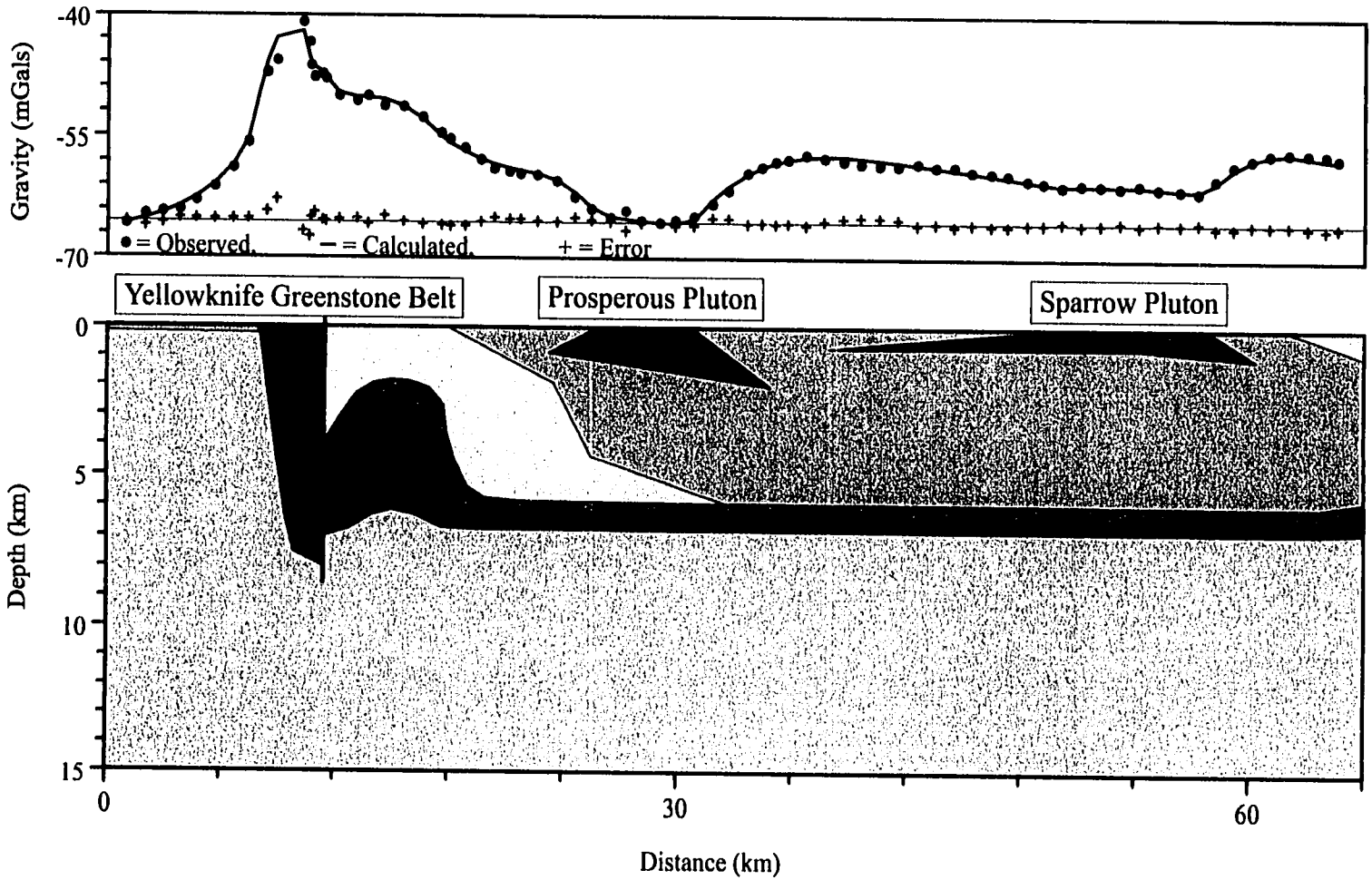

Figure 3.8. Yellowknife profile showing the greenstone to the east of the Yellowknife River Fault Zone (vertical red line) extending to 8 km depth, 1 km deeper than the greenstone to the west of the fault zone.

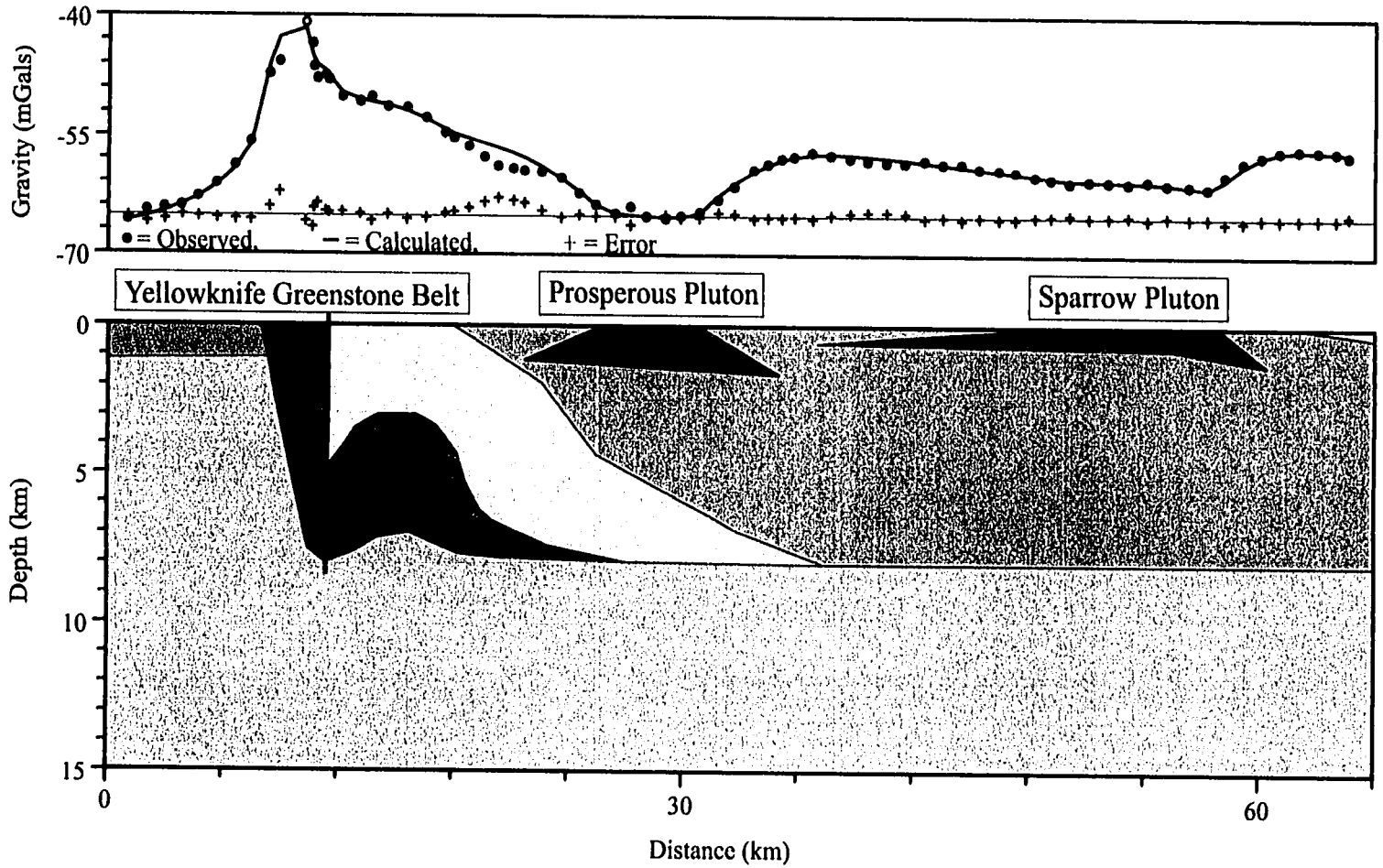

Figure 3.9. Preferred model for the Yellowknife gravity profile with no greenstones extending beneath the metasediments of the Yellowknife Basin. Depth to basement is 8 km. The vertical red line represents the Yellowknife River Fault Zone.

greenstones extend beneath the metasediments, the dip of the greenstone belt west of the YRFZ increases slightly, and east of the fault zone the top of the anticline increases in depth to about 3 km.

The shape and depth extent of the Prosperous and Sparrow Plutons are constrained. The Prosperous Pluton (western pluton) has a laccolithic shape, dipping to the east, with a thickness of about 2 km. This is consistent with the field and magnetic fabric studies of Ham and Benn (1998). The Sparrow Pluton is laccolithic and is approximately 1 km in thickness. In this model it is shown to outcrop at the surface. This is not entirely accurate, as the Ingraham Trail passes just to the south of the pluton. However, it is close enough to the surface for this model to be valid. The main body of the pluton is thicker, as can be seen in the Cameron 2 and Cameron 3 profiles (discussed below). At the extreme western end of the profile, there is a very thin (250 m) Defeat Suite pluton. In the model in which no greenstones extend beneath the metasediments, this Defeat Pluton increases to more than 1 km in depth, while the other plutons do not change in depth or shape; however, because the pluton is at the end of the profile it is difficult to model accurately due to far field effects.

In addition to the constraints on the shape of the plutons, the shape of the isograd between the high and low grade metasediments is constrained, and is the same in the model without the greenstones beneath the metasediments.

Figure 3.10 shows a depth range model for the Yellowknife Profile. The preferred depth to basement of 8 km is shown with 6 km depth, where it becomes too shallow (shown by the calculated profile), and 10 km depth, where it begins to become too deep (a subtle

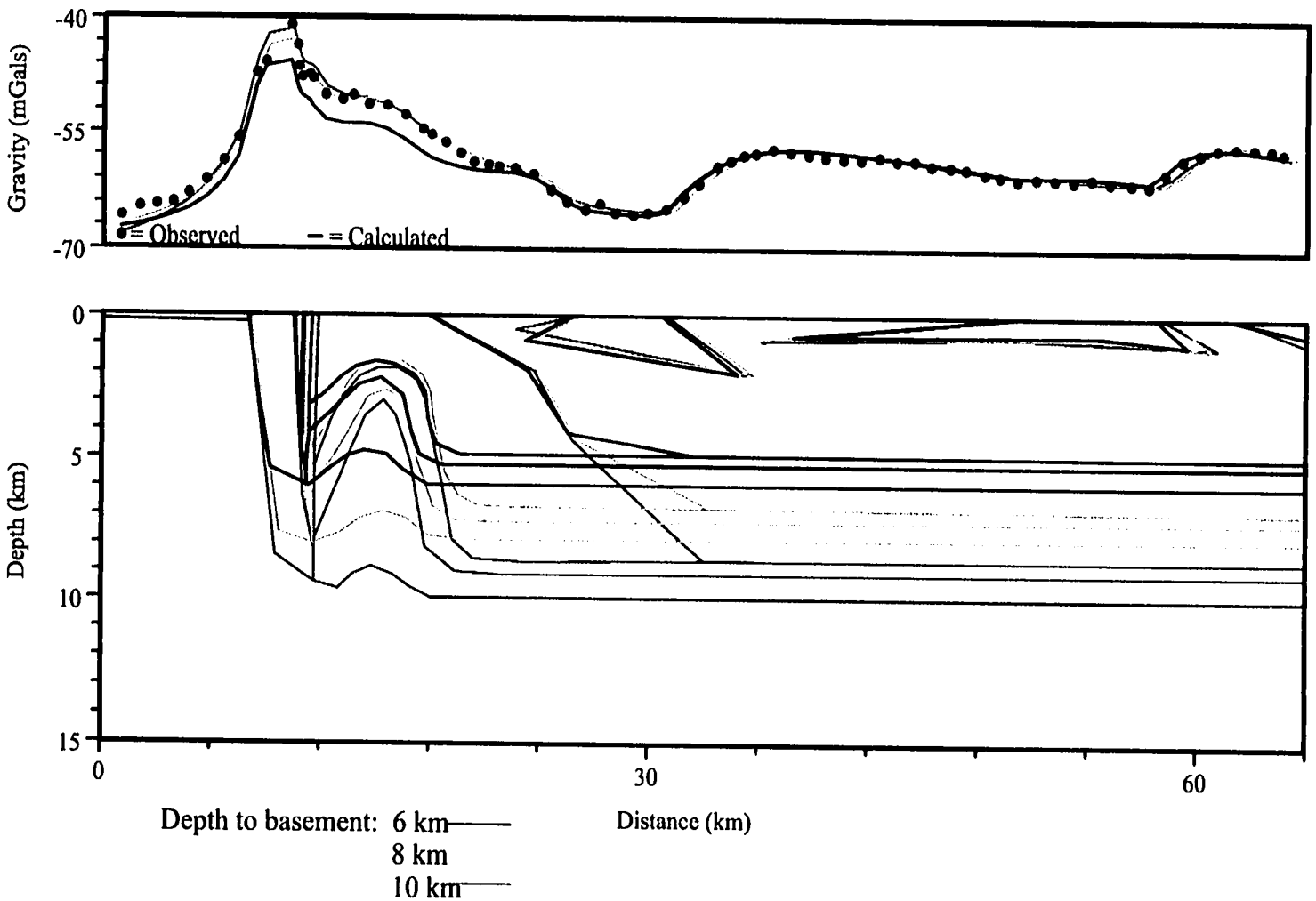

Figure 3.10. Range of models for the Yellowknife gravity profile. The preferred depth to basement is 8 km. Models are also shown for 6 km and 11 km depth to basement, which are to shallow and too deep respectively.

change, but the calculated does not fit well, particularly at the extreme western end of the profile). With changing depth-to-basement, the shape and dip of the greenstone belt to the west of the YRFZ remains consistent and the top of the anticline of folded greenstones to the east of the YRFZ stays at about 1.5 km depth. The shape and depth extent of the plutons also remains constant.

3.3 The Cameron 1 Profile

The Cameron 1 Profile crosses the Sleepy Dragon Complex and the data positions and their re-projection are shown in Figure 3.11. The Bouguer gravity values are plotted against the distance along the profile (Fig. 3.12). Note the three prominent gravity highs. The western one corresponds to the Cameron River Greenstone Belt and the eastern two correspond to the Beaulieu River Greenstone Belt. The broad gravity low in the centre of the profile is due to the Morose Pluton and the small gravity low between the two eastern gravity highs corresponds to the Amacher Pluton, which intrudes the Beaulieu River Greenstone Belt. The eastern end of the profile crosses back into metasediments.

The Cameron 1 Profile can be reasonably modelled with (Fig. 3.13) or without (Fig. 3.14) the greenstone belts extending beneath the metasediments. The preferred depth-to-basement is 9 km. The isograd between the low- and high-grade metasediments is the same as the one further south that is present in the Yellowknife profile, and to be consistent it must dip shallowly to the east. It should also be noted that the metasediments east of the Beaulieu River Greenstone Belt are high-grade metasediments, but were given the low-grade density of

Figure 3.11. The Cameron 1 profile superimposed on the regional geology of the Yellowknife Domain (from Hoffman and Hall, 1993). The purple line shows the profile's re-projection.

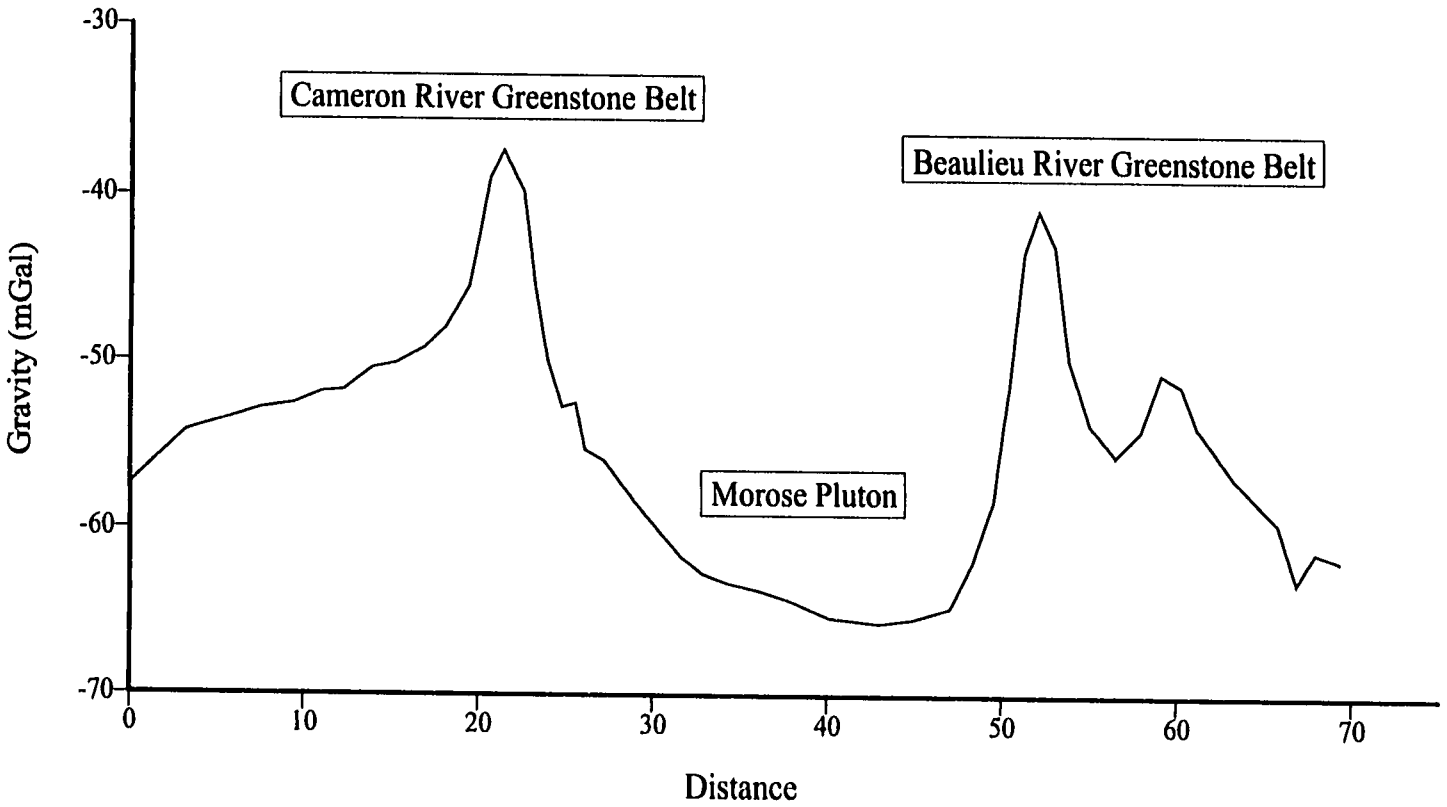

Figure 3.12. Cameron 1 Bouguer gravity profile.

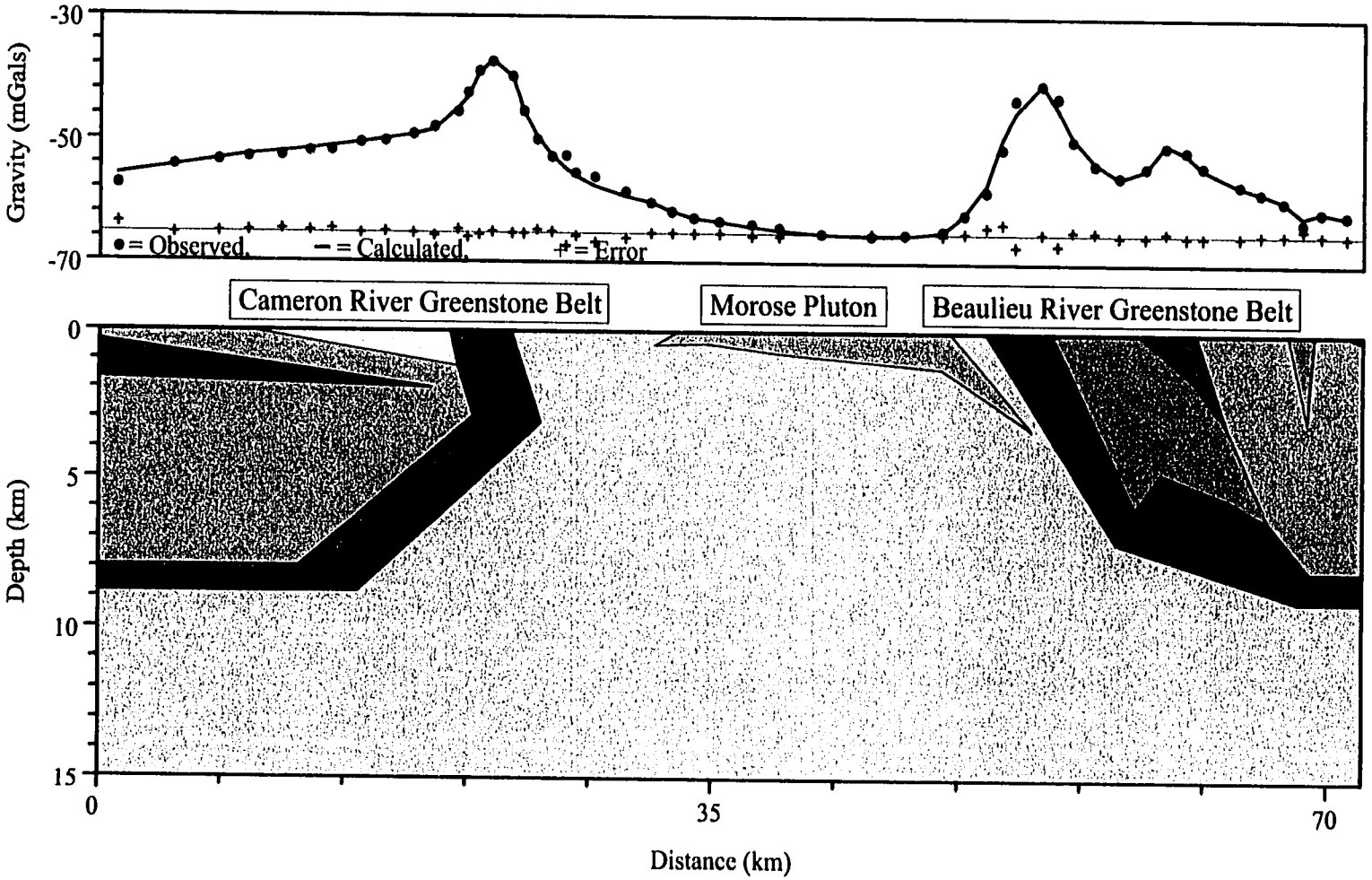

Figure 3.13. Model for the Cameron 1 gravity profile showing the greenstone belt extending beneath the metasediments of the Yellowknife Basin. Depth to basement is 9 km.

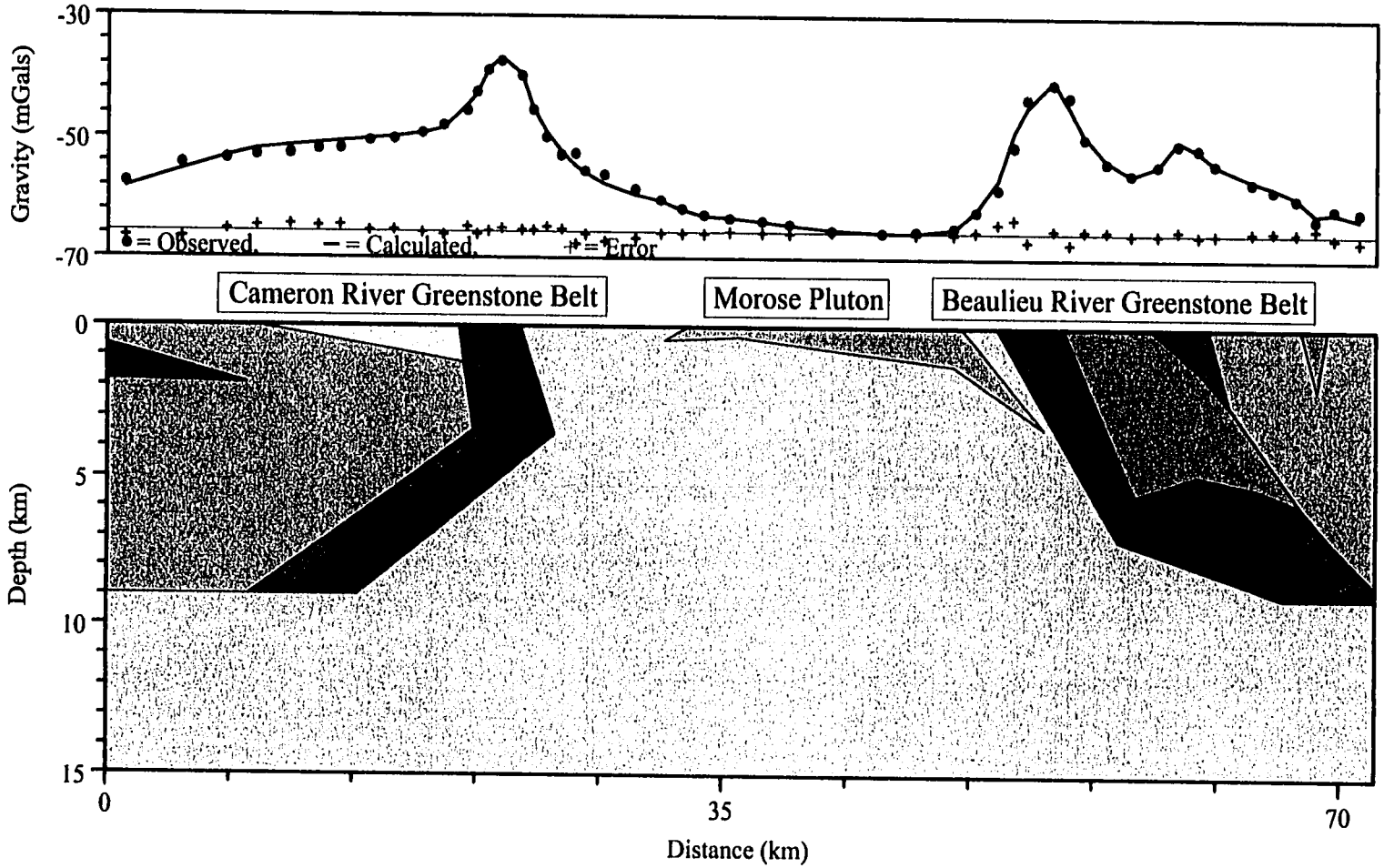

Figure 3.14. Model for the Cameron 1 gravity profile with no greenstones extending beneath the metasediments of the Yellowknife Basin. Depth to basement is 9 km.

2.73 g/cm^3 because the high-grade density of 2.78 g/cm^3 would not work in the model. These rock may have a lower than the average density for the high-grade metasediments, and this can be tested by performing density measurements on rocks from that area.

The Cameron River Greenstone Belt (CRGB) dips steeply to the east and extends to a depth of approximately 3.3 k, where its dip turns to the west and it shallows and extends to the maximum depth of 9 km. Without the greenstone belt extending beneath the metasediments, the CRGB turns to dip to the west at about 3.5 km. The greenstone belt maintains a constant thickness of about 2.5 km in both models. The Beaulieu River Greenstone Belt (BRGB) dips moderately to the east and maintains a constant thickness of about 3.5 km. This thickness is due to the folding of the belt into an anticline/syncline pair. At a depth of approximately 6 km, the dip shallows and continues to the maximum depth of 9 km. In the model in which the greenstone belt does not extend beneath the metasediments, the only change is that the belt thins slightly with depth before reaching 9 km depth.

In the model in which the greenstones are present beneath the metasediments, the Prosperous Suite pluton that is immediately west of the profile is required to dip shallowly to the east, and it extends almost to the greenstone belt. In contrast, with no greenstones extending beneath the metasediments, the Prosperous pluton does not need to extend as far to the east. This seems to be a more realistic interpretation, as the pluton outcrops 20 km to the west of the Cameron River Greenstone Belt. This is the main difference between the model with the greenstones present beneath the metasediments and the one without. The shape and depth extent of the Morose Pluton is extremely well defined. It is laccolithic and dips

shallowly to the east, with a thickness of about 1 km. The Amacher Pluton forms the core of the anticline in the BRGB, and both limbs extend to a depth of about 6 km. The small Defeat Suite pluton to the east of the BRGB extends to a depth of 3 km. The isograd in the model dips shallowly to the east.

The range of models (Fig. 3.15) shows the preferred depth-to-basement of 9 km, as well as 7 km depth (too shallow) and 11 km depth (maximum possible depth to basement). Thus, the minimum and maximum depths-to-basement are 8 km and 11 km respectively. The model for 7 km depth begin to get too shallow, as the calculated profile does not fit the observed profile well. It is a subtle change, but significant. Also, at this depth, the belt begins to thicken with depth. If a constant thickness is assumed for the unit, then this also favours a minimum depth of 8 km. The maximum depth is considered to be 11 km because of the constraints of the model, not the fit of the profile. The Prosperous pluton to the west extends so far east, it almost touches the Cameron River Greenstone Belt. This was taken to be the cut off for maximum depth, assuming that the pluton does not cut across the greenstone belt. The range of models shows that the dips and dip directions of the greenstone belts that outcrop at the surface are consistent, as well as the depth at which they fold under the metasediments. The isograd to the west shallows with decreasing depth to basement. The shape and depth extent of the other plutons remain constant with changing depth-to-basement.

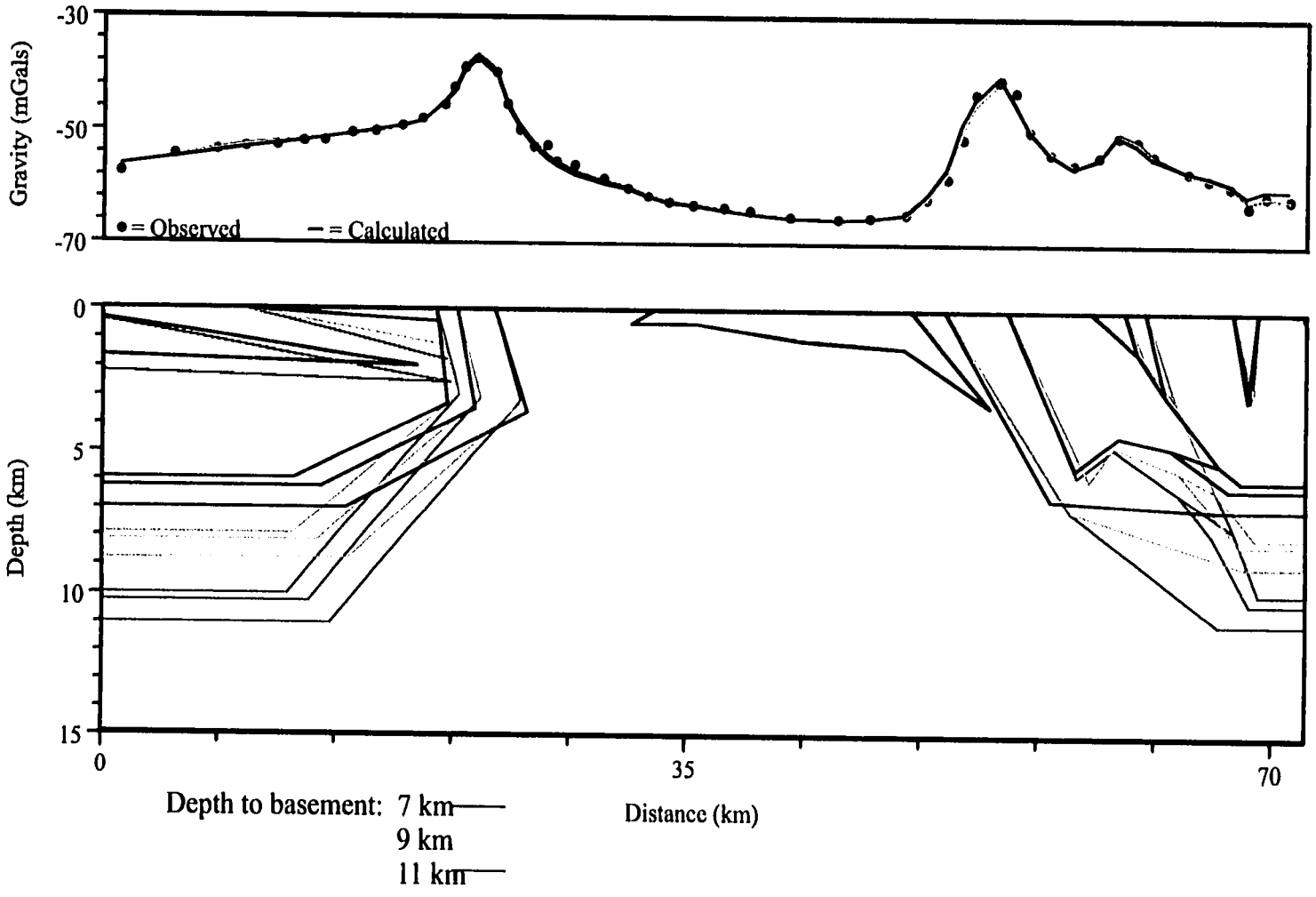

Figure 3.15. Range of models for the Cameron 1 gravity profile. The preferred depth to basement is 9 km. Models are also shown for 7 km and 11 km, which are too shallow and too deep respectively.

3.4 The Cameron 2 Profile

The Cameron 2 Profile extends southwest from the Morose Pluton in the Sleepy Dragon Complex and then west across the Hidden Lake and Sparrow Plutons of the Prosperous Suite, where it joins the Yellowknife Profile. The profile and its re-projection are shown in Figure 3.16. The Bouguer gravity values are plotted against the distance along the profile (Fig. 3.17). There are no sharp gravity highs present, but there is a central, broad high and a broad gravity low to the west. The low is interpreted to correspond to the Prosperous plutons and the high is interpreted to correspond to the greenstone belt to the southeast of the profile continuing at depth.

To be consistent with the other models, the preferred depth-to-basement is 8 km. This will be explained when the range of the models is discussed below. The profile can be modelled adequately with (Fig. 3.18) or without (Fig. 3.19) greenstones extending beneath the metasediments. In the model in which the greenstone belt extends beneath the metasediments, it thickens to about 1.75 km in the northeast, before folding at the edge of the Sleepy Dragon Complex, where it thins out as it approaches the surface. It pinches out at about 3 km depth. In the model where the greenstone belt does not extend beneath the metasediments (Fig. 3.19), the 1.75 km thick package of greenstones is still necessary to match the calculated profile to the observed profile.

The dip of the contact at the edge of the Sleepy Dragon Complex is moderate to steep to the east. The thickened greenstone belt is interpreted as the northwestern extension of the greenstone complex at the southern edge of the Sleepy Dragon Complex. This package of

Figure 3.16. The Cameron 2 profile superimposed on the regional geology of the Yellowknife Domain (from Hoffman and Hall, 1993). The purple lines shows the profile's re-projection.

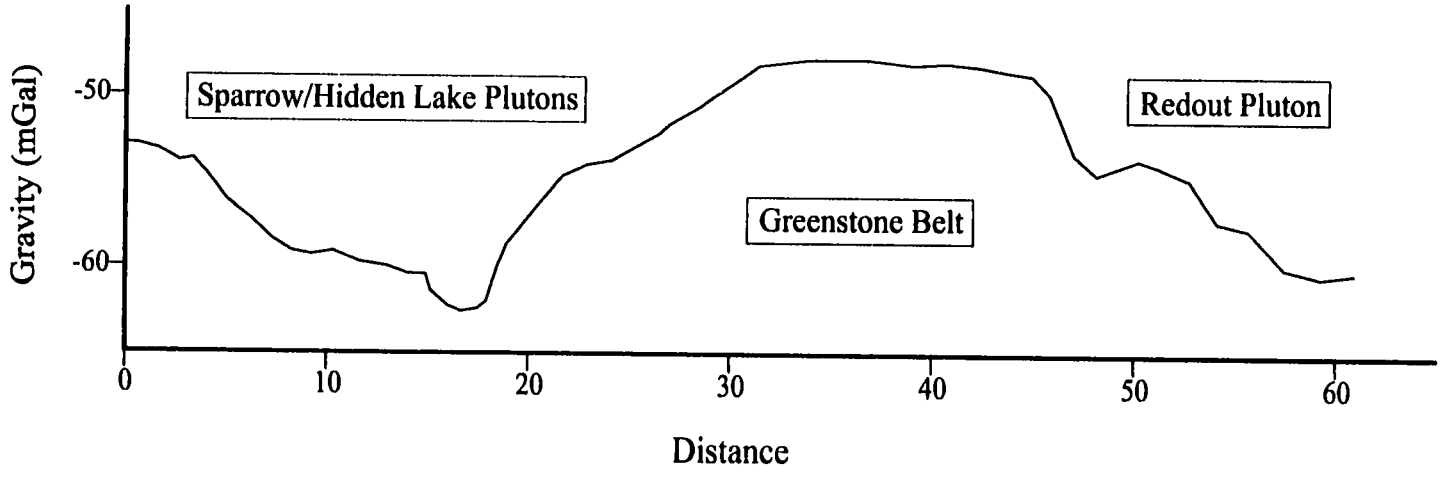

Figure 3.17. Cameron 2 Bouguer gravity profile.

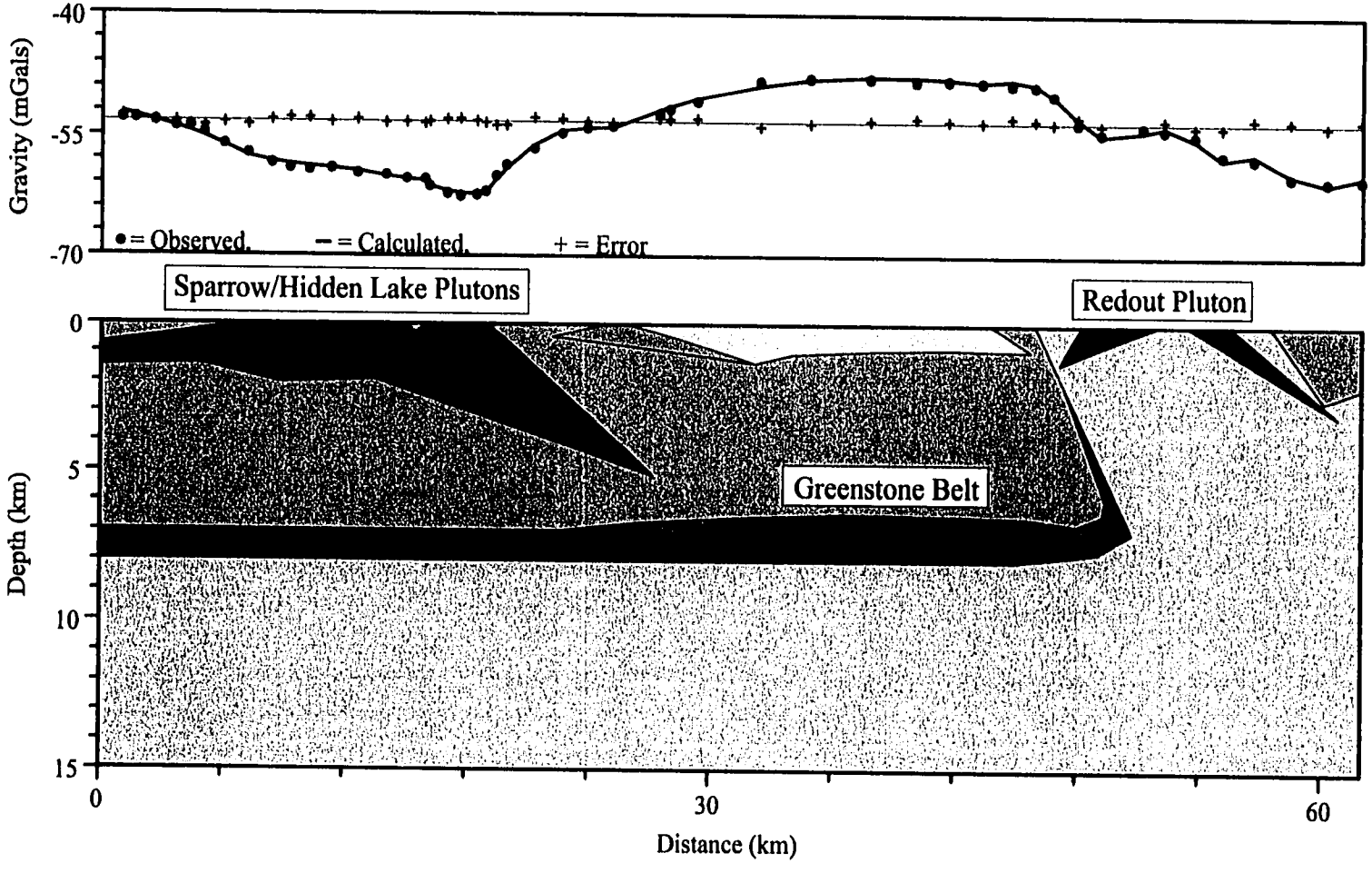

Figure 3.18. Model for the Cameron 2 gravity profile showing the greenstone belt extending beneath the metasediments of the Yellowknife Basin. Depth to basement is 8 km.

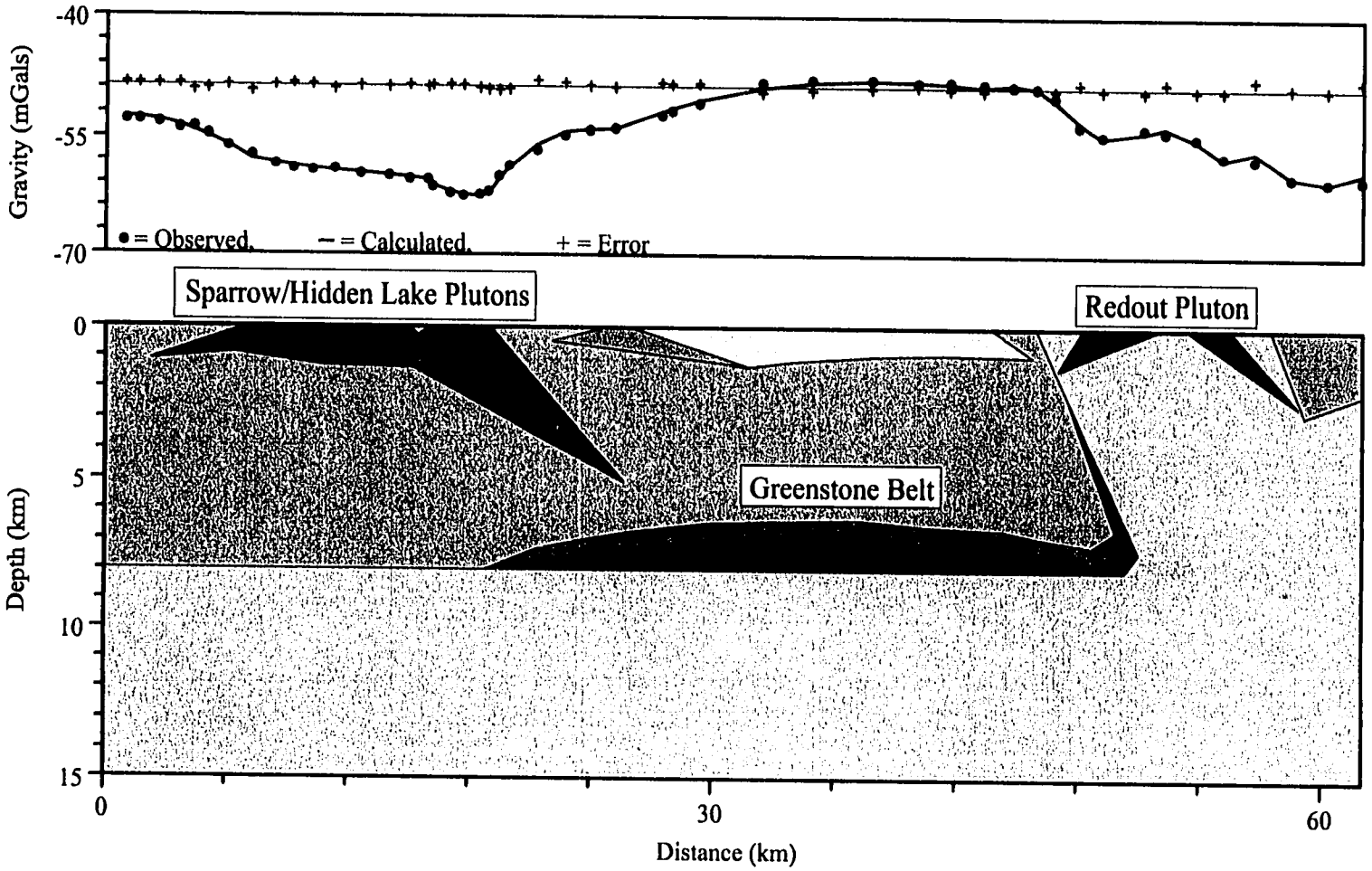

Figure 3.19. Model for the Cameron 2 gravity profile with no greenstones extending beneath the metasediments of the Yellowknife Basin. Depth to basement is 8 km.

greenstones at the southern edge of the Sleepy Dragon Complex also affects the northeastern end of the profile, although it is not crossed by the profile itself. Thus, a large body with the average density used for the basalts, was included in the model to the east of the profile (not shown in model). Without this body, the northeastern end of the calculated profile is approximately 10 mGal lower than the observed profile.

The Sparrow and Hidden Lake Plutons merge at a depth of about 400 m in the model, suggesting that the Hidden Lake Pluton cuts across the older Sparrow Pluton. These plutons are about 2 km thick and dip moderately to the east, with a maximum depth of 5 km. The plutons extends past the edge of the model to the west. In the model without the greenstones extending beneath the metasediments, the Sparrow and Hidden Lake Plutons still merge at about 400 m beneath the surface and the pluton still dips to the east with a maximum depth of 5 km. However, the plutons are smaller, with a thickness of about 1.5 km, and do not extend as far to the west. There is also a small Defeat Suite pluton to the east of the Hidden Lake Pluton, which is a thin body about 750 m thick and dipping shallowly to the east. The Redout Pluton is a thin body, about 1 km thick. Where crossed by the profile it is looks as though there are two separate plutons, but the pluton as a whole is folded and dips slightly to the northeast. The Morose Pluton appears to be approximately 2.5 km thick at its southern edge. This is about 2 km thicker than modelled in the Cameron 1 Profile. As explained in section 3.4, the ends of profiles are often difficult to model accurately, due to far field effects, so the Cameron 1 Profile is a better representation of the Morose Pluton. The thickness of the pluton edge could probably be modified by changing the properties of the dense body to

the east of the profile (described above). It is also important to note that, in both models, the area of low-grade metasedimentary rocks extends to a shallow depth of about 1 km.

The range of models in Figure 3.20 shows the preferred depth-to-basement of 8 km, as well as at 6 km and 10 km. The 6 km depth-to-basement is considered to be to the minimum, assuming the Sparrow/Hidden Lake Pluton does not cut across the greenstone belt. The maximum depth was not determined. The model was taken to a depth of 18 km to the top of the basement and the calculated profile still fit the observed very well. Thus, a depth of 8 km was chosen, in order to be consistent with the Yellowknife and Cameron 1 models. As the depth-to-basement shallows. The thickness of the greenstone belt remains unchanged. The dip of the Sparrow/Hidden Lake Pluton became more shallow and its maximum depth decreases, although its thickness and shape remained unchanged. To the northeast, the Redout and Morose Plutons became slightly more shallow with increasing depth-to-basement. The small Defeat Suite pluton and the area of low-grade metasediments do not vary with changing depth-to-basement, nor does the dip of the basement-metasediment contact.

3.5 The Cameron 3 Profile

The Cameron 3 Profile and its re-projection are shown in Figure 3.21. The Bouguer gravity values are plotted against the distance along the profile (Fig. 3.22). There are no major gravity highs or lows, but there are broad lows related to the presence of thin plutons at the surface.

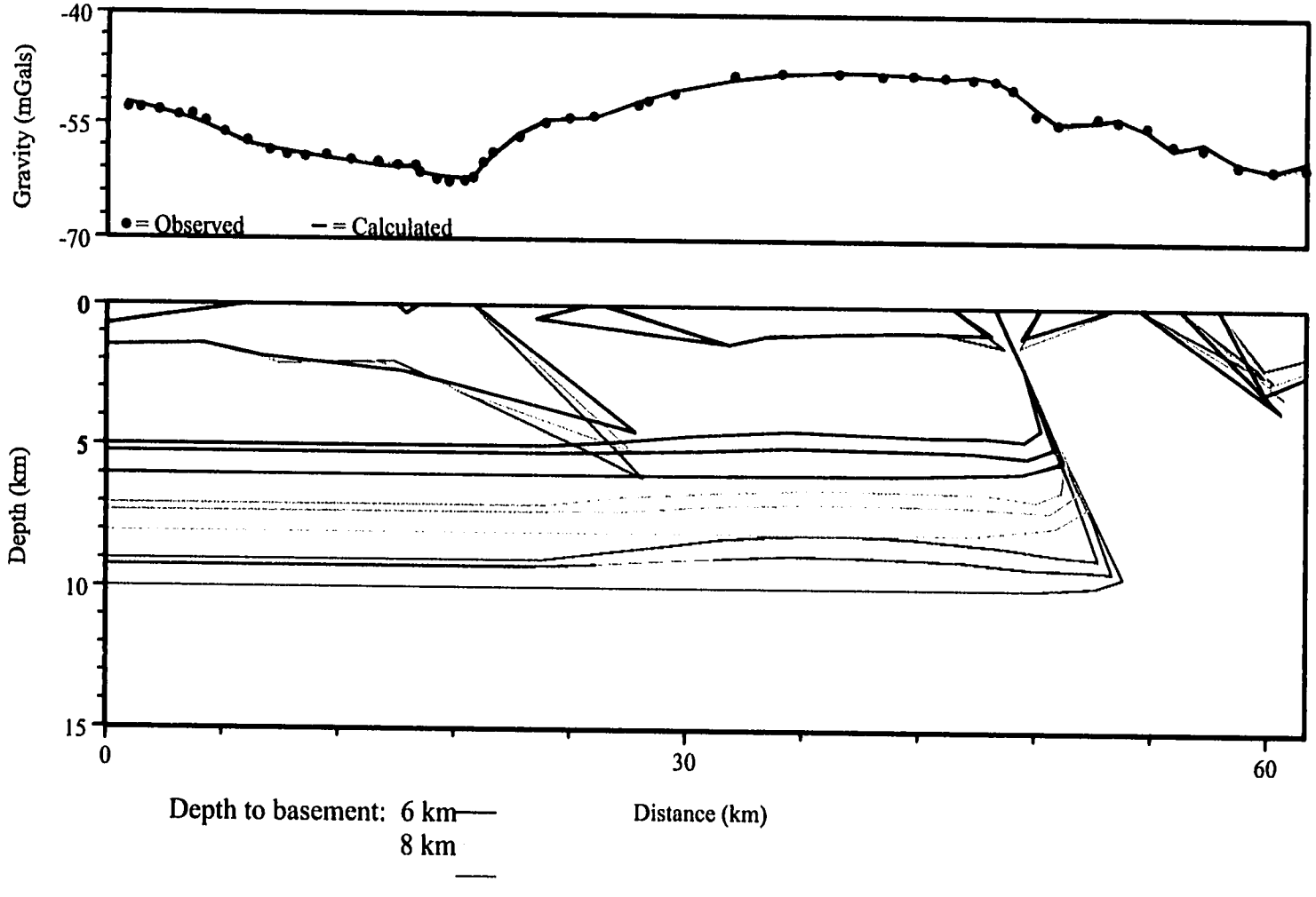

Figure 3.20. Range of models for the Cameron 2 gravity profile. The preferred depth to basement is 8 km. Models are also shown for 6 km and 10 km. These do not vary significantly from the 8 km profile, but are considered to be too shallow and too deep respectively (see text).

Figure 3.21. The Cameron 3 profile superimposed on the regional geology of the Yellowknife Domain (from Hoffman and Hall, 1993). The purple line shows the profile's re-projection.

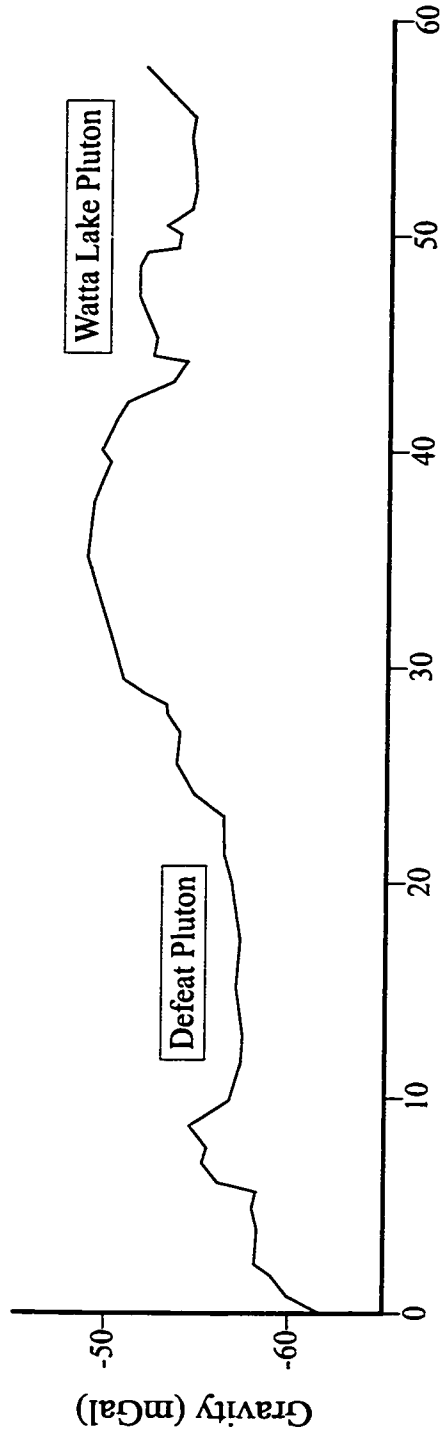

Figure 3.22. Cameron 3 Bouguer gravity profile.

This profile crosses the central part of the basin. Thus, it does not cross any greenstone belts that outcrop at the surface. The simplest model is a flat-bottomed basin and, since there is no control on the shapes, thicknesses, or densities of bodies at depth, this is what has been used in the model. Due to the flat bottom the presence (Fig. 3.23) or absence (Fig. 3.24) of a greenstone belt beneath the metasediments does not change the model, nor does increasing or decreasing the depth-to-basement.

The advantage of the Cameron 3 Profile is that it helps constrain the depth extent and shape of the plutons it crosses. At its northern end, the profile crosses the Sparrow and Hidden Lake Plutons and, as with the Cameron 2 Profile, it shows them merging at a depth of about 300-400 m. The Sparrow/Hidden Lake Plutons are approximately 2 km thick in this model, as in the Cameron 2 model with greenstones underlying the metasediments, but does not dip considerably. The northern corner of the Defeat Pluton is cut by the Sparrow/Hidden Lake Plutons at depth. It is about 2 km thick and flat-lying. The Watta Lake Pluton of the Defeat Suite at the southern end of the profile, is also relatively flat-lying and is about 1.5 km thick. The small Defeat Suite pluton that lies between the Defeat and Watta Lake Plutons is small and extends to almost 1 km depth.

The depth range for the Cameron 3 Profile is presented in Figure 3.25 to show that the depth to basement does not affect the model.

3.6 Discussion

An important result of the modelling is that the shapes and depth extents of the

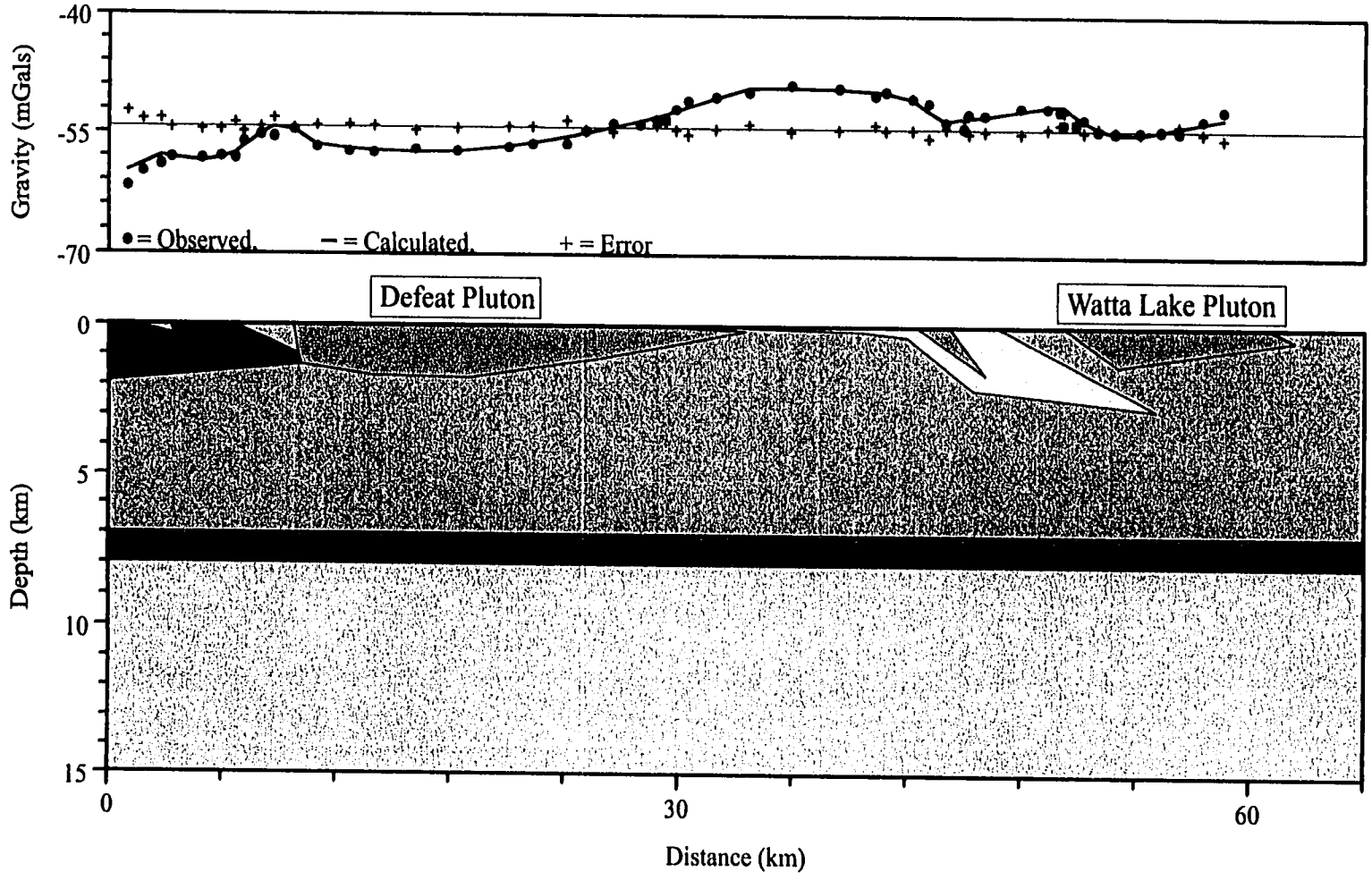

Figure 3.23. Model for the Cameron 3 gravity profile showing the greenstone belt extending beneath the metasediments of the Yellowknife Basin. Depth to basement is 8 km.

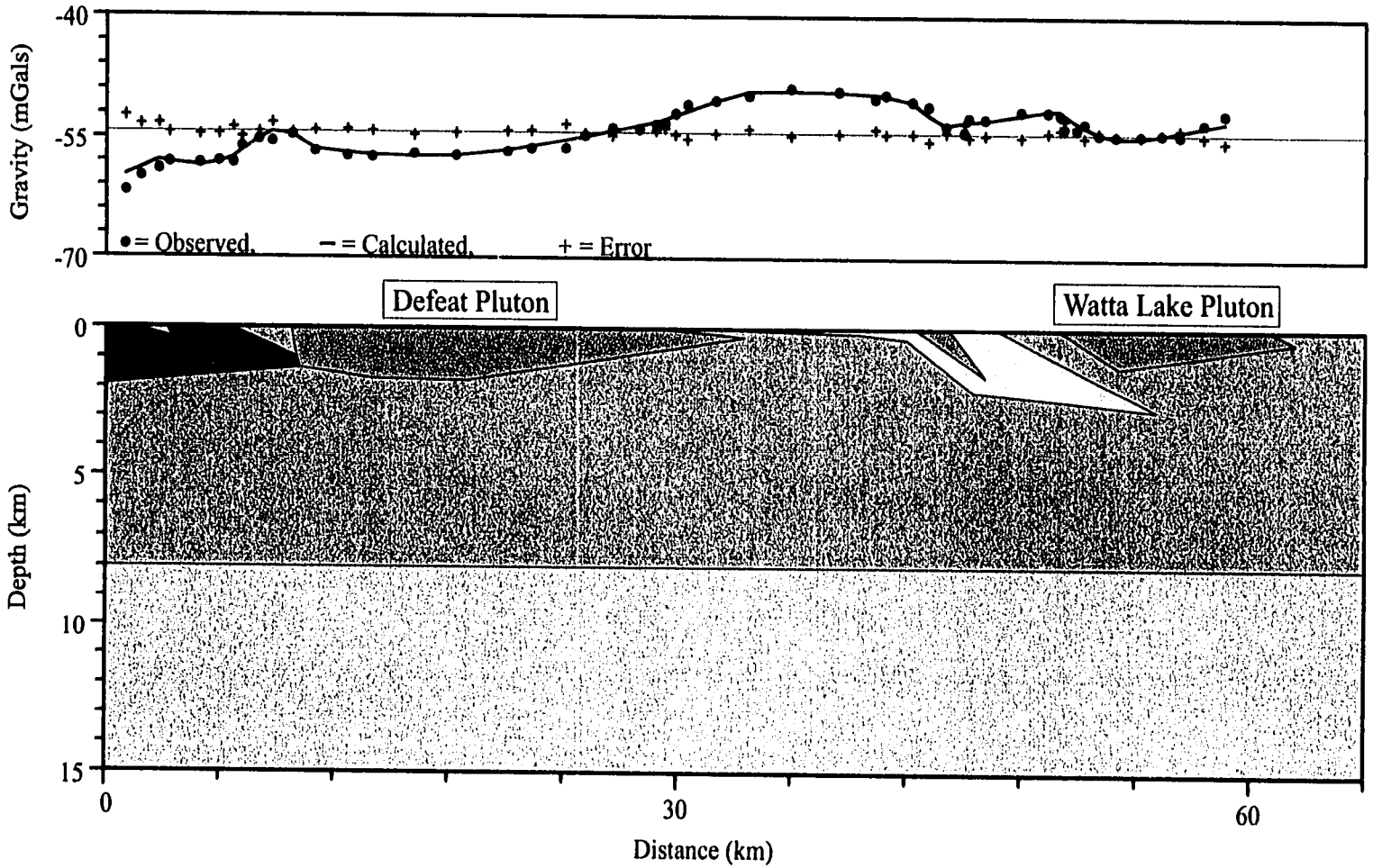

Figure. 24. Model for the Cameron 3 gravity profile with no greenstones extending beneath the metasediments of the Yellowknife Basin. Depth to basement is 8 km.

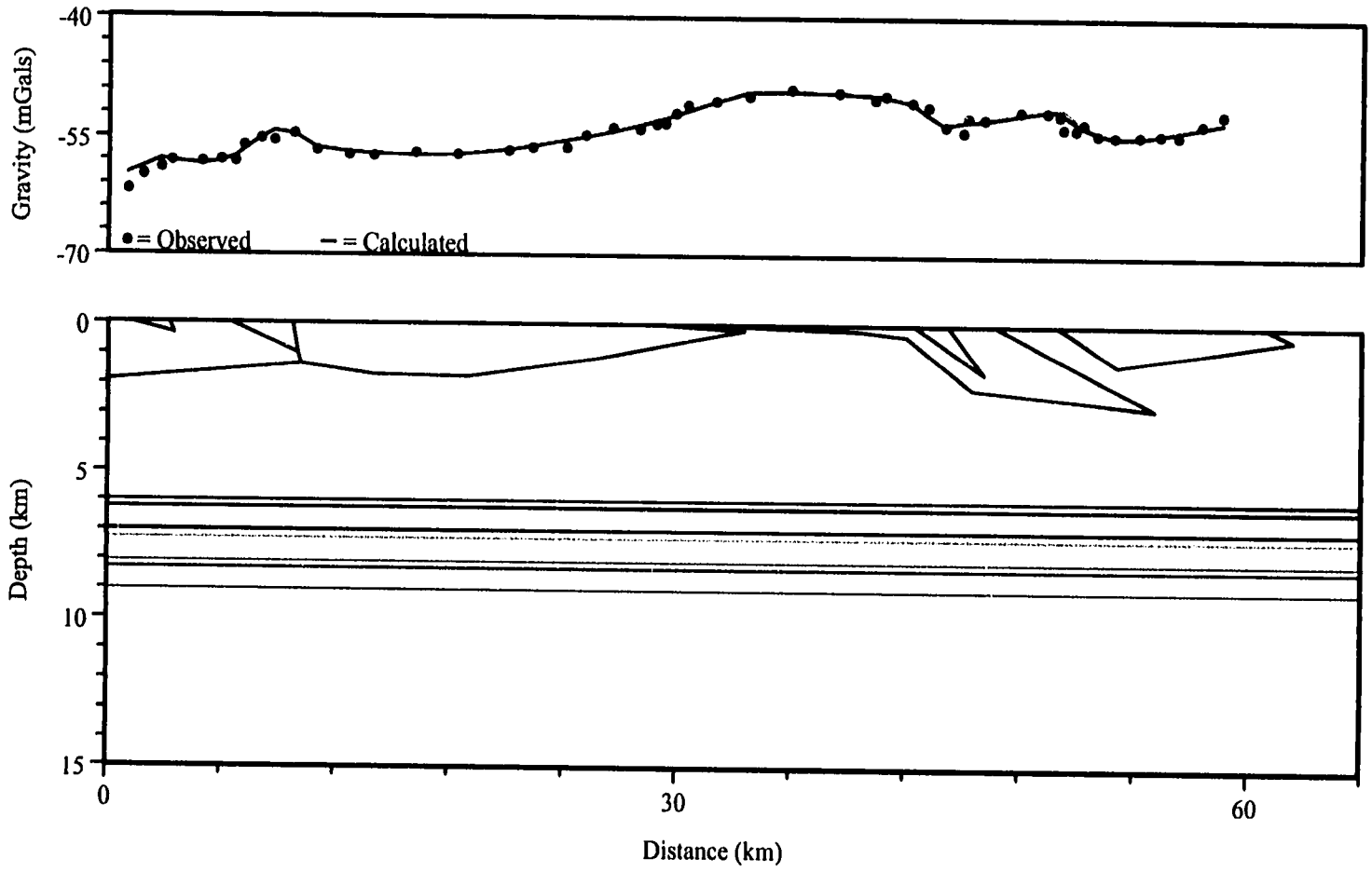

Depth to basement: 7 km——
8 km
9 km——

Figure 3.25. Range of models for the Cameron 3 gravity profile. Because of the flat nature of the basement and the greenstone belt a depth range for the top of the basement could not be estimated. Therefore, the depth was placed at 8 km to be consistent with the preferred depth of the other profiles.

plutons in the region are well constrained. They were all found to be laccolithic in shape and range in thickness from 1-2 km. A few of them are flat-lying, but most are folded and dip to the east. An exception to this is the Amacher pluton, which is a more vertically-elongate body, with a greater depth-extent; however this pluton is known to reside in the core of an anticline and it is reasonable to assume that it was horizontal upon emplacement and was later folded. In section 1.28, it was discussed that some of the plutons or plutonic suites may have overlapped in time with folding events. Thus, the plutons were emplaced in a compressional environment, and folding probably took place during or after emplacement. Benn et al. (1999) propose a laccolithic emplacement model for plutons in which there is a major discontinuity present, such as a major unconformity or the brittle-ductile transition or a change in rock strength, that acts as a trap for the rising magma, causing it to pool and displace the roof rocks vertically. If there is such an unconformity present in the Yellowknife Basin, is has not been identified or it has eroded away. The cross-section in Fig. 3.26 (contributed by Wouter Bleeker), which shows the western half of the Slave Province, suggests a laccolithic shape for many of the plutons in the area, correlating well with the models. It is important to note that the isograd to the east of the Prosperous and Defeat Suites dips shallowly to the east, as predicted by the gravity models presented here.

The modelling did not confirm or rule out the presence of the greenstone belt beneath the metasediments of the Yellowknife Basin. Although one scenario seems to be favoured over the other in some of the models, both can be modelled reasonably. The minimum depth-to-basement was easy to determine in the profiles, exclusive of the Cameron 3 Profile,

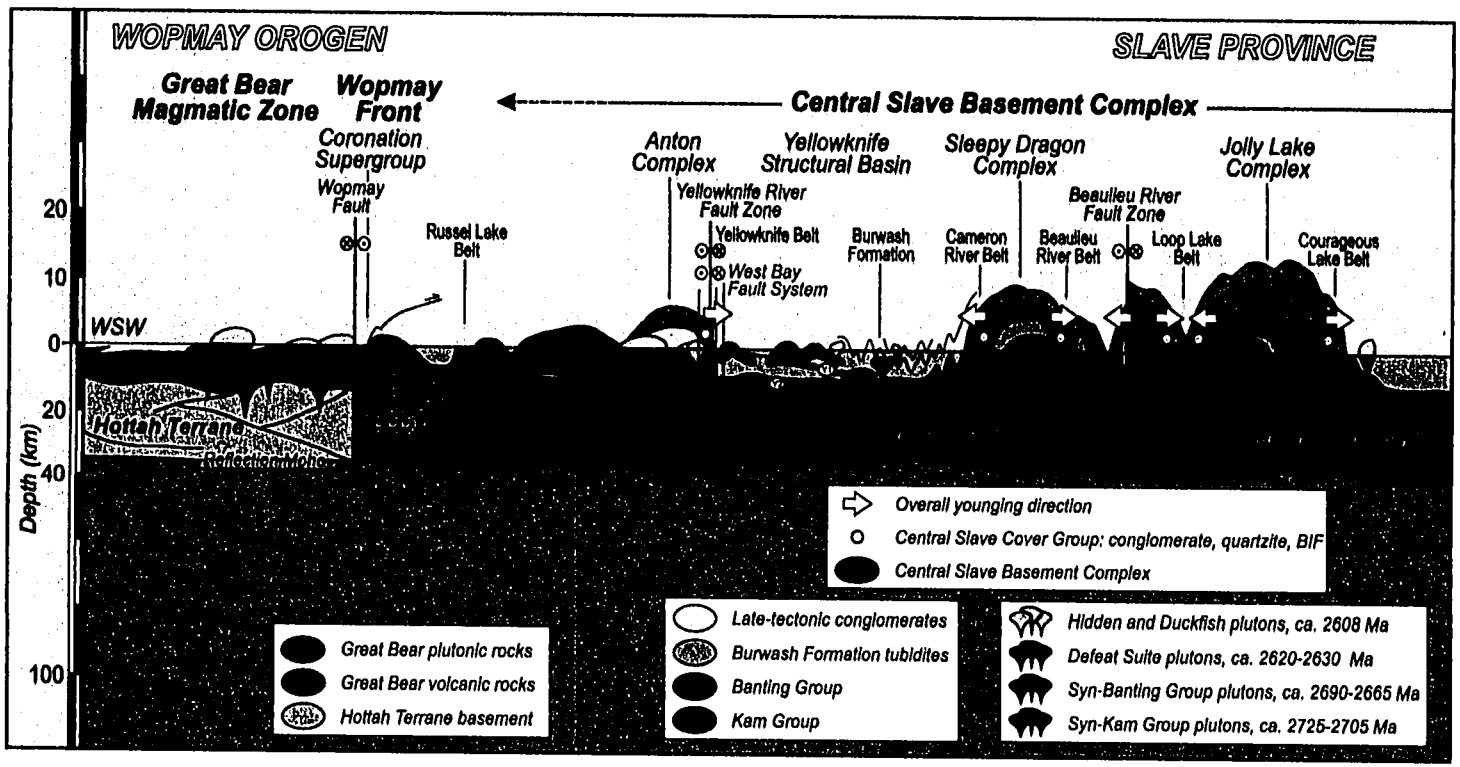

Figure 3.26. Cross-section across the western half of the Slave Province (courtesy of Wouter Bleeker). The Sleepy Dragon Complex, Yellowknife Basin and Yellowknife Greenstone belt are represented in the section.

but the maximum depth-to-basement was more difficult to determine. This is a result of the relatively short length of the profiles. However, the depth-to-basement is constrained at 8-9 km depth with a fair degree of confidence (except in the Cameron 3 Profile) and this is independent of whether the greenstone belt is present beneath the metasediments or not.

For the Yellowknife Profile, the model in which no greenstones extend beneath the metasediments (Fig. 3.9) did not fit the eastern part of the broad high very well, suggesting that the presence of a higher density material beneath the metasediments may be required. Similarly, with the presence of the greenstone belt beneath the metasediments in the Cameron 2 Profile (Fig. 3.18), the Sparrow/Hidden Lake Plutons are of comparable thickness to the same plutons in the Cameron 3 model (Fig. 3.23), whereas, without the greenstone (Fig. 3.19), they are about 0.5 km thinner.

In contrast to this, in the Cameron 1 Profile, the model without the greenstone belt extending beneath the metasediments (Fig. 3.14) gives a more reasonable shape to the Prosperous Suite pluton west of the profile. However, this does not mean that the pluton could not extend as far to the east as the model with the greenstones (Fig. 3.13) suggests.

The modelling provides good constraints on the dips and dip directions of the bodies and the various contacts and it correlates well with Figure 3.26. The dips and dips directions of the greenstone belts have been well constrained, where they outcrop at the surface, dipping moderately to steeply to the east. This is demonstrated by the Cameron 1 and Cameron 2 Profiles, which both cross the Cameron River Greenstone Belt and give a similar steep dip toward the east for the belt. The dips of the greenstone belts are shown in the cross-section as

vertical to steeply dipping, correlating well with the models. Thus, the models provide a further constraint on the nature of the Yellowknife Basin as a structural basin.

A three dimensional view of the models (Fig. 3.27a-d) was constructed by placing the models of the four profiles together in the proper orientation with respect to one another. The figures show the view from the south, north, east-southeast, and west-northwest respectively. In Figure 3.27a, the units are labelled and the lines above the profiles represent the now-eroded portions of the units. This creates a good conceptual model of what the Yellowknife Basin looks like if, indeed, the greenstone belt extends beneath the metasediments of the basin. Where the Yellowknife, Cameron 1, and Cameron 2 Profiles cross, it can be seen that the depth extent and shape of the Sparrow/Hidden Lake Plutons are consistent between the three profiles. This relationship can be seen wherever the profiles meet or cross and each view in Fig. 3.27a-d shows the relationship of the units from a different perspective.

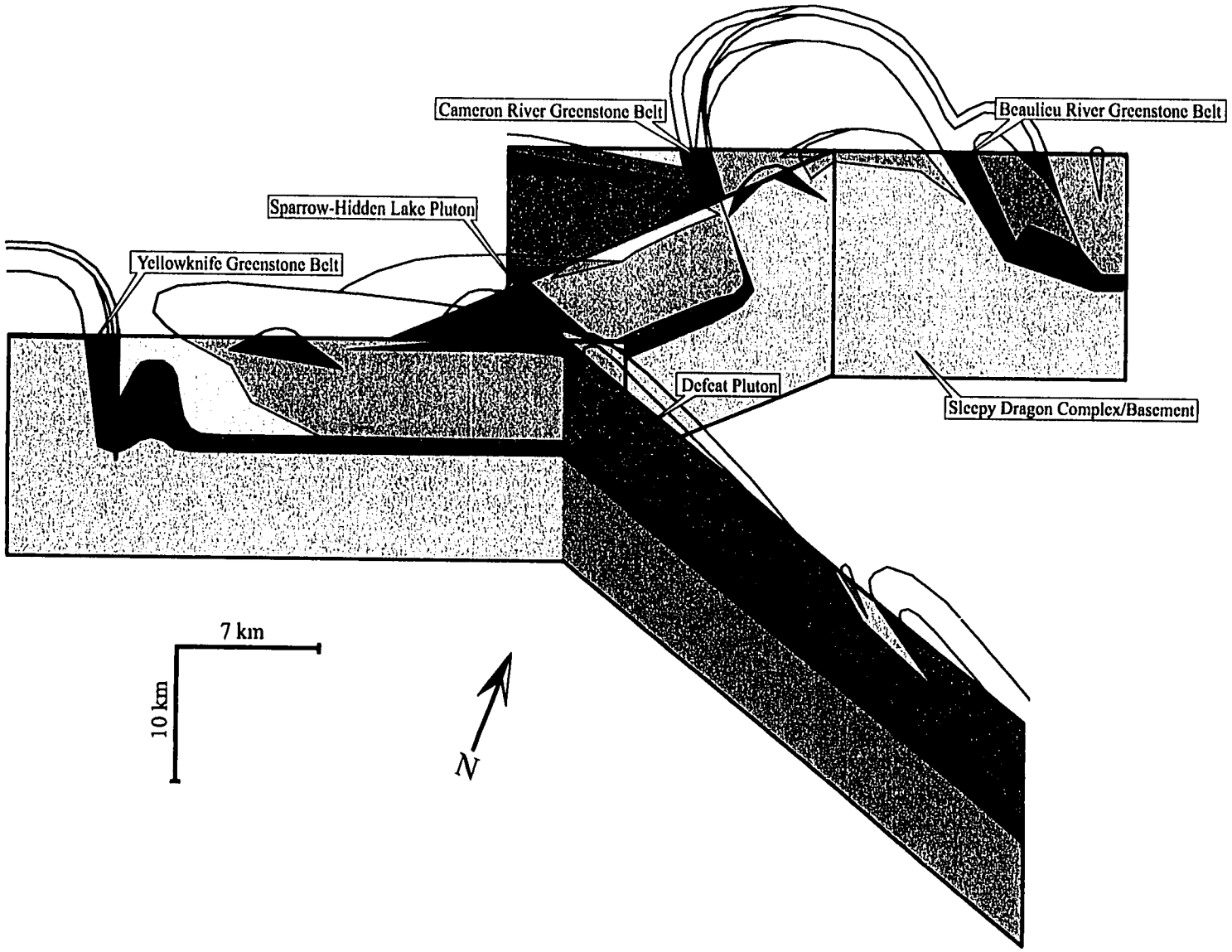

Figure 3.27a. A 3-D model composed of the four profiles. The relationships between the various contacts can be seen, as well as that between the Sparrow and Hidden Lake Plutons. The view is from the south, and Figures 34b-d show the same model viewed from different directions.

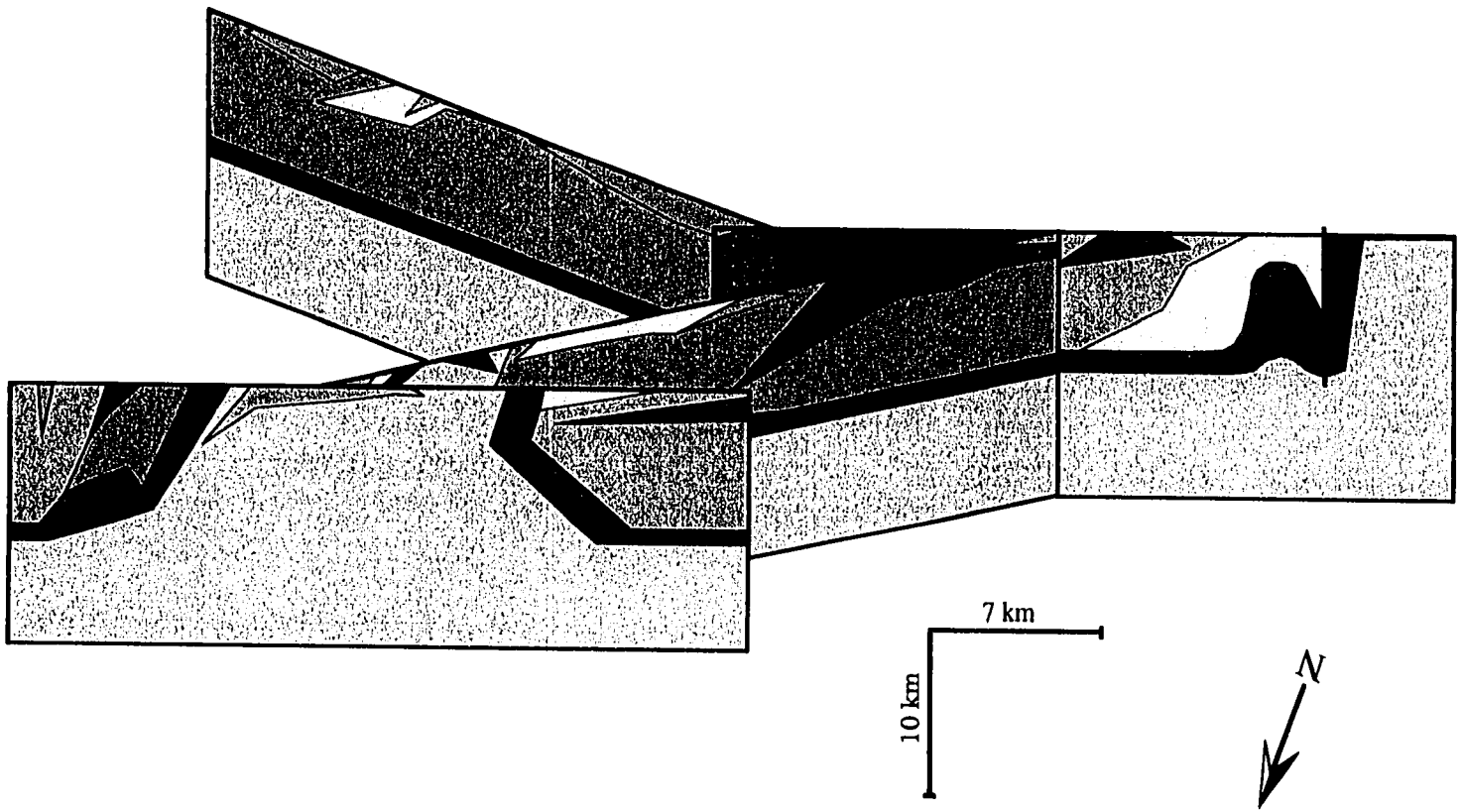

Figure 3.27b. A 3-D model of the four profiles showing their relationship to each other. View is from the north. Refer to Fig. 37a for correlation of units.

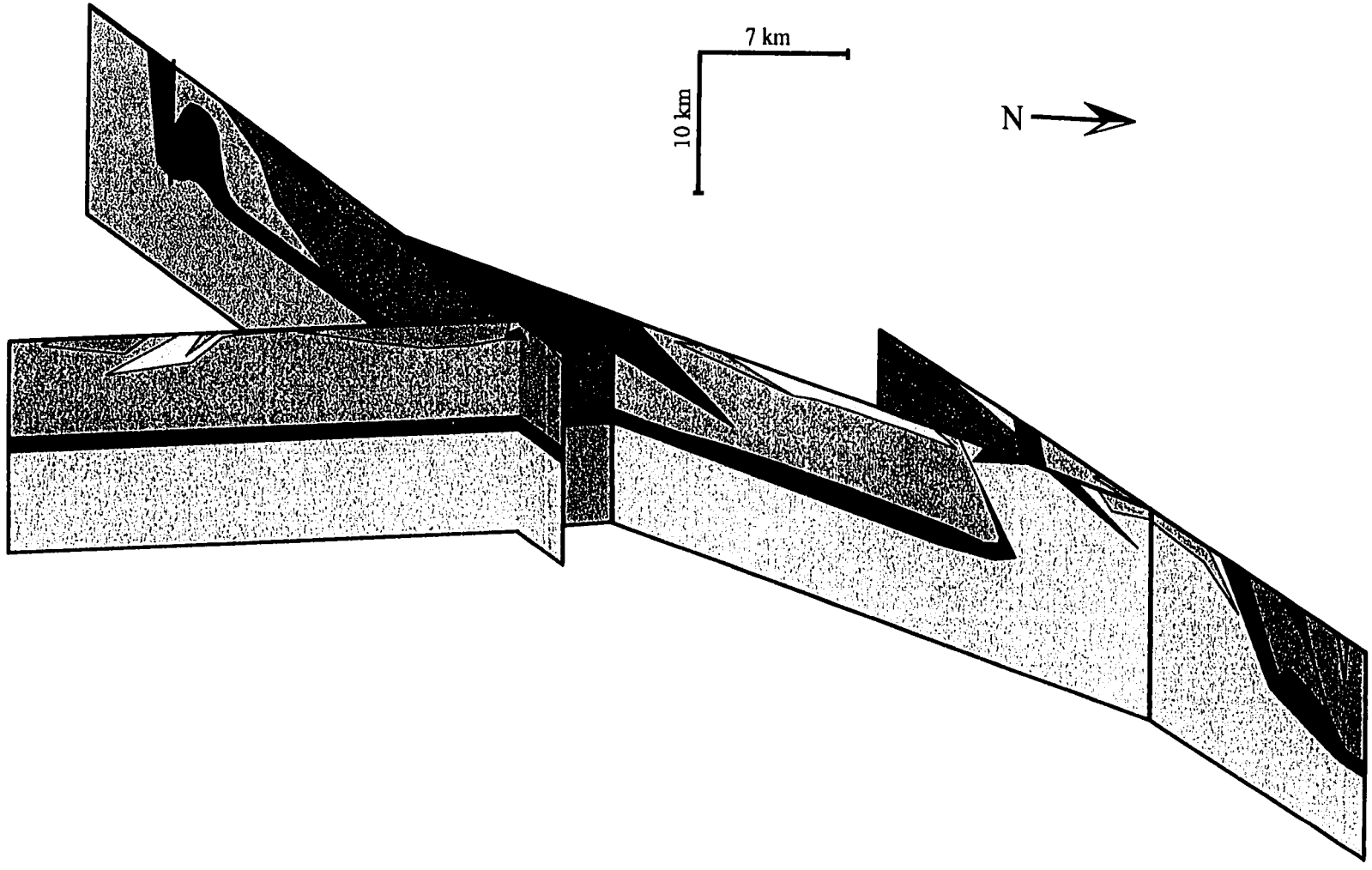

Figure 3.27c. A 3-D model of the four profiles showing their relationship to each other. View is from the east-southeast. Refer to Fig. 37a for correlation of units.

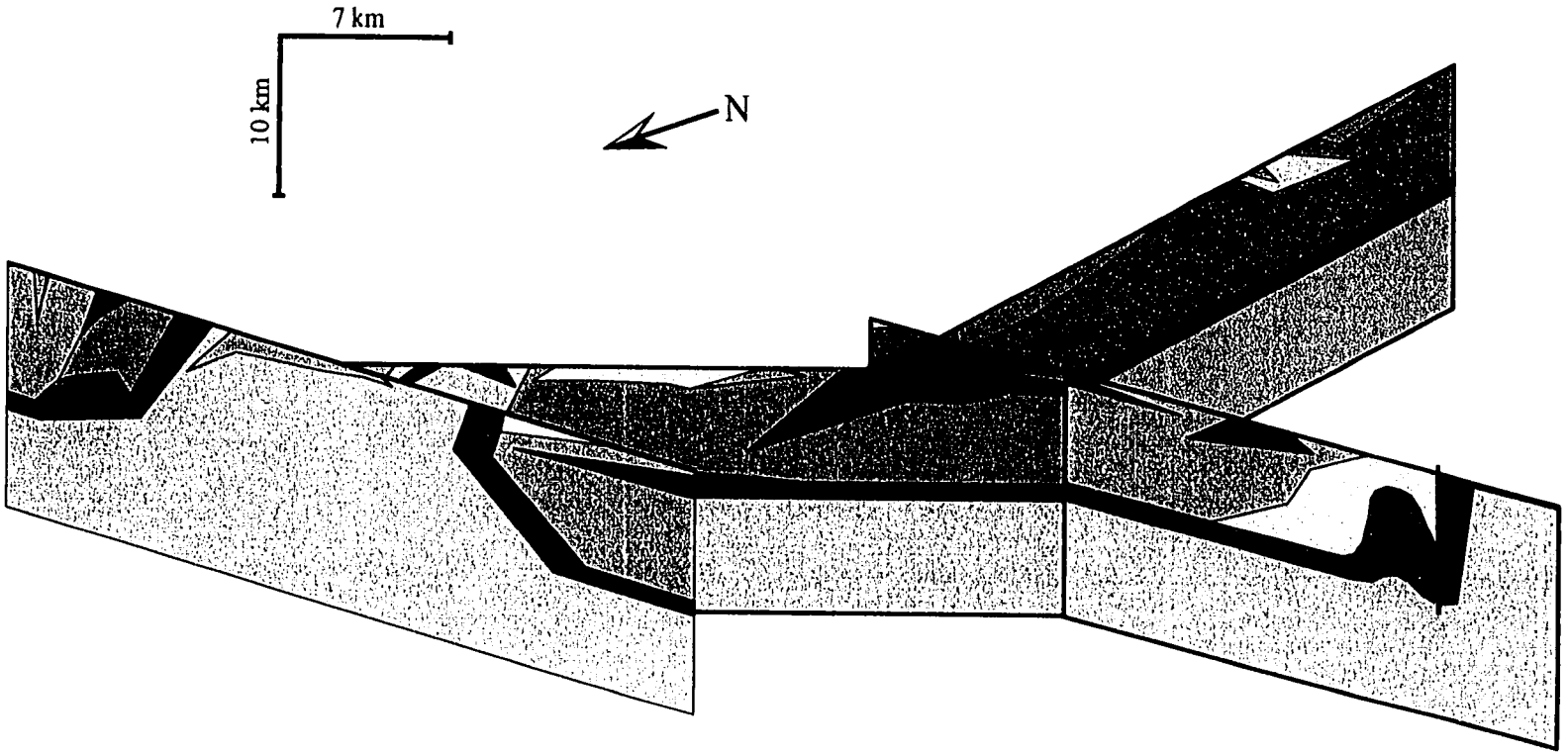

Figure 3.27d. A 3-D model of the four profiles showing their relationship to each other. View is from the west-northwest. Refer to Fig. 37a for correlation of units.

Chapter 4: Reconstruction of the Great Slave Lake Shear Zone

4.1 Introduction

The Great Slave Lake Shear Zone (GSLSZ) forms the southern boundary of the Slave Structural Province. It was active at 2.0-1.9 Ga and is approximately 1200 km long, running southwest from the eastern edge of the Thelon Tectonic Zone to the foothills of the Rocky Mountains. The displacement along the GSLSZ is dextral and the maximum motion along the shear zone is about 700 km. A little less than half of the shear zone is exposed at the surface at its northeastern end, while in the southwest it lies beneath Paleozoic Cover. However, the GSLSZ stands out very well on the aeromagnetic map of Canada as a sharp truncation of the units to the north and south of it (Fig. 4.1). A map of the terrane boundaries can be seen in Figure 4.2. The shear zone is associated with a weak gravity anomaly which shows up on the map as a subtle truncation of units to the north and south of the shear zone (Fig. 4.3). The geology of the GSLSZ is discussed in section 1.52.

The GSLSZ accommodated the convergence, collision, and post-collisional indentation of the Slave Structural Province with the Western Churchill Province. At about 100 Ma following the collision between the SSP and the Western Churchill Province, the Bathurst and MacDonald Fault Zones were formed as a result of the collision of the Hottah Terrane with the western edge of the Slave Province. Thus, before the reconstruction of the GSLSZ can be done, it is essential to remove the effects of this conjugate fault system.

The following section will discuss the removal of the effects of the Bathurst and MacDonald Fault Zones, and the geometry of the compression. Then, the reconstruction of

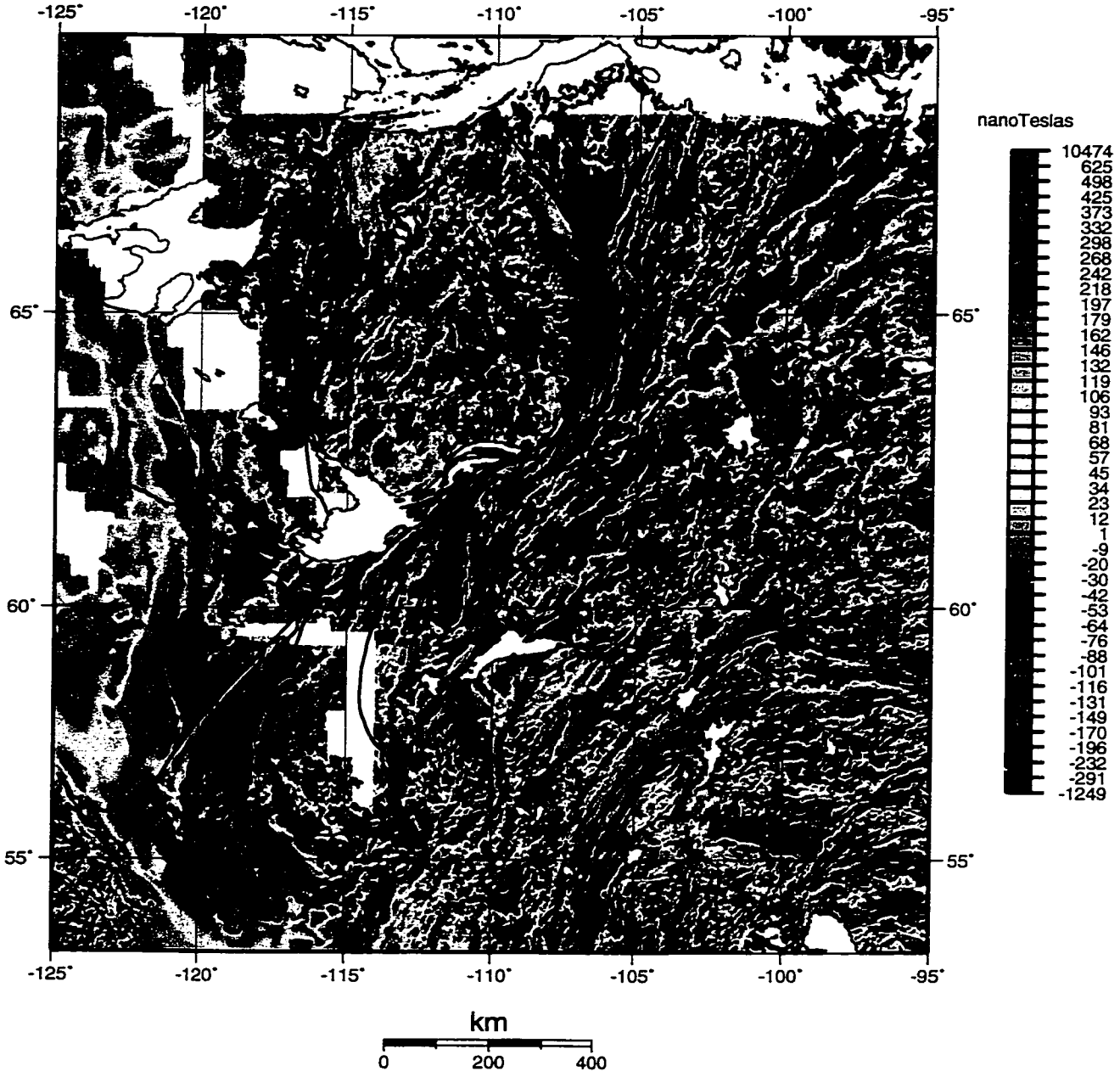

Figure 4.1. The regional aeromagnetic map showing the truncation of units to the north and south of the GSLSZ. The trace of the GSLSZ, the Bathurst and MacDonald Fault Zones, and the terrane boundaries are superimposed on the map.

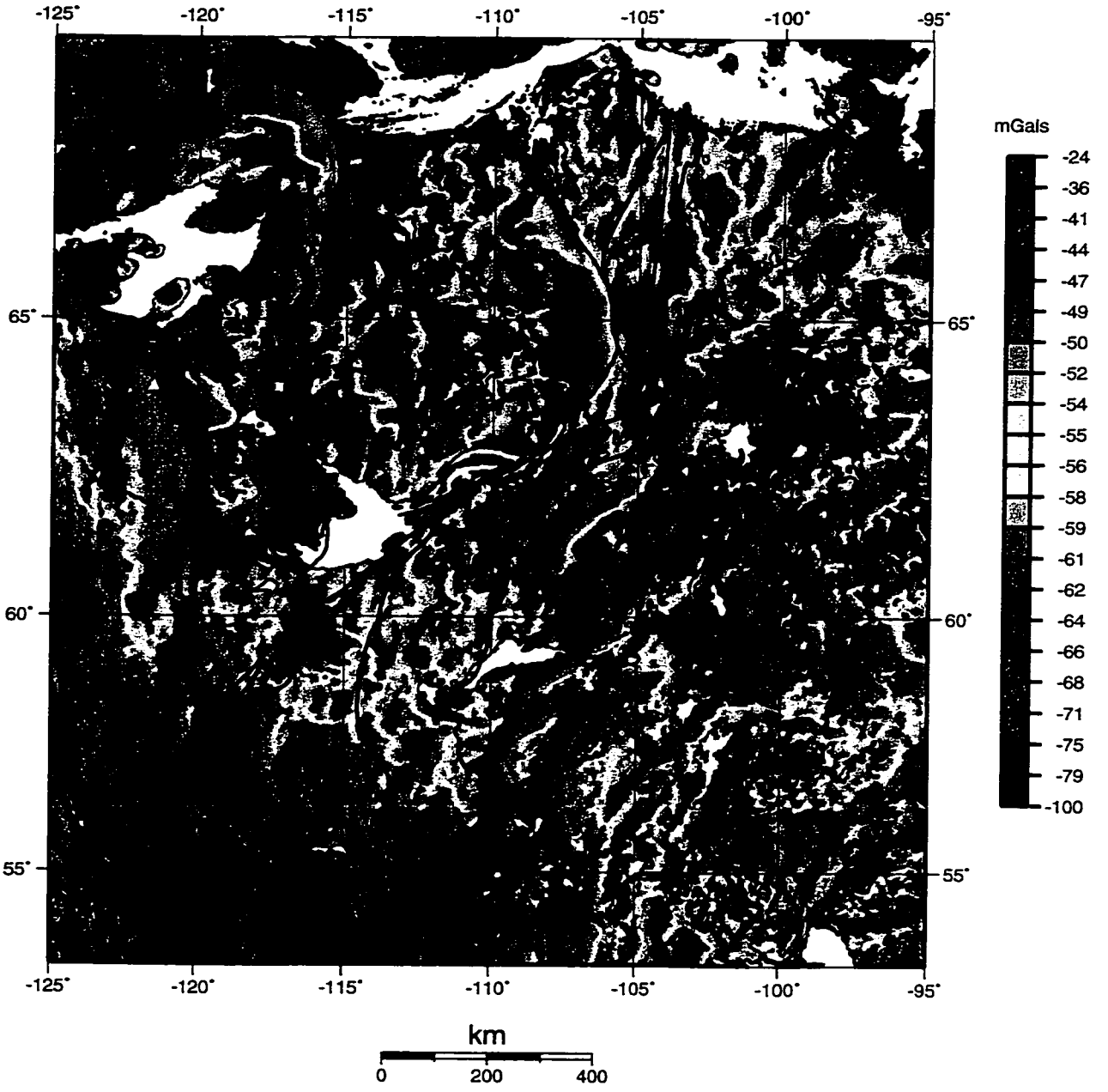

Figure 4.2. The regional Bouguer gravity map showing the trace of the GSLSZ, the Bathurst and MacDonald Fault Zones, and the terrane boundaries superimposed on the map.

the GSLSZ will be presented, with a description of the method used and the rationale behind it.

4.2 The Bathurst and MacDonald Fault Zones

The Bathurst and MacDonald Fault Zones are a conjugate set of transcurrent faults (Fig. 4.3), which bound the Slave Structural Province to the northeast and southeast respectively. The Bathurst Fault Zone trends northwest and the MacDonald Fault Zone parallels the GSLSZ in the south, trending northeast. The motion along these faults is strike-slip; the Bathurst Fault is sinistral and the MacDonald Fault is dextral. The Bathurst Fault has two large fault splays, which visibly displace the Thelon Magmatic Zone on the aeromagnetic map. The MacDonald Fault has one major fault splay, which is interpreted here as the reactivation of the McKee Fault, a splay of the GSLSZ.

The indentation of one body into another must be accompanied by compression and/or escape of some material. Gibb (1978) presents such a model for the Slave-Churchill indentation, in which he postulates compression of material at the apex of the indentor, as well as the escape of small blocks of material to the north and south of the wedge. He inferred the faults that allowed for this escape from magnetic lows in the regional aeromagnetic data and assumed indentation normal to the Slave-Churchill boundary.

The model presented here is a variation on Gibb's model, with compression in the apex of the indentor and the escape of one small block of material to the north (compression is accommodated by thrusting and subduction). Three scenarios were examined as

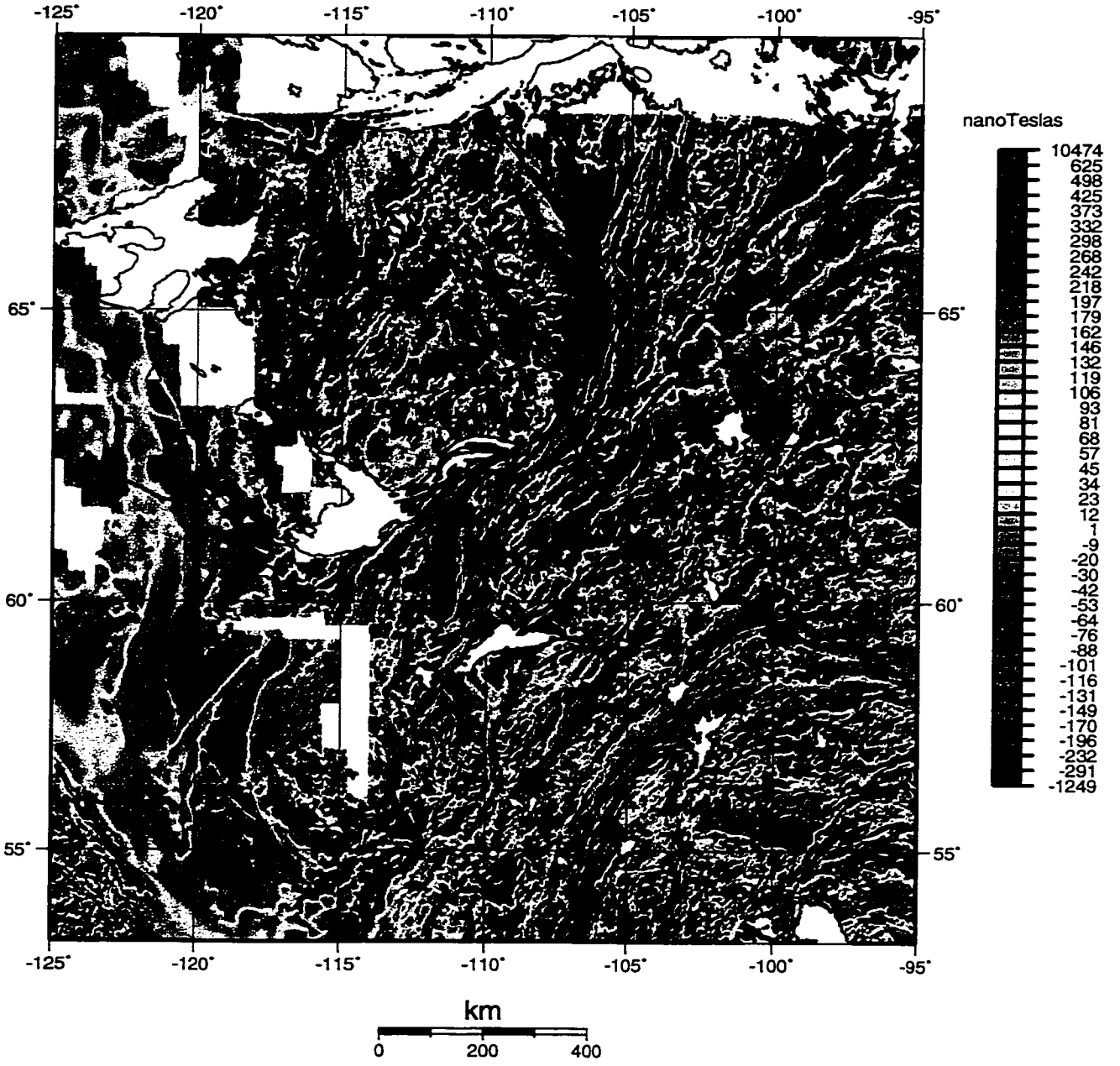

Figure 4.3. The Bathurst (northern) and MacDonald (southern) fault zones superimposed on the regional aeromagnetic map.

possibilities for the geometry of the indentation. In all three scenarios, the motion along the fault splays were reconstructed, in order to undo the deformation, by a simple cut and paste procedure in order to align the magnetic fabric of the regional aeromagnetic map along each fault. The motion along the reactivated McKee fault accommodates clockwise rotation of a block of material.

The first scenario is a simple compression model, with no escape of material (Fig. 4.4). Motion along the fault splays were reconstructed, but along the main faults the motion is highly transpressive. This does not fit well with the known transcurrent motion of the fault zones. Therefore, this scenario can be ruled out.

The second scenario includes the escape of a small block of material to the north, along a strike-slip fault at the western edge of the Thelon Magmatic Zone (Fig. 4.5). Again, the fault splays were reconstructed. However, in this scenario, strike-slip motion is only possible along the northwestern half of the Bathurst Fault; the southeastern portion would still undergo a large amount of transpression. Thus, this scenario can also be ruled out.

The third and final scenario is similar to the second in that it incorporates compression and escape of a northern block of material (Fig. 4.6). The escape fault has been inferred from the regional aeromagnetic map, and trends north-south from the southeastern end of the Bathurst Fault to the Queen Maude Gulf. This is the preferred model, as it accommodates transcurrent motion along the entire Bathurst Fault, as well as the MacDonald Fault and the fault splays.

The Bathurst Fault displaces the Thelon Magmatic Zone approximately 18 km, which

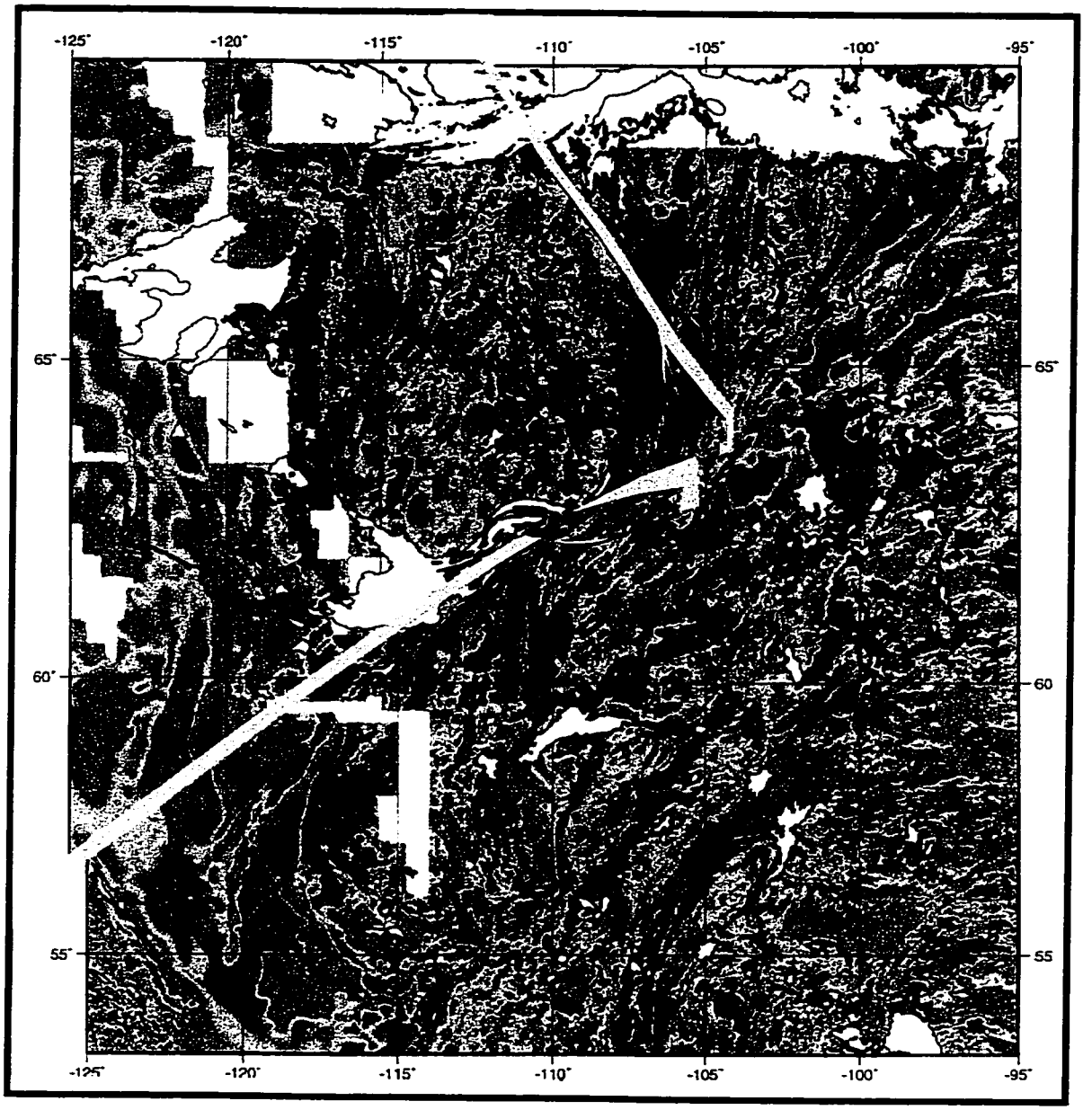

Figure 4.4. A simple compression model for movement along the Bathurst and MacDonald Fault Zones. There is no escape of material. Areas that would experience compression are shaded in gray.

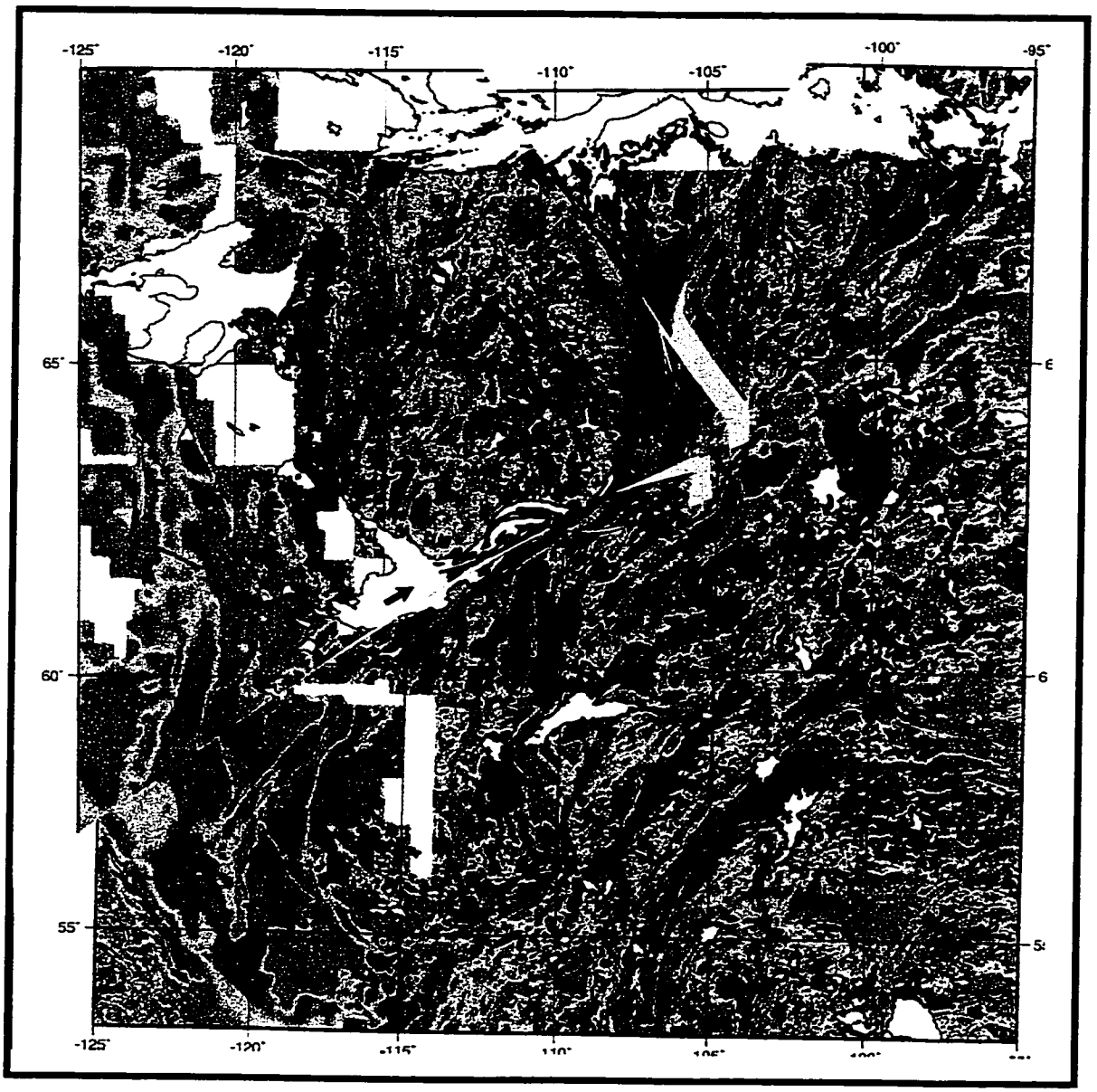

Figure 4.5. A model for movement along the Bathurst and MacDonald Fault Zones, with both compression and escape to accommodate the indentation. The escape fault is located at the western edge of the Thelon Magmatic Zone. Areas that would experience compression are shaded in gray.

Figure 4.6. The preferred model for movement along the Bathurst and MacDonald Fault Zones. There is compression and escape of material to accommodate the indentation. The escape fault is inferred from the regional aeromagnetic map. Areas that would experience compression are shaded in gray.

is consistent with the results of Thomas et al. (1976). Its northern and southern fault splays displace the Thelon Zone about 20 km and 10 km respectively. The MacDonald Fault Zone's displacement is closer to the Thomas et al. (1976) estimate of 70 km. The motion along the reactivated McKee Fault splay accommodates approximately 15° of rotation of a small block of material.

Thus, there are two primary results of this model. The model shows that escape probably played a role in the indentation of the Slave Province into the western Churchill. The escape fault, inferred from the regional magnetic map, accommodates the escape extremely well. In addition the model indicates that the indentation was directed more toward the northeast than the assumed eastward indentation of Gibb's (1978) model.

The strain pattern was constructed by extracting the present day magnetic values at their paleo positions and then gridding these values against the present day latitude and longitude. The strain pattern resulting from the reconstruction is shown in Figure 4.7 and the final result of the reconstruction is shown in Figure 4.8, with the terrane boundaries superimposed on the aeromagnetic map (note that the areas of compression are not filled with gray as in Figures 4.4-4.6). This reconstructed framework is the starting point in the reconstruction of the GSLSZ.

4.3 Reconstruction of the Great Slave Lake Shear Zone

When determining the strain pattern resulting from the convergence and subsequent collision between the Slave Province and the Western Churchill Province, it is important to

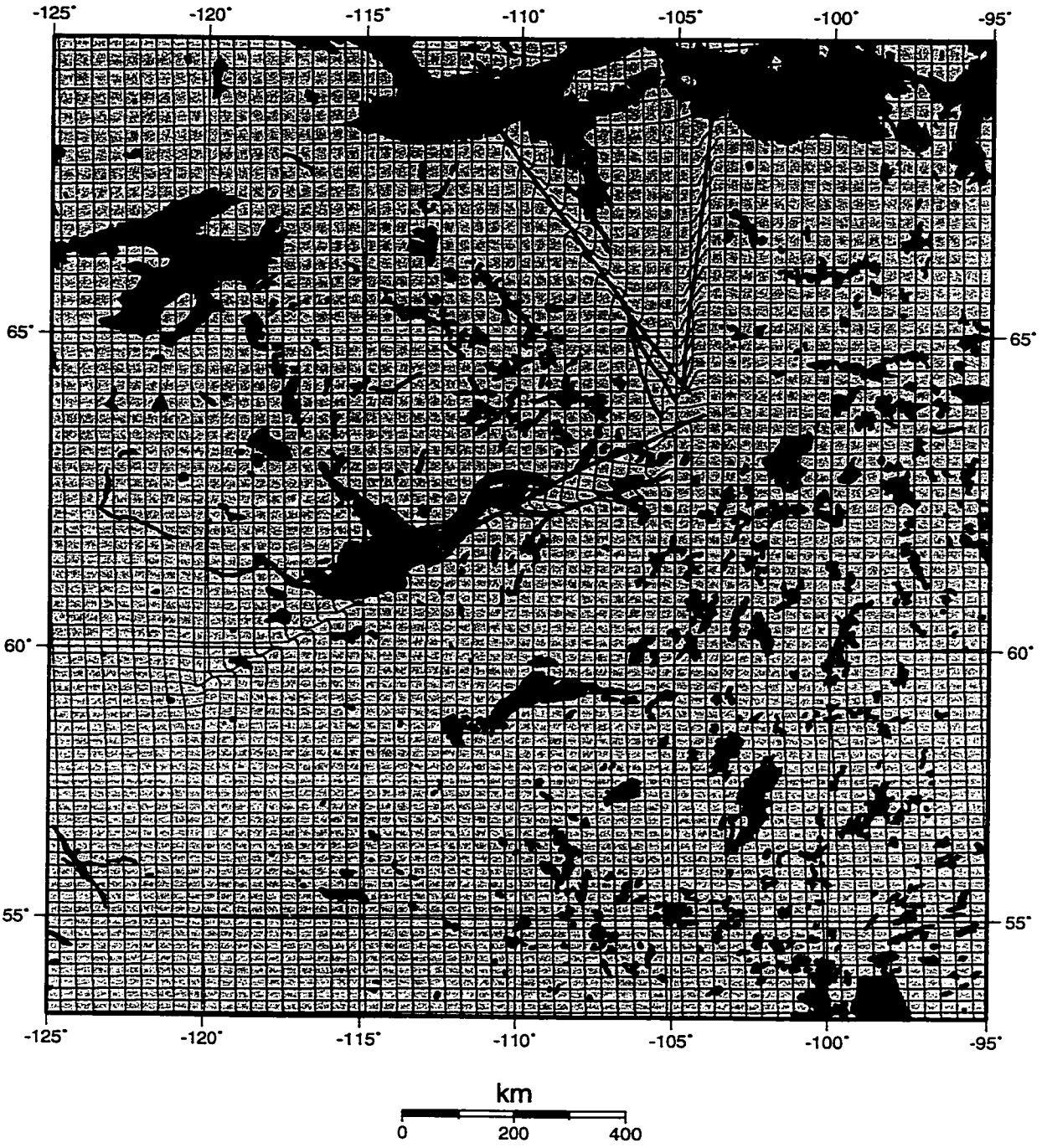

Figure 4.7. A contour map showing the strain pattern resulting from the reconstruction of the Bathurst and MacDonald Fault Zones.

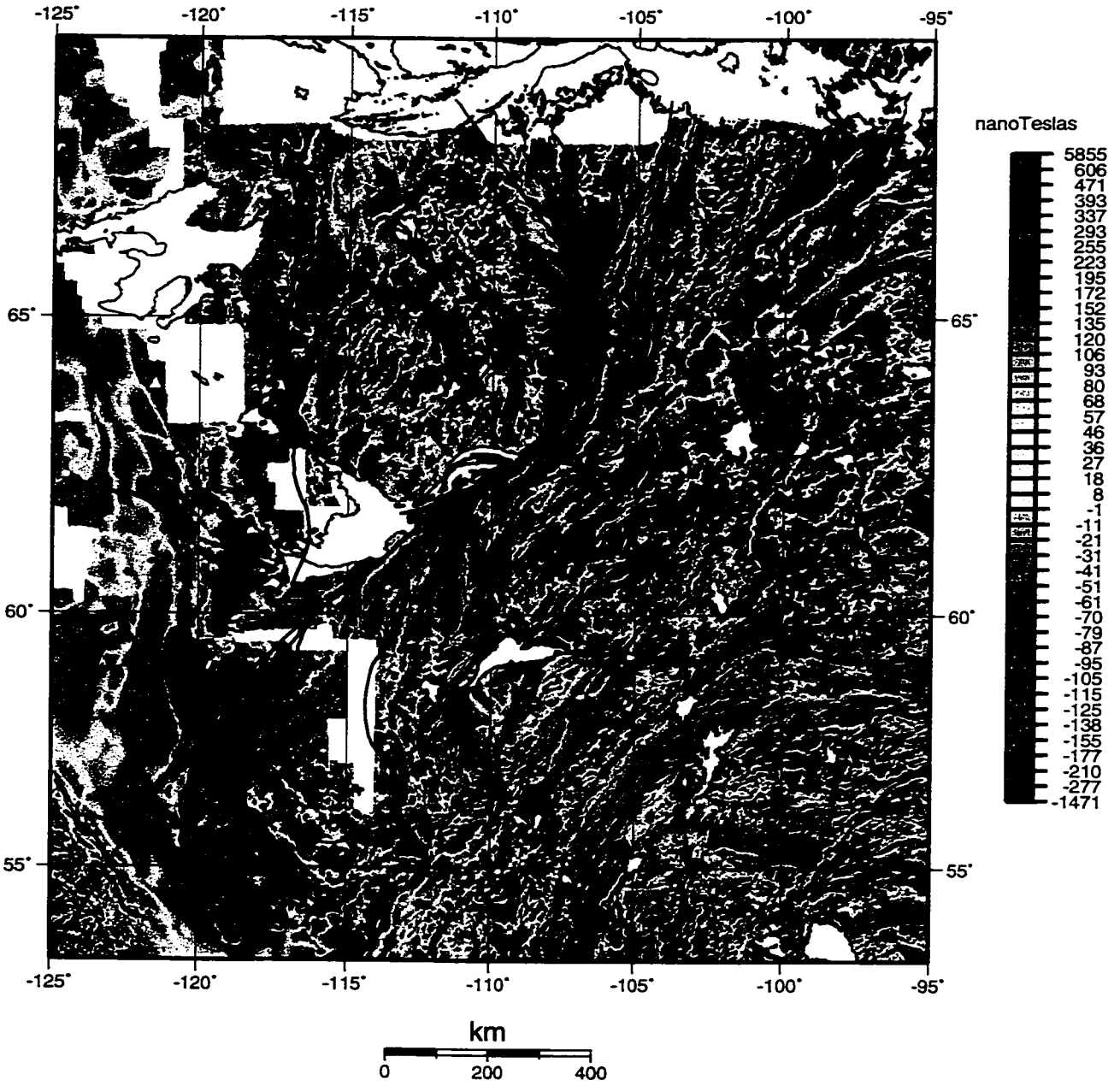

Figure 4.8. The regional aeromagnetic map after the effects of the Bathurst and MacDonald Faults are removed. Strained areas (shaded in gray in Fig. 4.4-4.6) indicate areas that will experience compression. The terrane boundaries and fault traces are superimposed on the map.

consider the conditions prior to collision, particularly the respective plate geometries. Figure 4.9 shows a cartoon depicting nine possible combinations of plate geometries, which include combinations of curved and straight geometries. Scenarios A-C have a straight Churchill geometry, D-F have a curved Churchill geometry trending to the northeast, and G-I have a curved Churchill geometry trending northwest. We realize that these are the extreme cases and that there are other possible plate geometries that could be considered, but we have reduced the scenarios to those that would result in the bulk of the compression occurring in the CSP north of the shear zone.

The convergence direction of the Slave Province relative to the Churchill Province was to the northeast at a small angle to the direction of the shear zone (Hoffman, 1987). Of the combinations in Figure 4.9, figures C and F can be ruled out as possibilities. In C, the geometries are straight and parallel. As the SSP converges and collides with the CSP, the geometries will collide and the strain will be distributed evenly along the contact between them. This does not account for the high amount of compression north of the GSLSZ, perpendicular to the trend of the Thelon Magmatic Zone, compared to south of the shear zone. In F, the Slave geometry remains straight, but the Churchill geometry is curved such that, as they converge, the SSP will first come in contact with the Churchill south of the shear zone. This will result in greater compression south of the shear zone. Again, this is inconsistent with the bulk of the compression having taken place north of the shear zone, and the shear zone is more likely to form in the Slave Province rather than in the Churchill Province.

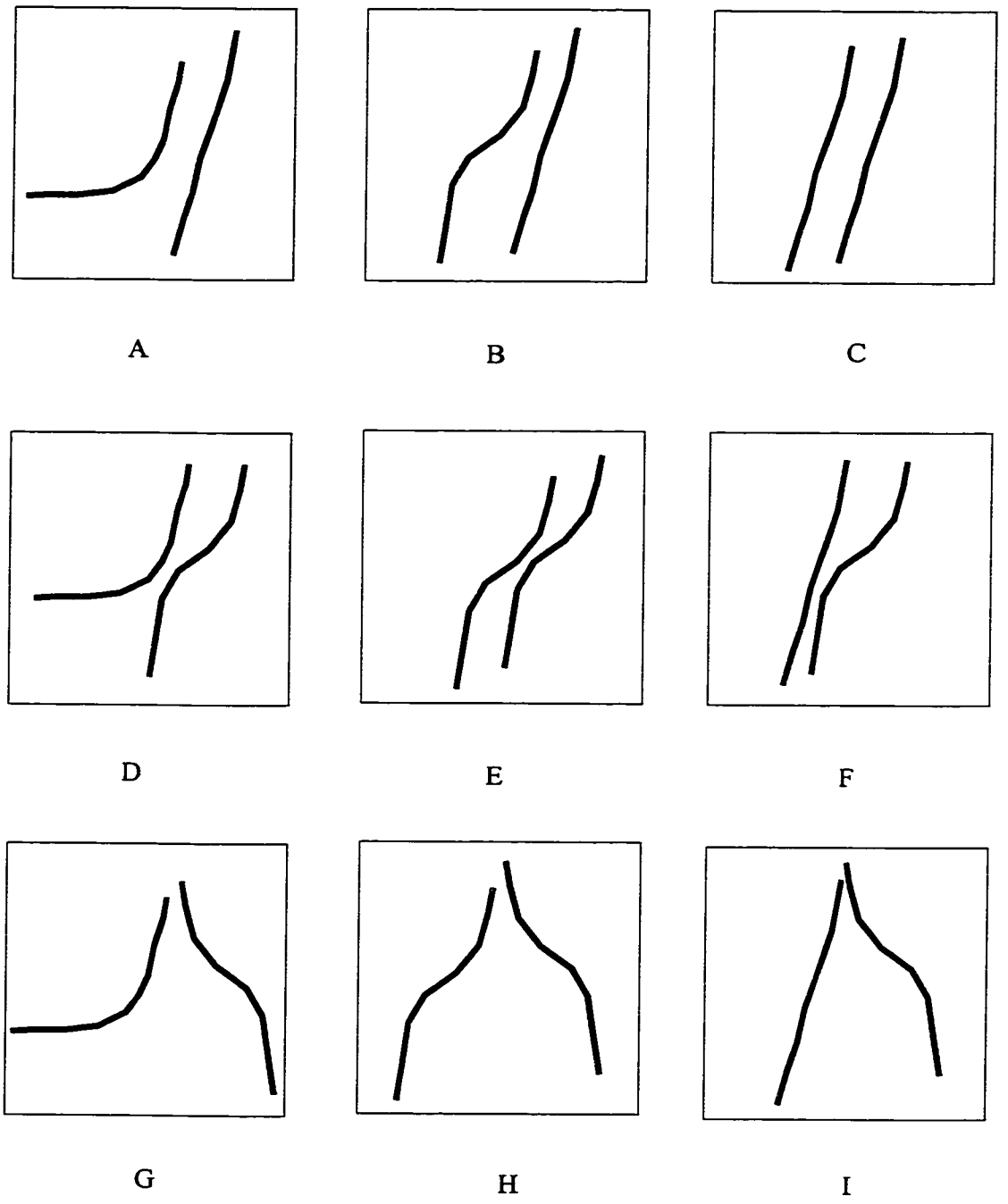

Figure 4.9. Presented here are different possible plate geometries for the Slave Province (red) and the Western Churchill Province (blue) at the time of convergence and collision. Figures A-C, D-F, and G-I show combinations of different Slave geometries with a relatively straight Churchill geometry, a curved (northeast-trending) Churchill geometry, and a curved (northwest-trending) geometry, respectively.

Scenario E considers the situation where both geometries are curved and parallel. In this situation compression will be evenly distributed north and south of the shear zone.

The other six scenarios result in the largest amount of compression taking place north of the GSLSZ. In B, the Churchill geometry is straight and the Slave geometry is curved, such that when collision takes place, the northern part of the Slave comes in contact with the Churchill Province first, creating the greater amount of compression there. In scenarios H and I, the northwest-trending, curved Churchill geometry collides with a northeast-trending, curved SSP geometry and a straight SSP geometry respectively. In scenarios A, straight Churchill geometry, and D, curved Churchill geometry, the Slave Province's geometry is not continuous, but curves to the west, forming a block of material with a defined southern boundary. Senarios D and E are supported by geological (geochronology and kinematic) evidence. Hanmer et al.(1995) proposes a jagged northeast-trending Churchill plate geometry. They suggest that two reentrants were present: one located at the Virgin River Shear Zone (which may have accommodated the docking of the Buffalo Head Terrane) and the other located at the GSLSZ. In the case of the GSLSZ, older (pre-2.56 Ga) mylonites are present, which supports this as having been the location of the reentrant. It would appear that these reentrants controlled the orientation of the shear zones to some degree.

The following reconstruction is based on scenario D, since it is the simplest case and the southern extent of the SSP is unknown. This method can be applied to the other scenarios as well, but due to time constraints it was not possible to do so in this study.

The primary fault trace of the GSLSZ conforms to a small circle about the pole of

relative motion between the SSP and the CSP (Fig. 4.10; error limits have not been calculated). This pole is located at 31.5N and 88Wand fits the small circle with a standard deviation of approximately 2 km. In order to restore the motion along the shear zone, the shear zone, the terrane boundaries, and the data from the regional magnetic grid were transformed in the coordinate system of the rotation pole so that the shear zone lies on a common latitude. The terrane boundaries were then rotated in segments, anticlockwise, with the southern end of each segment anchored. This results in an east-west translation of the units bordering the shear zone, unshearing them and removing the compression from the units north of the shear zone, and gives a value for each point, which is equal to the shift in longitude.

These data were gridded to produce a grid of the value of the longitudinal shift in the present day latitude and longitude coordinates. The data were extracted from this grid and the values were added to the present-day longitude values to give the paleo-longitudes. The data were transformed back into the original framework and the present-day latitude and longitude values were gridded as a function of the paleo-values. The contour map depicting the strain patterns of these grids are shown in Fig. 4.11. Note the large, stretched area north of the shear zone indicating that a large amount of compression occurred. There is also a small area south of the shear zone, just to the south of the larger area, that underwent compression due to the large amount of transpression experienced by the northeastern segment of the shear zone (Hanmer et al., 1992).

In the transformed framework, the magnetic data were used to extract the values from

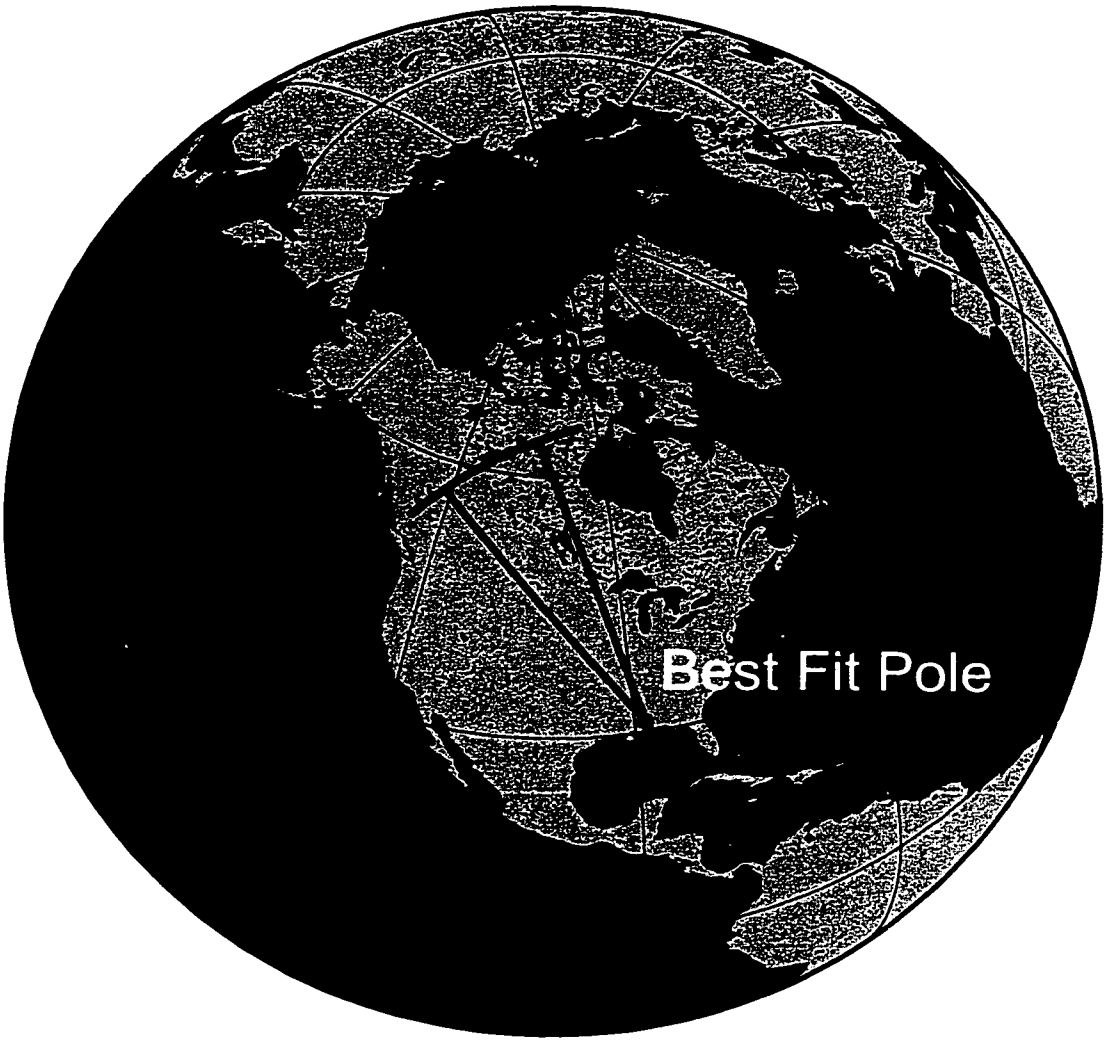

Figure 4.10. The trace of the Great Slave Lake Shear Zone conforms to a small circle about a pole at 31.5N and 88W. The Root Mean Square fit is approximately 2 km.

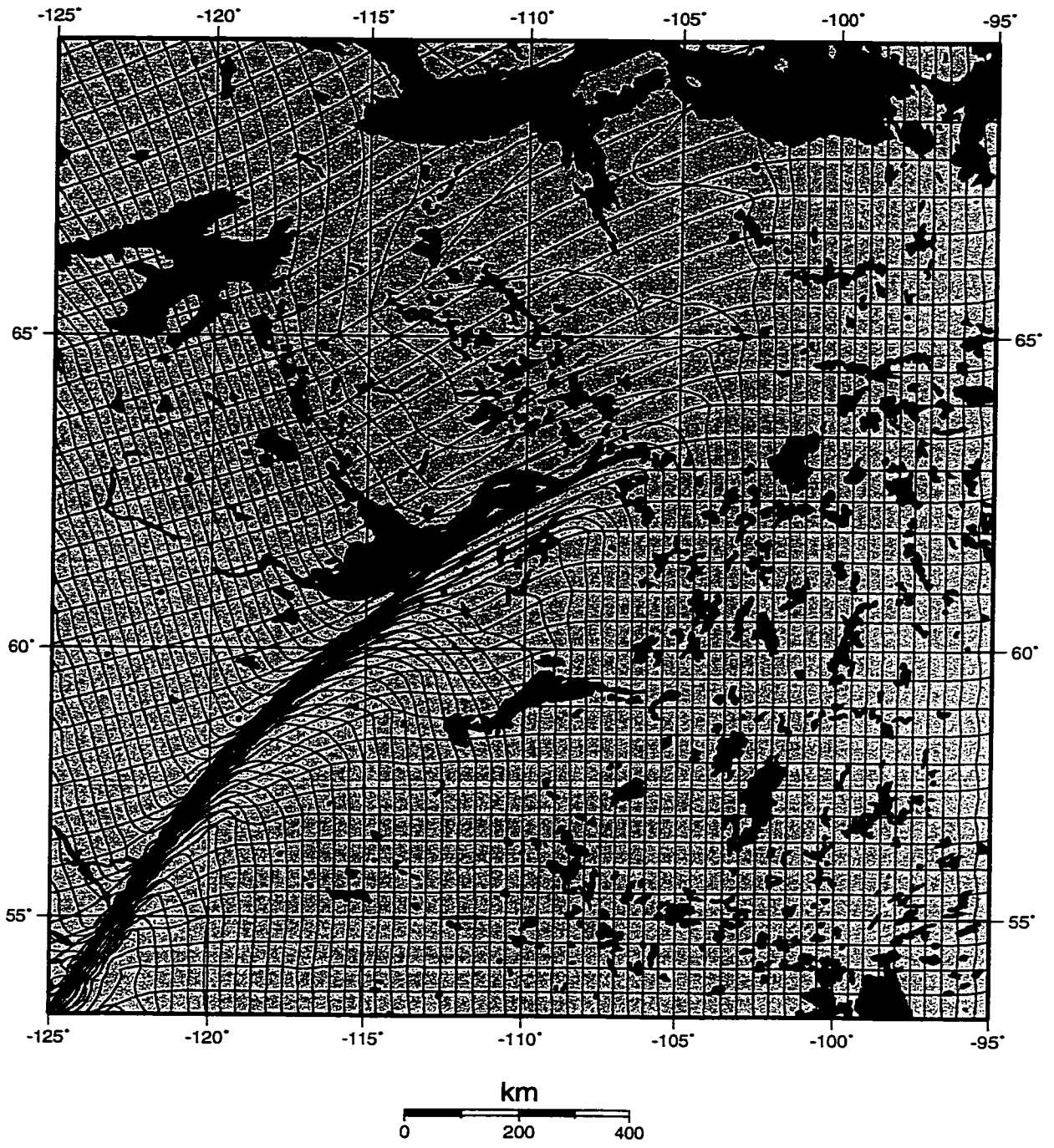

Figure 4.11. The contour map showing the strain pattern resulting from the reconstruction of the Great Slave Lake Shear Zone.

the grid of the translation values in the present-day coordinate system. This set of data was then transformed into the original framework and gridded to give the pre-collisional strain pattern of the magnetic data in the present-day coordinate system (Fig. 4.12). Note that the areas that undergo compression during the collision are blocked in white, as the mechanism of compression is unknown and we do not know what was there prior to collision.

4.4 Discussion

One of the most significant features of the strain pattern of the reconstruction is the rotation of the Slave Province as it converged and collided with the western Churchill Province. In the reconstruction presented here, this rotation was approximately 16° in a clockwise direction, and is attributed to the curved nature of the shear zone. This is because a clockwise rotation of the SSP with respect to the Western Churchill Province would result in sinistral motion along the Thelon Tectonic Zone, and motion along the Thelon Tectonic Zone has been documented as dextral (Hanmer and Lucas, 1985 and Hanmer, 1988). The other significant result of the reconstruction is the location of the areas that underwent compression during the convergence and subsequent collision. The largest area of compression to the north has been partially taken up by the Thelon Magmatic Zone (as can be seen on the present day magnetic map). It is important to remember that the Thelon/Taltson Magmatic Zone was being formed at the same time the convergence and collision were taking place and that there was other material involved in the compression. The smaller area of compression occurs to the south of the larger one and south of the shear zone. The eastern

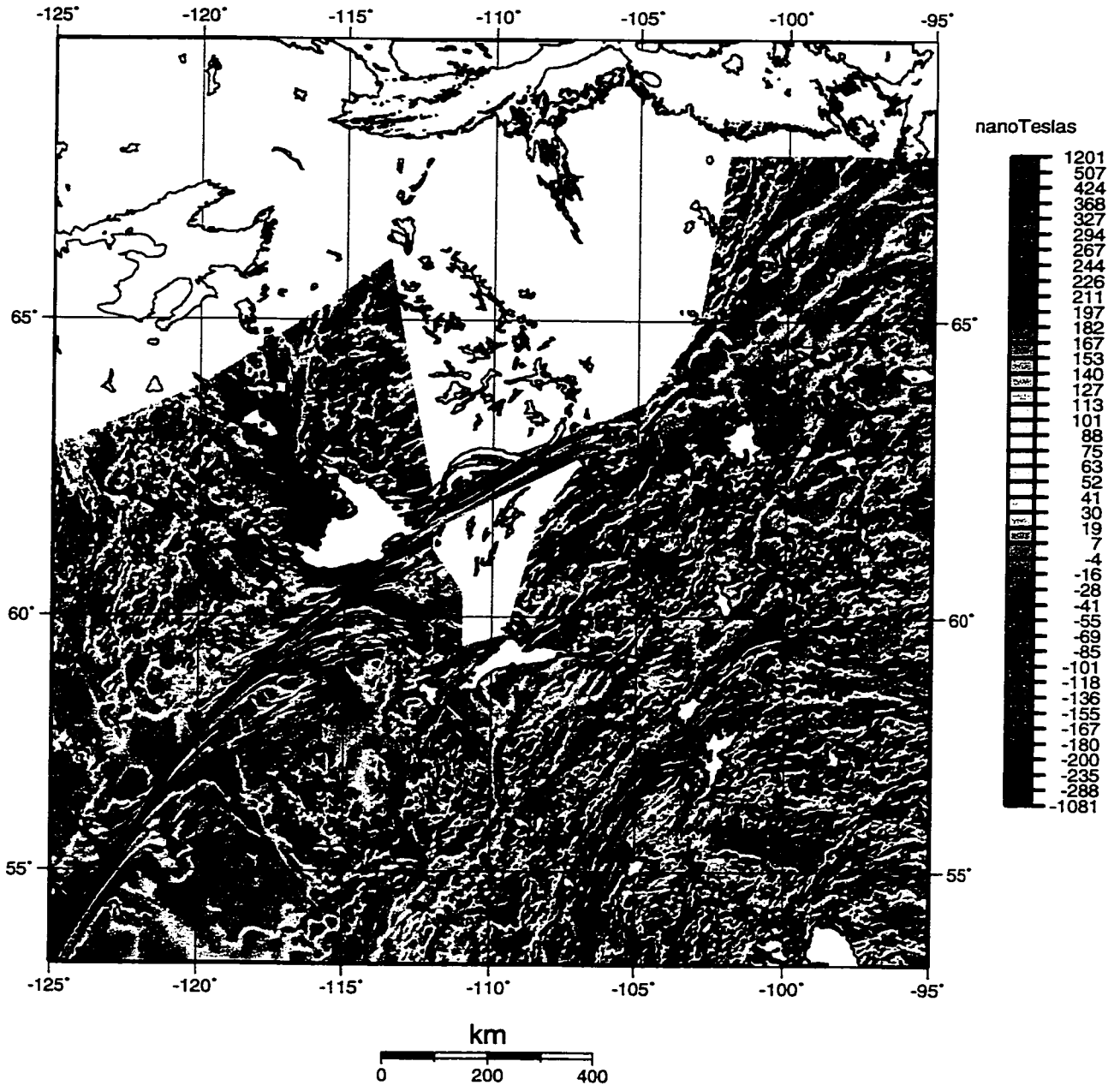

Figure 4.12. The regional aeromagnetic map after the reconstruction of strike-slip motion along the GSLSZ. The areas blocked out in white are areas where compression takes place during the convergence and collision.

boundary of this area coincides with the northeastern limit of the shear zone so compression would be expected here, as no compression occurs east of this or of the eastern limit of the Thelon Magmatic Zone.

In the present reconstruction, the Slave Province is juxtaposed against the units south of the shear zone, except for the Taltson Magmatic Zone, which lines up with the Thelon Magmatic Zone. This is expected as they are the only two units that have been demonstrated, on the basis of geological, geochemical, and geochronological studies, to belong to the same unit (see sections 1.36 and 1.37). The ages and geology of the other units south of the shear zone are quite distinct from those of the Slave Province that lies to the north, and they are older than the shear zone. It is possible that some or all of the units south of the shear zone were lost in the compression that took place to the north. It is also possible that these units never continued further to the north. In light of this, the present reconstruction cannot aid in the correlation of the units.

This reconstruction represents only one stage, that of strike-slip motion, in the collisional process and the development of the GSLSZ. The earlier dip-slip component and any later movement has not been addressed. The mechanism of escape has not been used in this model as no possible escape faults could be identified from the regional aeromagnetics (although it is suggested in the regional geology by the presence of N-S-trending sinistral and dextral mylonites present along the eastern boundary of the Taltson Magmatic Zone; Hanmer et al., 1992). It is assumed that the present erosion surface shows the ductile component of the shear zone and that the brittle component has been eroded away. Thus, escape tectonics

may have played a significant role in the collisional process.

This reconstruction has helped to constrain the geometry of the convergence and collision between the Slave Province and the western Churchill Province. In the future this method may be applied to the other plate geometries shown in Fig. 4.8. This may further constrain the geometry of the relative motion between the two provinces and it may also help to constrain the plate geometries themselves.

Conclusions

This was a two part study focussed on: 1) gravity modelling of profiles in the south-central Slave Structural Province and 2) a reconstruction of the Great Slave Lake Shear Zone using the regional magnetic fabric. Each part focuses on a unique aspect of craton building.

In the Slave Province the gravity modelling provides excellent constraints on the shapes and depth extents of the plutons are also extremely well constrained, defining them as laccolithic units 1-2 km thick, which have a folded geometry. The plutons were emplaced in a compressional environment and folding probably took place during or after folding. In addition, the depth extent and shapes of the greenstone belts, where they outcrop at the surface, are well constrained by the gravity modelling, indicating that they dip steeply to the east. This agrees with the cross-section in Fig. 3.26.

It was not possible to confirm or rule out the presence of the greenstone belt beneath the metasediments of the Yellowknife Basin, one of the original goals of this study, as either model is feasible. Despite this, the depth-to-basement has been fairly well constrained at about 8-9 km, regardless of the presence or absence of the greenstones beneath the metasediments. Although this basin may have had a history of extension, considerable compression has taken place, both natural phases of craton construction. In the future, generation of a 3-D model may aid in further interpretation.

In the second phase of the study, a larger and more recent phase of craton building was examined. Different combinations of plate geometries for the Slave and Churchill Provinces were considered, but the model was only applied to one of them. The

reconstruction of the GSLSZ did not result in correlation of the units to the north and south of the shear zone, except for the correlation of the Thelon and Taltson Magmatic Zones as one unit, but it did constrain the geometry of the motion along the shear zone, showing a northeast movement of the Slave Province relative to the Churchill Province (similar to the motion of the Hottah Terrane with respect to the Slave Province). It also resulted in a 16° rotation of the Slave Province with respect to the Churchill province.

Before the reconstruction along the shear zone could be done, the effects of the Bathurst and MacDonald Fault Zones had to be removed. The same method was applied to both reconstructions and it was found that escape tectonics probably played a role in the indentation of the Slave Province into the Churchill Province. In addition, the motion of the indentation was directed toward the northwest, indicating that the motion of the Hottah Terrane was northwest with respect to the Slave Province.

Thus, the two phases to this study show different aspects of craton formation and compression. Each event is widely separated in time, but may have developed in similar stages, and they both contributed to the formation of what is now the North American Craton.

References

Benn, K., Roest, W., Rochette, P., Evens, N.G., and Pignotta, G.S., 1999. *Geophysical and structural signatures of syntectonic batholith construction: the South Mountain Batholith, Meguma Terrane, Nova Scotia*; in Geophys. J. Int., v. 136, p. 144-158.

Bleeker, W. and Beaumont-Smith, C., 1995. *Thematic structural studies in the Slave Province: preliminary results and implications for the Yellowknife Domain, Northwest Territories*; in Current Research 1995-C, Geological Survey of Canada, p.87-96.

Bleeker, W, Villeneuve, M., and Bethune, K., 1997. *Thematic structural studies in the Slave Province, Northwest Territories: contrasting basement/cover relationships on the western and southwestern flanks of the Sleepy Dragon Complex*; in Current Research 1997-C, Geological Survey of Canada, p. 27-37.

Bleeker, W. and Ketchum, J., 1998. *The Central Slave Basement Complex: its autochthonous cover, décollement, and structural topology*; in Current Research 1998-C, Geological Survey of Canada, p. 9-19.

Bleeker, W., Cooper, R.V., Berrigan, M.E., Roest, W.R., and Hendry, K.A.B., 1998. *Detailed gravity profiles across the Sleepy Dragon Complex and adjacent parts of the Yellowknife Domain, Slave Structural Province: preliminary data*; in Current Research 1998-C, Geological Survey of Canada, p. 1-8.

Bleeker, W and Davis, W.J.,1999. *The 1991-1996 Slave Province NATMAP Project:*

Introduction; in Can. J. Earth Sci., in press.

Bostock, H.H., 1987. *Geology of the south half of the Taltson Lake map area, District of MacKenzie*; in Current Research, Part A, Geological Survey of Canada, Paper 87-1A, p. 443-450.

Bostock, H.H., van Breemen, O., and Loveridge, W.D., 1987. *Proterozoic geochronology in the Taltson Magmatic Zone, N.W.T.*; in Radiogenic Age and Isotopic Studies: Report 1, Geological Survey of Canada, Paper 87-2, p. 73-80.

Bowring, S.A. and Podosek, F.A., 1989. *Nd isotopic evidence from Wopmay Orogen for 2.0-2.4 Ga crust in western North America*; in Earth Planet. Sci. Lett., v. 94, p. 217-230.

Culshaw, N., 1990. *Post-collisional oblique convergence along the Thelon Tectonic Zone, north of the Bathurst Fault, NWT, Canada*; in J. Struct. Geol., v. 13, p. 501-516.

Davis, W.J. and Henger, E., 1991. *Neodymuim isotopic evidence for the tectonic assembly of Late Archean crust in the Slave Province, northwest Canada*; in Contrib. Mineral Petrol., v. 111, p. 493-504.

Davis, W.J and Bleeker, W., in press. Timing of Plutonism, Deformation and Metamorphism in the Yellowknife Domain, Slave Province, CJES.

Dods, S.D., Teskey, D.J., and Hood, P.J., 1985. *The new series of 1:1 000 000-scale magnetic anomaly maps of the Geological Survey of Canada: Compilation techniques and interpretation*; in W.J. Hinze (ed), The Utility of Regional Gravity and Magnetic Anomaly Maps,Society of Exploration Geophysicists, Tulsa, Oklahoma, p. 69-87.

Fraser, J.A., Hoffman, P.F., Irvine, T.N., and Mursky, G., 1972. *The Bear Province*; in R.A

Price and R.J.W. Douglas (eds), Variations in Tectonic Styles in Canada, Geological Association of Canada, Special Paper 11, p. 454-503.

Fyson, W.K., 1981. *Complex evolution of folds and cleavages in Archean rocks, Yellowknife, N.W.T.*; in Can. J. Earth Sci., v. 19, p. 878-893.

Gibb, R.A., 1978. *Slave-Churchill collision tectonics*; in Nature, v. 271, p. 50-52.

Ham, N.M., Benn, K., and Bleeker, W., 1998. *The late Archean Prosperous Granite Suite: syn-D2 laccoliths in the Yellowknife Domain, Slave Province*; in F. Cook and P. Erdmer (compilers), Slave-Northern Cordillera Lithospheric Evolution (SNORCLE) Transect and Cordilleran Tectonics Workshop Meeting (March 6-8), Simon Fraser Unviersity, Lithoprobe Report No. 64, p. 36.

Hanmer, S.,1988. *Great Slave Lake Shear Zone, Canadian Shield: reconstructed vertical profile of a crustal-scale fault zone*; in Tectonophysics, v. 149, p. 245-264.

Hanmer, S. and Lucas, S.B., 1985. *Anatomy of a ductile transcurrent shear: Great Slave Lake Shear Zone, District of MacKenzie, NWT (preliminary report)*; in Current Research, Part B, Geological Survey of Canada, Paper 85-1B, p. 7-22.

Hanmer, S., Bowring, S., van Breemen, O., and Parrish, R., 1992. *Great Slave Lake shear zone, NW Canada: mylonitic record of Early Proterozoic continental convergence, collision and indentation*; in J. Struct. Geol., v. 14, no. 7, p. 757-773.

Hanmer, S., Williams, M., and Kopf, C., 1995. *Striding-Athabasca mylonite zone: Implications for Archean and Early Proterozoic tectonics of the western Canadian Shield*; in J. Earth. Sci., v. 32, p. 178-196.

Helmstaedt, H. and Padgham, W.A., 1985. *A new look at the stratigraphy of the Yellowknife Supergroup at Yellowknife, N.W.T. – implications for the age of gold-bearing shear zones and Archean basin evolution*; in Can. J. Earth Sci., v. 23, p. 454-475.

Helmstaedt, H., Padgham, W.A., and Brophy, J.A., 1986. *Multiple dikes in Lower Kam Group, Yellowknife greenstone belt: Evidence for Archean sea-floor spreading?*; in Geology, v.14, p. 562-566.

Henderson, J.B., 1985. *Geology of the Yellowknife-Hearne Lake area, District of MacKenzie: a segment across an Archean Basin*; Geological Survey of Canada, Memoir 414.

Henderson, J.B., 1985. *Geology, Yellowknife-Hearne Lake, District of MacKenzie, Northwest Territories*; Geological Survey of Canada, Map 1601A, scale 1:250 000.

Hildebrand, R.S., Hoffman, P.F., and Bowring, S.A., 1987. *Tectono-magmatic evolution of the 1.9-Ga Great Bear Magmatic Zone, Wopmay Orogen, northwestern Canada*; in J. Vol. and Geotherm. Res., v. 32, p. 99-118.

Hildebrand, R.S., Bowring, S.A., Andrew, K.P.E., Gibbins, S.F., and Squires, G.C., 1987. *Geological investigations in Calder River map area, central Wopmay Orogen, District of MacKenzie*; in Current Research, Part A, Geological Survey of Canada, Paper 87-1A, p. 699-711.

Hildebrand, R.S., Bowring, S.A., and Housh, T., 1990. *The medial zone of the Wopmay orogen, District of MacKenzie*; in Current Research, Part C, Geological Survey of Canada, Paper 90-1C, p. 167-176.

Hoffman, P.F., 1980. *Wopmay Orogen: a Wilson Cycle of Early Proterozoic age in the northwest of the Canadian Shield*; in D.W. Strangeway (ed), The Continental Crust and its Mineral Resources, Geol. Assoc. Can., Special Paper 20, p. 523-549.

Hoffman, P.F., 1987. *Continental transform tectonics: Great Slave Lake shear zone (ca. 1.9 Ga), northwestern Canada*; in Geology, v. 15,p. 785-788.

Hoffman, P.F. and McGlynn, J.C., 1977. *Great Bear Batholith: a volcano-plutonic depression*; in W.R.A. Baragar, L.C. Coleman, and J.M. Hall (eds), Volcanic Regimes in Canada, Geol. Assoc. Can., Special Paper 16, p. 170-192.

Hoffman, P.F. and Hall, L, 1983. *Geology, Slave craton and environs, District of Mackenzie, Northwest Territories*; Geological Survey of Canada, Open File 2559.

Hoffman, P.F. and Bowring, S.A., 1984. *Short-lived 1.9 Ga continental margin and its destruction, Wopmay orogen, northwest Canada*; in Geology, v. 12, p. 68-7.

Housh, T., Bowring, S.A., and Villeneuve, M., 1989. *Lead isotope study of Early Proterozoic Wopmay Orogen, NW Canada: Role of Continental Crust in arc magamtism*; in J. Geol., v. 97, p. 735-747.

Isachsen, C.E. and Bowring, S.A., 1994. *Evolution of the Slave Craton*; in Geology, v. 22, p. 917-920.

Isachsen, C.E. and Bowring, S.A., 1997. *The Bell Lake group and Anton Complex: a basement-cover sequence beneath the Archean Yellowknife greenstone belt revealed and implicated in greenstone belt formation*; in Can. J. Earth Sci., v. 34, P. 169-189.

James, D.T., 1986. *Geology of the Moraine Lake area District of MacKenzie; Part 2: a*

transect across part of the Thelon Tectonic Zone; in Current Research, Part A, Geological Survey of Canada, Paper 86-1A, p. 417-421.

James, D.T., van Breemen, O., and Loveridge, W.D., 1988. *Early Proterozoic U-Pb zircon ages for granitoid rocks from the Moraine Lake transect, Thelon Tectonic Zone, District of MacKenzie*; in Radiogenic Age and Isotopic Studies: Report 2, Geological Survey of Canada, Paper 88-2, p. 67-72.

Kusky, T.M., 1988. *Thrusting Between the Cameron River Greenstone Belt and the Sleepy Dragon Complex, Slave Province, District of MacKenzie*; in Cont. Geol. N.W.T., v. 3, p. 97-101.

Kusky, T.M., 1990. *Evidence for Archean ocean opening and closing in the southern Slave Province*; in Tectonics, v. 9, no. 6, p. 1533-1563.

Luyendyk, A.P.J., 1997. *Processing of airborne magnetic data*; in AGSO J. Aust. Geol. Geophys., v. 17, no. 2, p. 31-38.

McGlynn, J.C. and Henderson, J.B., 1970. *Archean volcanism and sedimentation in the Slave Structural Province*; in A.J. Baer (ed), Symposium on basins and geosynclines of the Canadian Shield, Geological Survey of Canada, Paper 70-40, p. 31-44.

McGlynn, J.C. and Henderson, J.B., 1972. *The Slave Province*; in R.A. Price and R.G.W. Douglas (eds), Variations on Tectonic Styles, Geol. Assoc. of Can., Special Paper 11, p. 506-526.

King, J.E., Barrette, P.D., and Relf, C.D., 1987. *Contrasting styles of basement deformation ad longitudinal extension in the metamorphic-internal zone of Wopmay Orogen,*

N.W.T.; in Current Research, Part A, Geological Survey of Canada, Paper 87-1A, p. 515-531.

Lambert, M.B., 1988. *Cameron River and Beaulieu River Volcanic Belts of the Archean Yellowknife Supergroup, District of MacKenzie, Northwest Territories*; Geological Survey of Canada, Bulletin 382.

MacLachlan, K. and Helmstaedt, H., 1995. *Geology and geochemistry of an Archean mafic dike complex in the Chan Formation: basis for a revised plate-tectonic model of the Yellowknife greenstone belt*; in Can. J. Earth Sci., v. 32, p. 614-630.

Redford, S.W., Gupta, V.K., Paterson, N.R., Kwan, K.C.H., and MacLeod, I.N., . *Ontario Master Aeromagnetic Grid: A Blueprint for Detailed Compilation of Magnetic Data on a Regional Scale*; in 60th Annual International Meeting, Expanded Abstracts, Society of Exploration Geophysicists, Tulsa, OK, p. 617-619.

Roest, W. and Pilkington, M., 1994. *Restoring post-impact deformation at Sudbury: A circular argument*; in Geophys. Res. Lett., v. 21, p. 959-962.

Ross, G.M., Parrish, R.R., Villeneuve, M.E., and Bowring, S.A., 1990. *Geophysics and geochronology of the crystalline basement of the Alberta Basin, western Canada*; in Can. J. Earth Sci., v. 28, p. 512-522.

Snyder, D.. Roberts, B., and Bleeker, W., 1999. *More thoughts about the nature of bright reflections in the upper crust near Yellowknife*; in F. Cook and P. Erdmer (compilers), Slave-Northern Cordillera Lithospheric Evolution (SNORCLE) Transect and Cordilleran Tectonics Workshop Meeting (March 5-7), University of Calgary,

Lithoprobe Report No. 69, p. 37-39.

Spark, R., Benn, K., Bleeker, W., Roest, W., 1999. *Syn-D2 plutonism in the southern Slave Province: evidence from magnetic fabrics and field mapping*; in F. Cook and P. Erdmer (compilers), Slave-Northern Cordillera Lithospheric Evolution (SNORCLE) Transect and Cordilleran Tectonics Workshop Meeting (March 5-7), University of Calgary, Lithoprobe Report No. 69, p. 42-45.

St-Onge, M.R., 1981. *"Normal" and "inverted" metamorphic isograds and their relation to syntectonic Proterozoic batholiths in the Wopmay Orogen, Northwest Territories, Canada*; in Tectonophysics, v. 76, p. 295-316.

St-Onge, M.R. and King, J.E., 1987. *Evolution of regional metamorphism during backarc stretching and subsequent crustal shortening in the 1.9 Ga Wopmay Orogen, Canada*; in Phil. Trans. R. Soc. Lond., v. A 321, p. 199-218.

Thomas, M.D., Gibb, R.A., and Quince, J.R., 1976. *New evidence from offset aeromagnetic anomalies for transcurrent faulting associated with the Bathurst and MacDonald faults, Northwest Territories*; in Can. J. Earth Sci., v. 13, no. 9, p. 1244-1250.

Thompson, P.H., Culshaw, N., Buchanan, J.R., and Manojlovic, P., 1986. *Geology of the Slave Province and Thelon Tectonic Zone in the Tinney Hills-Overby Lake (west half) map area, District of MacKenzie*; in Current Research, Part A, Geological Survey of Canada, Paper 86-1A, p. 275-289.

Thorpe, R.I., Cumming, G.L., and Mortensen, J.K., 1992. *A significant Pb isotope boundary in the Slave Province and its probable relation to ancient basement in the western*

Slave Province; in Project Summaries: Canada – Northwest Territories Mineral Development Subsudiary Agreement, Geological Survey of Canada, Open File 2484, p. 179-184.

Tirrul, R., 1983. *Structure cross-sections across Asiak Foreland Thrust and Fold Belt, Wopmay Orogen, District of MacKenzie*; in Current Research, Part B, Geological Survey of Canada, Paper 83-1B, p. 253-260.

van Breemen, O., Davis, W.J., and King, J.E., 1992. *Temporal distribution of granitoid plutonic rocks in the Archean Slave Province, northwest Canadian Shield*; in Can. J. Earth Sci., v. 29, p. 2186-2199.

Villeneuve, M.E., Ross, G.M., Thériault, R.J., Miles, W., Parrish, R.R., and Broome, J., 1993. *Tectonic subdivision and U-Pb geochronology of the crystalline basement of the Alberta Basin, western Canada*; Geological Survey of Canada, Bulletin 447.

Appendix A

DENSITY AND SUSCEPTABILITY MEASUREMENTS OF YELLOWKNIFE DOMAIN ROCKS

#	Sample #	Rock Unit	Lithology	Wdry grams	Wwet grams	Wdry-Wwet	Density grams/cm3	W.F. %	Susc.1	Susc. 2	Susc. 3	Ave. Susc.
	Formulae:			1000.0	500.0	500.0	1.99					
	Error:						ca. 0.005					
	Sleepy Dragon Complex:											
	BNB95-051	Sleepy Dragon Complex	Old metatonalite, Webb Lake	2302.0	1435.0	867.0	2.65		0.08	0.07	0.05	0.06
	BNB97-018A	Sleepy Dragon Complex	Grey metatonalite, Brown Lake	1172.1	736.5	435.6	2.68		0.2	0.17		0.18
	BNB96-046	Sleepy Dragon Complex	Mylonitized metatonalite/granodiorite	1480.8	965.8	515.0	2.87		0.08	0.1		0.09
	BNB97-055	Sleepy Dragon Complex	Oldest transposed dyke swarm in SDC, Patterson Lake	1835.6	1234.8	600.8	3.05	<10%	0.65	0.65		0.65
	BNB96-050A	Sleepy Dragon Complex	Kfsp megacrystic granodiorite, Patterson Lk.	1087.5	681.1	406.4	2.67		1.39	1.32		1.36
	BNB96-052A	Sleepy Dragon Complex	Biotite tonalite-granodiorite, Patterson Lk.	2331.1	1454.8	876.3	2.65		0.07	0.11		0.09
	BNB97-089	Sleepy Dragon Complex	Foliated, fine-grained hbl-bi tonalite	1078.9	684.7	392.2	2.74		0.4	0.4		0.4
	BNB97-009	Sleepy Dragon Complex	Pre-Morose Suite, foliated quartz diorite, Morose Lake	2536.2	1634.3	901.9	2.80		0.71	0.74		0.72
	BNB95-065	Sleepy Dragon Complex	Pre-Morose Suite, hbl-bi metatonalite	2321.7	1476.3	845.4	2.74		0.2	0.22	0.32	0.25
	BNB96-033	Sleepy Dragon Complex	Melanocratic tonalite, east of Patterson Lk.	880.2	562.8	317.4	2.77		0.26	0.24	0.21	0.24
	BNB97-078	Sleepy Dragon Complex	Intrusive granodiorite, Sleepy Dragon Lake	1713.6	1082.2	631.4	2.71		15.1	14.5	14	14.5
	BNB97-073	Sleepy Dragon Complex	Ross Lake granodiorite	2374.7	1478.0	896.7	2.64		3.26	2.34	3.01	2.87
	Central Slave Cover Group:											
	BNB96-028C	Patterson Lake Formation	Quartzite, weakly fuchsitic	895.9	565.4	330.5	2.70		0.03	0.02		0.02
	BNB96-030A	Patterson Lake Formation	Gritty, graded beds in BIF	2335.2	1474.7	860.5	2.71		0.19	0.16		0.18
	BNB94-105A	Dwyer Lake Formation	Quartzite, fuchsitic	1768.5	1122.9	645.6	2.73		0	0	0	0
	BNB97-008	Dwyer Lake Formation	Fuchsitic, chromite-bearing quartzite	1251.7	784.4	467.3	2.67		0.01	0.02	0.03	0.02
	BNB96-028A	Patterson Lake Formation	Serpentinized ultramafic sill	2118.9	1355.2	763.7	2.77		51			51
	Average iron formation											
	BNB94-105B	Dwyer Lake Formation	Banded iron formation	918.1	631.6	286.5	3.20		861			861
	BNB98-141	Amacher Lake Formation	Banded iron formation	2022.9	1408.6	614.3	3.28		541	592	614	582
	BNB95-078	Patterson Lake Formation	Oxide BIF						866	813	842	840
	BNB96-029B	Patterson Lake Formation	Oxide/silicate BIF						435	438		436
	BNB96-030C	Patterson Lake Formation	Quartzite schist						0.04	0.03		0.04
	Mafic volcanic rocks:											
	BNB95-053B	Cameron River basalts	Pillow basalt, some fractures	2858.6	1901.8	956.8	2.98		0.93			0.93
	BNB96-066D	Cameron River basalts	Pillowed mafic flow	808.0	526.3	281.7	2.86		0.47			0.47
	BNB96-036B	Cameron River basalts	Massive amphibolite, probably dyke or sill	1004.4	677.4	327.0	3.06		0.92			0.92
	BNB97-055	Old transposed gabbro dykes	Oldest transposed dyke swarm in SDC, Patterson Lake	1835.6	1234.8	600.8	3.05		0.65	0.65		0.65
	BNB94-128	Tumpline Lake volcanics	Pillowed mafic flow, Tumpline Lake						0.64	0.68	1.07	0.86
	Felsic volcanic rocks:											
	BNB94-102A	Victory Lake rhyolite	Foliated rhyolite	2316.3	1441.6	874.7	2.64					
	BNB94-135	Tumpline Lake volcanics	Intermediate volcaniclastic lapillistone	1029.8	648.2	381.6	2.69					
	BNB97-102	Sherrie rhyolite	Flow banded rhyolite	1756.3	1098.7	657.6	2.66		0.03	0.05	0.04	0.04
	BNB97-101	Cameron River rhyolite	Flow banded rhyolite	2345.4	1455.7	889.7	2.63		0.02			0.02
	Amacher Tonalite:											
	BNB97-088	Amacher tonalite	Chloritized quartz-porphyritic tonalite	883.2	555.2	328.0	2.69		0.12	0.1		0.11
	BNB98-142	Amacher tonalite	Metatonalite, Amacher Lake	703.1	442.8	260.3	2.69		0.2			0.2

Burwash Formation, low grade:												
	BNB94-004	Burwash Formation, biotite grade	Gritty metagreywacke	578.2	366.1	212.1	2.72		0.3			0.3
	BNB94-007	Burwash Formation, sub-biotite grade	Fine sandy to slaty metagreywacke	1927.7	1219.3	708.4	2.71		0.27	0.25	0.22	0.25
	BNB94-016	Burwash Formation, biotite grade	Metagreywacke with concretions						0.26	0.26		0.26
	BNB94-019	Burwash Formation, biotite grade	Thinly bedded metagreywacke	601.1	382.7	218.4	2.74		0.34	0.36	0.32	0.34
	BNB94-043	Burwash Formation, biotite grade	Silty to shaly metagreywacke	2440.8	1561.4	879.4	2.77		0.3	0.32	0.31	0.31
	BNB94-074	Burwash Formation, biotite grade	Sandy metagreywacke	1375.9	872.7	503.2	2.73		0.19	0.19	0.22	0.2
	BNB94-112	Burwash Formation, biotite grade	Metagreywacke	453.3	290.1	163.2	2.77		0.68	0.76	1.22	0.89
	BNB95-046	Burwash Formation, biotite grade	Coarse, pebbly metagreywacke, Hearne Lake	2757.9	1755.9	1002.0	2.74		0.42	0.58		0.5
	BNB95-047	Burwash Formation, biotite grade	Gritty metagreywacke, Hearne Lake	723.4	465.6	257.8	2.80					
	BNB98-DDH 97L	Beechy Lake Group metagreywacke	Thinly bedded greywacke, ca. 50% slate	895.7	572.5	323.2	2.76					
	BNB98-090A	Beechy Lake Group, biotite grade	Typical low-grade metagreywacke, Gold Lake	990.0	619.0	371.0	2.66		0.2	0.2		0.2
	BNB98-098A	Beechy Lake Group, biotite grade	Feldspathic coarse greywacke, NW of Back River	1087.5	681.4	406.1	2.67		0.14			0.14
	BNB95-038	Burwash Formation, with tuff layers	Shaly turbidite with 50% felsic tuff						0.25	0.33		0.29
Burwash Formation, medium grade:												
	BNB94-066A	Burwash Formation, cordierite grade	Metagreywacke, first cordierite	900.6	576.6	324.0	2.77		0.54	0.6		0.52
	BNB94-055	Burwash Formation, cordierite grade	Cordierite bearing metagreywacke	1654.2	1059.1	595.1	2.77		0.32	0.33	0.4	0.35
	BNB94-053	Burwash Formation, cordierite grade	Cordierite bearing metagreywacke	845.3	539.5	305.8	2.76		0.41	0.4		0.4
	BNB94-079	Burwash Formation, cordierite grade	Typical cordierite grade metagreywacke, Watta Lake	1428.1	910.2	517.9	2.75		0.33	0.38	0.39	0.37
	BNB95-028	Burwash Formation, cordierite grade	Typical cordierite grade metagreywacke, Victory Lake	1735.7	1101.2	634.5	2.73		0.37	0.38		0.38
	BNB94-116	Burwash Formation, cordierite grade	Typical cordierite grade, porphyroblast-rich	1417.0	934.4	482.6	2.93		0.58	0.48	0.55	0.54
Defeat Suite granitoids, Wool Bay diorite:												
	BNB96-062	Defeat Suite, Wool Bay diorite	Hornblende diorite	2014.7	1327.3	687.4	2.92		0.41	0.52	0.43	0.45
	BNB96-062	Defeat Suite, Wool Bay diorite	Hornblende diorite	694.0	456.0	238.0	2.91		0.49	0.39	0.54	0.47
Defeat Suite granitoids, tonalites:												
	BNB94-026	Defeat Suite, Upper Watta Lake stock	Biotite tonalite, leucocratic	1232.2	768.7	463.5	2.65		0.09	0.1		0.1
	BNB94-057A	Defeat Suite, Watta Lake pluton	Coarse biotite tonalite	1841.3	1167.9	673.4	2.73		0.15	0.17	0.18	0.17
	BNB97-097	Defeat Suite, Watta Lake pluton	Central phase, massive	648.8	405.3	243.5	2.66		12.4	11.8		12.1
	BNB97-096	Defeat Suite, Watta Lake pluton	Marginal phase, coarse bi-tonalite	615.2	384.1	231.1	2.65		0.13	0.14		0.14
	BNB97-092	Defeat pluton	Central phase, massive, quartz-porphyritic	2293.1	1437.2	855.9	2.67		8.71	8.64		8.68
	BNB97-091	Defeat pluton	Eastern marginal phase	1685.1	1060.8	624.3	2.69		16.1	14.9		15.5
Hidden Lake pluton:												
	BNB96-013	Hidden Lake granodiorite	Marginal phase	1543.6	955.7	587.9	2.62		0.04	0.05	0.06	0.05
	BNB96-015A	Hidden Lake granodiorite	Biotite granodiorite, central phase	1143.3	709.1	434.2	2.63		0.02	0.04		0.03
Prosperous Suite granitoids:												
	BNB96-022	Prosperous Suite	Sparrow pluton, typical	1791.7	1110.6	681.1	2.62		0.03	0.02	0.04	0.03
	BNB96-024B	Prosperous Suite	Sparrow pluton, typical	1396.3	867.8	528.5	2.63		0.04			0.04
	BNB97-093	Sparrow Lake pluton	Foliated bi-ms granite	1873.6	1160.1	713.5	2.62		0.05	0.03	0.05	0.04
Redout Granite:												
	BNB97-090	Redout Granite	Pink bi-granite	576.9	356.7	220.2	2.61		0.1	0.11		0.1
	BNB97-084B	Redout Granite	Pink bi-granite	343.6	214.2	129.4	2.65		3.48	4.03		3.76
Morose-type granitoids:												
	BNB95-064B	Morose Granite	Typical	2021.6	1251.2	770.4	2.62		0.07	0.06	0.08	0.07
	BNB96-041	Morose Granite	Typical	2022.0	1255.2	766.8	2.63		0.07			0.07
	BNB97-017A	Morose-type granite	Morose-type granite, Brown Lake	1004.4	625.5	378.9	2.64		0.22			0.22
Proterozoic intrusives:												
	BNB98-140	Duck Lake intrusive sheet	Melanocratic gabbro						45.1	31.7	27.5	34.8